Structural Basis for Target Protein Regcognition by Thiredoxin

Maeda, Kenji; Svensson, Birte

Publication date:
2007

Document Version
Publisher's PDF, also known as Version of record

Structural Basis for Target Protein Recognition by Thioredoxin

by

Kenji Maeda

M. Sc.

University of Copenhagen,

Copenhagen, Denmark

This thesis is submitted for the Ph.D. degree at the Technical University of Denmark

Enzyme and Protein Chemistry, BioCentrum-DTU,

Technical University of Denmark,

Kgs Lyngby, Denmark

Acknowledgements

The present Ph.D. project was supported by a Ph.D. scholarship from the Technical University of Denmark, the Danish Technical Research Council (STVF, grant nr 26-03-0194) and the Carlsberg Foundation.

Professor Birte Svensson (Enzyme and Protein Chemistry, BioCentrum-DTU) is acknowledged for creating financial and scientific basis for this project and for daily supervision and discussions.

Professor Anette Henriksen (Biostructure Group, Carlsberg Laboratory) is acknowledged for making facilities of X-ray crystallography available for the present project, for supervision and support in theoretical and practical X-ray crystallography and for helpful discussions.

Associate Professor Per Hägglund (Enzyme and Protein Chemistry, BioCentrum-DTU) is acknowledged for daily support and for helpful discussions.

Associate Professor Christine Finnie (Enzyme and Protein Chemistry, BioCentrum-DTU) and Professor Jakob R. Winther (University of Copenhagen) are gratefully thanked for helpful discussions.

All technicians at Enzyme and Protein Chemistry, BioCentrum-DTU, and especially Karina Rasmussen, Mette Therese Christensen and Anne Blicher are acknowledged for technical assistance.

All former and present members of Enzyme and Protein Chemistry, BioCentrum-DTU, and Biostructure Group, Carlsberg Laboratory, are thanked for discussions and for creating excellent working environment.

Table of contents

Appendix I

Maeda, K., Hägglund, P., Finnie, C., and Svensson, B. (2006). Proteomics of disulphide and cysteine oxidoreduction. In Plant Proteomics, The Annual Plant Reviews, Vol. 28, Finnie, C., ed. (Blackwell Publishing: Oxford, UK), pp. 71-97.

Appendix II

Maeda, K., Hägglund, P., Finnie, C., Svensson, B., and Henriksen, A. (2006). Structural basis for target protein recognition by the protein disulfide reductase thioredoxin. Structure *14*, 1701–1710.

Abbreviations

2-DE, two-dimensional gel electrophoresis

ASA, accessible surface area

ASK1, apoptosis signal-regulating kinase-1

BASI, barley α–amylase/subtilisin inhibitor

DTNB, 5,5´-dithiobis(2-nitrobenzoic acid)

DTT, dithiothreitol

E°´, standard redox potential

EcTrx, *Escherichia coli* thioredoxin 1

ER, endoplasmic reticulum

Grx, glutaredoxin

GSH, reduced glutathione

GSSG, oxidized glutathione

GST, glutathione transferase

H_2O_2, hydrogen peroxide

HvTrxh1, barley thioredoxin h isoform 1

HvTrxh2, barley thioredoxin h isoform 2

HvTrxh2-S-S-BASI, the disulfide-linked complex of HvTrxh2 and BASI

IAM, iodoacetamide

IPTG, isopropyl β-D-1-thiogalactopyranoside

MR, molecular replacement

Mw, molecular weight

NO, nitric oxide

NTR, NADPH-dependent Trx reductase

Orp1, oxidant receptor peroxidase 1

PEG, polyethylene glycol

PDI, protein disulfide isomerase

PTM, post-translational modification

Rmsd, root-mean-square difference

RNS, reactive nitrogen species

ROS, reactive oxygen species

SOH, sulfenic acid

SO_2H, sulfinic acid

SO_3H, sulfonic acid

TCEP, Tris(2-carboxyethyl)phosphine

TFA, trifluoroacetic acid

TNB, 2-nitro- 5-thiobenzoate

Trx, thioredoxin

Thesis summary

Thioredoxin (Trx) is an ubiquitous protein disulfide reductase that possesses two redox active cysteines in the conserved active site sequence motif, Trp-Cys_N-Gly/Pro-Pro-Cys_C situated in the so called Trx-fold. The lack of insight into the protein substrate recognition mechanism of Trx has to date been a hindrance for comprehensive understanding of the functions and biological roles of Trx. This issue is addressed in the present study on two h-type Trxs, HvTrxh1 and HvTrxh2 from barley seeds. The crystal structure was determined for a stable, disulfide-linked complex of a HvTrxh2 mutant (Cys49Ser) and a mutant of an *in vitro* substrate α-amylase/subtilisin inhibitor (BASI) (Cys144Ser), as a reaction intermediate-mimic of Trx-catalyzed disulfide reduction. The resultant structure showed a sequence of BASI residues along a conserved hydrophobic groove constituted of three loop segments on HvTrxh2 surface, associated through several van der Waals contacts and three backbone-backbone hydrogen bonds resembling β-sheet formation. Moreover, a pattern of interactions essentially identical to that in HvTrxh2-S-S-BASI was observed in the structure of HvTrxh1 crystallized in the oxidized form. In the crystal lattice, HvTrxh1 formed a dimer, in which a loop segment from one molecule was situated along the hydrophobic groove at the active site of another molecule. The observed manner of protein recognition by Trx was similar in the central part to the glutathione recognition mechanisms of Trx-fold proteins glutaredoxin and glutathione transferase. This study suggests that the features of main chain conformation as well as charge property around disulfide bonds in protein substrates are important factors for interaction with Trx. Moreover, this study describes a detailed structural and biophysical comparison of the two coexisting h-type barley Trxs, HvTrxh1 and HvTrxh2.

Dansk Resumé

Thioredoxin (Trx) er en allestedsnærværende protein-disulfid-reduktase, som har to redox aktive cysteiner i det konserverede active site sekvensmotiv, Trp-Cys_N-Gly/Pro-Pro-Cys_C, placeret på den såkaldte Trx-fold. Mangelen på indblik i mekanismen bag Trxs substratgenkendelse har indtil idag været en forhindring til at opnå fuld forståelse for Trxs funktioner og biologiske rolle. Denne problemstilling bliver behandlet i det nærværende undersøgelse af to h-type Trx'er, HvTrxh1 and HvTrxh2 fra bygkerner. Krystalstrukturen er blevet bestemt for et stabilt, disulfidbundet kompleks af en HvTrxh2 mutant (Cys49Ser) og en mutant af et *in vitro* substrat, α-amylase/subtilisin inhibitor (BASI) (Cys144Ser), som repræsenterer et intermediat i Trx-katalyseret disulfid-reduktion. Den resulterende struktur viste en sekvens af BASI-rester langs en konserveret hydrofob rende bestående af tre loop segmenter på HvTrxh2 overfladen forbundet med en række van der Waals kontakter og tre backbone-backbone hydrogenbindinger, som ligner en β-sheet-dannelse. Desuden blev et mønster af interaktioner, der grundlæggende var identisk med det der ses i HvTrxh2-S-S-BASI, observeret i strukturen af HvTrxh1, som blev krystalliseret i den oxiderede form. I krystalgitteret dannede HvTrxh1 en dimer, hvori et loop segment fra det ene molekyle var placeret langs den hydrofobe rende i det andet molekyle. Den centrale del af denne observerede mechanismer for Trxs protein-genkendelse var sammenlignelig med glutathion-genkendelses mekanismer for Trx-fold-proteinerne, glutaredoxin og glutathion-transferase. Det nærværende arbejde foreslår, at såvel backbones konformation som ladningsfordelingen omkring disulfidbroer i protein-substrater er vigtige faktorer for interaktion med Trx. Desuden beskrives i det nærværende arbejde en detaljeret strukturel og biofysisk sammenligning af de to sameksisterende h-type byg Trx'er, HvTrxh1 and HvTrxh2.

Chapter 1

Introduction

1.1 Reactive nature of cysteine residues in proteins

The proteome in a given cell or organelle of an organism is dynamic and changes both in terms of protein composition and post-translational modifications (PTMs). PTMs of specific amino acid residues can alter the properties and functions of proteins and are major regulatory mechanisms in diverse physiological processes.

Cysteine residues in protein three-dimensional structures are most commonly observed in the free thiol form or in the oxidized and paired form, in which two cysteine side chains are covalently cross-linked *via* a disulfide bond. Cysteine is the most reactive amino acid residue present in proteins apart from the rare selenocysteine and is often located in the active sites of enzymes. It can also have a structural role, for example, in iron–sulfur centers of metal proteins. A disulfide bond provides an additional covalent bond between two sequentially separated cysteine residues and is therefore an important stabilizing factor of protein structures.

Cysteine residues in various proteins can alter the redox status upon changes in the redox homeostasis. The cysteine thiol group is susceptible to several reversible and irreversible oxidative modifications including formation of sulfenic acid (SOH), sulfinic acid (SO_2H), sulfonic acid (SO_3H) and mixed disulfides with low-molecular-weight thiols such as glutathione, cysteine and homocysteine. Cysteine in the thiol form can furthermore react reversibly with nitric oxide (NO) to give a nitrosothiol. As cysteine often has catalytic or structural roles in proteins, such modifications can profoundly influence protein function. A wide variety of biological redox compounds, including proteins catalyzing cysteine redox modifications, regulate an array of biological processes. Several of these redox proteins such as protein disulfide isomerase (PDI)

have central roles in protein folding and function and have been studied for many decades (Wilkinson and Gilbert, 2004). Sulphiredoxin (Biteau et al., 2003) that can reduce cysteine SO_2H, have been discovered recently, emphasizing the fact that our knowledge of thiol modification mechanisms is still incomplete. The expressions of these proteins in turn are often adjusted in response to cellular redox signals, and thus create highly complex regulatory networks.

1.2 Control of cellular redox status

Reactive oxygen/nitrogen species (ROS/RNS) such as hydrogen peroxide (H_2O_2), superoxide, singlet oxygen, NO and the hydroxyl radical can cause damage to biological macromolecules, including lipids, nucleic acids and proteins, and are very reactive against protein thiols. ROS production takes place, for instance, in the electron transport chain of the respiratory pathway in the mitochondrion, while ROS primarily are produced by chloroplasts and peroxisomes in plant tissues (Bailly, 2004).

A coordinated system for detoxification of ROS is required to remove the different toxic by-products of metabolism. The major control of cellular redox status is the ascorbate–glutathione cycle (Potters et al., 2002). The enzymes of the ascorbate–glutathione cycle in plants occur in the chloroplast, mitochondrion and cytosol. Glutathione, the tripeptide glutamyl–cysteinyl–glycine, is the dominant low molecular weight (Mw) thiol in the cell, present at millimolar concentrations. The ratio of reduced (GSH) to oxidized (GSSG) glutathione is the major determinant of the cellular redox balance including the thiol/disulfide redox status. This ratio is around 100:1 in the cytoplasm of eukaryotic cells (Hwang et al., 1992) and the maintenance of the GSH/GSSG ratio is coupled by glutathione reductase to the availability of NADPH. The reducing environment of the cytosol does not favor disulfide formation. Disulfides

formed in cytosolic proteins are therefore likely to be transient and highly sensitive to changes in the redox status of the cell. In contrast to the cytoplasm the GSH/GSSG ratio is around 3:1 in the endoplasmic reticulum (ER). This more oxidizing environment favors disulfide bond formation. PDI catalyses disulfide formation and isomerization in the ER, and is responsible for the correct disulfide pairing in nascent secretory proteins. Although PDI has also been identified in chloroplasts of the unicellular green alga *Chlamydomonas reinhardtti* (Trebitsh et al., 2001), disulfide bonds are typically found in proteins that are processed *via* the secretory pathway.

In addition to the role of glutathione in maintenance and regulation of the cellular redox state, glutathionylation of thiol groups in proteins protects them from irreversible oxidation by ROS. The glutaredoxin (Grx) system is responsible for the deglutathionylation, which also requires reducing power from NADPH, supplied *via* glutathione reductase. Another major system for regulation of protein thiol redox status is the thioredoxin (Trx) system that also uses reducing power from NADPH, *via* Trx reductases, to reduce disulfide bonds in proteins. Cellular redox control and protein thiol status are intimately linked in a complex regulatory network that is increasingly recognized as central to metabolism.

1.3 Cysteine PTMs as signal transduction mechanisms

For a long time cysteine PTMs have been considered as events of toxic effects that damage and dysfunctions cells under conditions of diseases and oxidative stress. In recent years, progressing numbers of studies have provided evidence for that controlled regulation of cellular redox status serves as a mechanism of signal transduction that often is mediated by cysteine PTMs. For example, cytokines and hormones stimulate the production of ROS in eukaryotic cells, which in low, untoxic concentrations act as

messengers that transduce signals and regulate various biological processes, including hormone biosynthesis, proliferation and apoptosis (Nakamura et al., 1997; Gamaley and Klyubin, 1999; Thannickal and Fanburg, 2000).

A small number of such signaling pathways controlled by intracellular redox conditions are to date characterized in detail. The redox regulations of yeast transcription factor Yap1 and its prokaryotic counterpart OxyR, both involved in the expression of antioxidant proteins in Trx and glutathione systems, are examples of well-studied signaling pathways mediated by cysteine PTMs (Toledano et al., 2004). In *Escherichia coli*, the stimulation of intracellular H_2O_2 release results in oxidation and formation of an intramolecular disulfide bond in OxyR that thereby alters the fold and activates the gene transcription (Åslund et al., 1999). In *Saccharomyces cerevisiae*, the corresponding mechanism of Yap1 regulation is more complicated. Firstly, H_2O_2 reacts with oxidant receptor peroxidase 1 (Orp1) to form a cysteine SOH. Yap1 is activated *via* specific protein-protein interaction involving the reaction between cysteine SOH of oxidized Orp1 with a dithiol in Yap1 that results in disulfide bond formation in Yap1 (Delaunay et al., 2000, 2002). The Trx system is likely to be responsible for the reduction and deactivation of Yap1, as Yap1 is constitutively oxidized and active in the Trx-deficient yeast strains (Izawa et al., 1999). The depletion of Grx genes, on the other hand, does not show the same effect (Izawa et al., 1999).

The redox regulation of mitogen-activated protein kinase pathway *via* apoptosis signal-regulating kinase-1 (ASK1) is another well-characterized example of cysteine PTM involved in signaling mechanisms. ASK1 is inactive when associated with the reduced form of Trx, but the ROS-mediated Trx oxidation leads to the dissociation of ASK1-Trx complex and the activation of ASK1 (Liu et al., 2000). These

and other examples signify that cysteine PTMs and protein redox regulations are prevalent events controlling biological activities in organisms.

1.4 Structures and functions of Trx and Trx superfamily proteins

Trx plays roles in cellular metabolic activities by donating electrons to enzymes such as ribonucleotide reductase, methionine sulfoxide reductases and peroxiredoxins, and in redox regulation of an array of target proteins ranging from mammalian transcription factors to plant enzymes involved in photosynthesis (Arnér and Holmgren, 2000).

Trx, Grx, PDI and prokaryotic disulfide bond formation proteins such as DsbA all belong to the Trx superfamily, sharing a conserved active site motif, Cys_N-Xxx_1-Xxx_2-Cys_C, situated in the Trx-fold with a βαβαββα topology (Martin, 1995). The overall fold of Trx is exceptionally well-conserved among species and constituted of a central five stranded β-sheet surrounded by four α-helices (**Figure 1.1**) (Holmgren et al., 1975). The two redox active cysteine residues in the Trx active site sequence motif Trp-Cys_N-Gly/Pro-Pro-Cys_C form an intramolecular disulfide in the oxidized state (**Figure 1.1**). Trx receives reducing equivalents from NADPH *via* NADP-dependent Trx reductase (NTR) or in plant chloroplast from ferredoxin *via* ferredoxin-dependent Trx (Buchanan and Balmer, 2005). For reduction of protein disulfides, the surface-exposed thiol group of Cys_N in the reduced Trx carries out the initial nucleophilic attack to form a transient intermolecular disulfide bond, linking Trx and the substrate at the transition state (Kallis and Holmgren, 1980). Cys_C subsequently attacks the transient disulfide bond and releases the reduced substrate with concomitant formation of the disulfide bond in Trx. For the efficient (de)protonation of the Cys_C thiol group, a conserved aspartic acid in the Trx core (referred to in the followings as Asp_C) acts as a general acid/base catalyst (**Figure 1.1**) (Chivers and Raines, 1997). Studies on *E. coli* Trx 1

(EcTrx) has demonstrated that the Trx active site ionizes singly either on Cys_N or Asp_C at the pK_a of 7.5, while the ionization on both groups occurs at pK_a of 9.2, because the Coulombic interaction between the two proximity anionic ions creates negative cooperativity (Chivers et al., 1997). The two pK_a values are referred as *microscopic* pK_as. The Cys_C thiol group of Trx ionizes at pK_a >11 (LeMaster, 1996; Chivers et al., 1997).

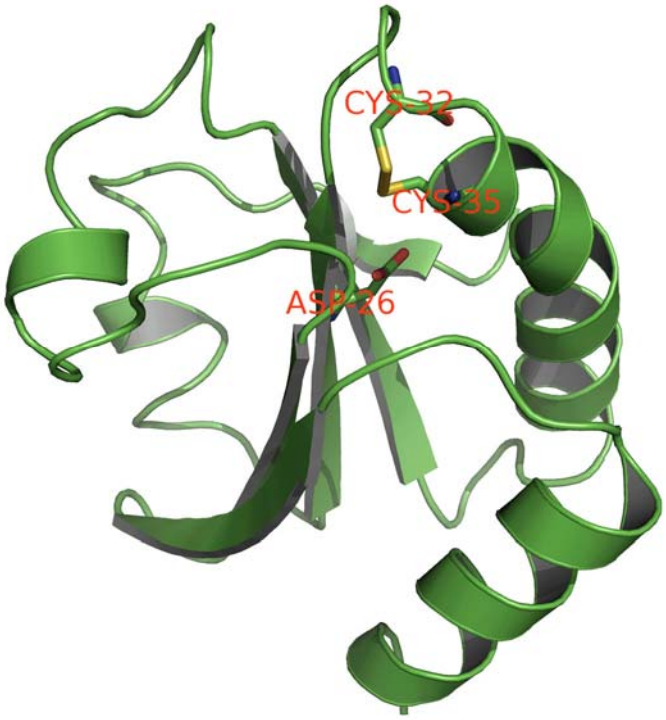

Figure 1.1 Cartoon display of the crystal structure of oxidized EcTrx (PDB entry 2TRX, molecule A; Katti et al., 1991). Stick representation shows the redox active cysteine pair, Cys32/Cys35 (Cys_N/Cys_C), and Asp 26 (Asp_C). Carbon, oxygen, nitrogen and sulfur are colored green, red, blue and yellow, respectively.

Grx typically contain the active site sequence motif Cys-Pro-Tyr-Cys, although several Grx genes in *A. thaliana* show variation in this sequence. Grx can accept

reducing equivalents either from NADPH *via* Grx reductase or from GSH (Holmgren, 1979a). Grx is, in terms of thermodynamics, a weaker reductant than Trx, by having standard redox potential of around –200 mV compared to about –270 mV for Trx (Åslund et al., 1997). In Grx, the thiol-pK_a value of Cys_N is strongly perturbed and exceptionally low, for example 3.5 in yeast Grx (Gan et al., 1990). In addition, the function of Grx is diverged from that of Trx in terms of kinetics and specificity, as solely Grx exhibits affinity towards glutathionylated proteins (Fernandes and Holmgren, 2004). Grx preferentially reduces glutathione mixed disulfides (Gravina and Mieyal, 1993) and accounts for the majority of deglutathionylation activity in human cells (Chrestensen et al., 2000). Whereas both Cys_N and Cys_C are essential in reduction of disulfide bonds by Trx, Cys_N is sufficient for protein deglutathionylation by Grx, because it can receive the glutathione group from *S*-glutathionylated proteins by a single nucleophilic attack (Yang et al., 1998). Grxs and Grx variants lacking Cys_C retain the reductase activity towards *S*-glutathionylated proteins (Yang et al., 1998), dehydroascorbate and cysteine SOH in peroxiredoxin (Rouhier et al., 2002a, b). Cys_C is replaced by serine in a number of Grxs from *A. thaliana* (Rouhier et al., 2004).

The *A. thaliana* genome includes at least 19 and 31 genes encoding for Trx and Grx, respectively, in contrast to human, yeast and *E. coli*, only containing a few Trx and Grx encoding genes (Meyer et al., 2002b; Rouhier et al., 2004). The numerous isoforms of plant Trxs are grouped into six types based on the primary structure. The f-, m-, x- and y-types are chloroplastic, the o-type is mitochondrial and the h-type is mainly cytosolic although it has also been identified in the nucleus, mitochondria and phloem sieve tubes (Buchanan and Balmer, 2005). Some of the coexisting Trx isoforms in plants have been demonstrated to have distinct physiological functions. For instance, the chloroplastic Trx f reduces fructose-1,6-bisphosphatase *in vitro* much more efficiently

than Trx m (Wolosiuk et al., 1979). The isoforms of h-type Trxs, which constitute the major Trx sub-group in plants (at least nine genes in *A. thaliana*), carry out distinct biological roles in yeast complementarity studies (Mouaheb et al., 1998; Sarkar et al., 2005; Traverso et al., 2007). Moreover, genes encoding *A. thaliana* Trx h isoforms are differentially regulated in response to pathogens and under oxidative stress (Reichheld et a., 2002; Laloi et al., 2004). Thus in plants, the presence of numerous Trx isoforms, in combination with other redox active components, constitutes a complex redox regulatory system.

1.5 Strategies to map the features of cysteine PTMs at the proteome level

In order to reveal the features of cysteine PTMs at the proteome level, various proteomics techniques have in recent years been developed. These techniques have been applied for the identification of proteins and individual cysteine residues that undergo oxidoreductions upon treatment with oxidants or reductants *in vitro* and *in vivo* (reviewed in Maeda et al., 2006a; Appendix I). Such approaches have led to, for instance, the identifications of over hundred proteins which are suggested to be reduced by the Trx system. However, most redox proteomics approaches developed so far have difficulties in providing solid evidence for that the PTMs of particular cysteines take place to significant extents under physiologically relevant conditions *in vivo*. The difficulties in achieving comprehensive mapping of the redox proteome stem *e.g.* from that the techniques are not able to analyze the relatively low-abundant proteins or membrane proteins, and moreover are mostly non-quantitative. Furthermore, individual cysteine residues can rapidly alter the redox status *via* dithiol/disulfide exchanging reactions unless the sample proteins stay in acidic solutions. However, the regular

sample handling procedures of proteomics often necessitate the application of buffers of higher pH values, as for instance in tryptic digestion.

Another major challenge in plotting redox regulatory pathways is the assignment of oxidants and reductants responsible *in vivo* for the individual cysteine PTMs involved in the signal transduction. The coexistence of numerous redox active compounds in biological environment makes such an assignment a highly challenging task. Approaches based on knock-out or knock-down of the individual oxidoreductases combined with techniques of proteomics can be useful, but insufficient for some cases. For instance, knock-down of Trx genes will not only alter the redox status of the downstream interaction partners, but the general cellular redox homeostasis, because Trx is responsible for the delivery of electrons to antioxidants proteins such as peroxiredoxins. For these reasons, detailed knowledge of the kinetic determinants for reactions between biological oxidoreductants can be a support for the understanding of redox-mediated signal transduction pathways. The susceptibility of cysteine residues to undergo oxidoreductions largely depends on the values of thiol-pK_a, but also on the specific interactions with oxidoreductants, as well-illustrated for the above-mentioned involvement of specific recognition of glutathionylated proteins in protein deglutathionylation by Grx.

Little is known currently about the substrate specificity of Trx, and it is still a matter of debate, to which extent the Trx-catalyzed disulfide reductions are governed by specific protein–protein interactions. Nevertheless, examinations of individual disulfide proteins and proteomics-based surveys for target proteins have shown substrate selectivity of Trx for certain protein disulfides (Østergaard et al., 2001; Yano et al., 2001; Maeda et al., 2004; Maeda et al., 2005). Moreover, mutational analysis of the redox regulation of fructose-1,6-bisphosphatase by chloroplastic Trx has suggested

charge complementarity to influence the specificity of Trx (de Lamotte-Guery et al., 1991; Geck et al., 1996; Mora-Garcia et al., 1998). However, the only structural studies to date on the interaction between Trx and target proteins are NMR structure determinations of two disulfide-bonded complexes between a mutant of human Trx and short synthetic peptide fragments derived from transcription factors NF-κB and Ref-1 (Qin et al., 1995; Qin et al., 1996). Protein disulfides can be structurally diverse in various aspects, such as their surface exposure and their locations in secondary structure elements, the dihedral angles around the disulfide bond, and the identity of the amino acids present at spatially and sequentially close locations (Bhattacharyya et al., 2004). Structural determination of Trx-substrate protein-protein complexes will possibly identify the substrate recognition site(s) on Trx structure, and structural motif(s) around disulfides of Trx targets recognized by Trx.

1.6 Barley Trx h isoforms HvTrxh1 and HvTrxh2

In proteome analysis of barley seeds based on two-dimensional gel electrophoresis (2-DE), two h-type Trx isoforms with 51% sequence identity were identified and termed HvTrxh1 and HvTrxh2 (Maeda et al., 2003). HvTrxh1 appeared in two spots with slightly different values of Mw in the 2D-gels of mature barley seeds, but the mass spectrometric analysis of the tryptic digests did not detected any PTMs or truncations that explain this observation. Detailed proteome analysis of the embryo, endosperm and aleurone layers from barley seeds in the mature state and six days after imbibition showed that the two Trxs have distinct patterns of spatial and temporal distribution. HvTrxh1 was abundant in all examined tissues of mature seeds. It remained abundant at similar levels in the embryo after imbibition, but diminished in endosperm and aleurone

layers. On the other hand, HvTrxh2 was mainly present in the embryo of mature seeds and decreased in the amount after imbibition.

In order to characterize the two barley Trxs, the encoding genes were cloned and the recombinant proteins produced in *E. coli* (Maeda et al., 2003). The protein disulfide reductase activities of the two barley Trxs were compared using the insulin assay (Holmgren, 1979b). In this assay, the efficiency of Trxs in catalyzing the reduction of insulin disulfides by dithiolthreitol (DTT) was measured, and the insulin reduction was followed spectrometrically based on the aggregation of the reduced insulin. Insulin reduction rates were ~30% higher for HvTrxh1 than HvTrxh2. HvTrxh1 is also a better substrate for *A. thaliana* NTR with ~3 fold lower K_m value than HvTrxh2.

H-type Trxs in cereal seeds have been shown to have positive influence on germination process, but little is yet known about their target proteins. Barley seed proteins susceptible to undergo reduction by HvTrxh1 and HvTrxh2 *in vitro* were identified using a proteomics technique, based on thiol-specific fluorescence labeling with monobromobimane and Cy5-maleimide, 2-DE and mass spectrometry (Maeda et al., 2004). The two Trxs reduced the same 16 seed proteins with various structures and functions. These possible Trx substrates include several endospermic enzyme inhibitors (α-amylase/subtilisin inhibitor (BASI) and trypsin/α-amylase inhibitors) and others. Subsequently, specific disulfide bonds reduced by Trx were identified in some of the Trx substrate proteins from barley seeds using another proteomics technique (Maeda et al., 2005). Although this technique was not quantitative, the BASI disulfide Cys144-Cys148 was clearly a preferred Trx-substrate, in comparison with several other disulfides in the barley seed proteome.

Objectives

The primary objective of the present Ph.D. project has been to reveal the structural background for the target protein recognition mechanism of Trx. The acquired knowledge will be useful as a tool to predict and understand the involvement of Trx in protein redox regulation and redox signaling pathways. Secondary, it has been intended to carry out comparative characterization of two barley Trx h isoforms, HvTrxh1 and HvTrxh2, with focus on their 3D structures, biophysical properties and substrate specificities.

Chapter 2 describes the crystal structure of a HvTrxh2 mutant Cys49Ser in a disulfide-linked complex with a BASI mutant Cys144Ser (HvTrxh2-S-S-BASI) as a reaction intermediate-mimic of the HvTrxh2-catalyzed reduction of the BASI disulfide Cys144-Cys148. This BASI disulfide, which previously was identified as an excellent *in vitro* target of Trx (Maeda et al., 2004, 2005), serves here as a model for the analysis of Trx-target protein interactions. The work is published in *Structure* (Maeda et al., 2006b) as the first reported structural study of a protein-protein complex of Trx and a target protein.

Chapter 3 describes crystal structures of HvTrxh1 and HvTrxh2. This work has focus on the comparison of the putative substrate recognition motifs in the two Trxs. Moreover, protein-protein interfaces in the HvTrxh1 crystal lattice, involving interactions between the putative substrate recognition motif and a loop motif of independent HvTrxh1 molecules, are discussed in detail. These interactions are considered to serve as a model for the general target recognition features of Trx. The

studies included in this chapter are described in a manuscript, which soon will be submitted to *Protein Science*.

Chapter 4 describes comparative biophysical characterization of HvTrxh1 and HvTrxh2. The values of the standard redox potential are determined for the two barley Trxs using a novel approach. The biophysical background for the distinct kinetic properties of the two Trxs is addressed based on the determination of thiol-pK_as of Cys_N and site-directed mutagenesis. The studies included in this chapter is described in a manuscript, which soon will be submitted to *Protein Science*.

Chapter 2

Structural basis for target protein recognition by the protein disulfide reductase thioredoxin

---

2.1 Summary

Thioredoxin (Trx) is ubiquitous and regulates various target proteins through disulfide bond reduction. We report the first structure of Trx (HvTrxh2 from barley) in a reaction intermediate complex with a protein substrate, barley α-amylase/subtilisin inhibitor (BASI). The crystal structure of this mixed disulfide shows a conserved hydrophobic motif in Trx interacting with a sequence of residues from BASI through van der Waals contacts and backbone-backbone hydrogen bonds. The observed structural complementarity suggests that the recognition of features around protein disulfides plays a major role in the specificity and protein disulfide reductase activity of Trx. This novel insight into the function of Trx constitutes a basis for comprehensive understanding of its biological role. Moreover, comparison with structurally related proteins shows that Trx shares a mechanism with glutaredoxin and glutathione transferase for correctly positioning substrate cysteine residues at the catalytic groups but possesses a unique structural element that allows recognition of protein disulfides.

2.2 Introduction

Our previous screenings for target proteins in barley seed extracts have shown that disulfide C144-C148 in BASI is reduced with high efficiency by h-type Trx, and that this disulfide is preferentially reduced compared to the other disulfide C43-C90 in BASI (Maeda et al., 2003; Maeda et al., 2004; Maeda et al., 2005). Here, the barley Trx h isoform 2 (HvTrxh2)-catalyzed disulfide reduction of BASI is used as a model system

to investigate structural requirements for recognition of a target protein disulfide bond by Trx. The crystal structure is solved for HvTrxh2-S-S-BASI, a trapped mixed disulfide that mimics the reaction intermediate of the reductase in complex with its target protein.

2.3 Results

2.3.1 Production of the HvTrxh2-S-S-BASI mixed disulfide

To form a kinetically stable complex mimicking the intermolecular mixed disulfide intermediate in the disulfide reductase reaction pathway of Trx (**Figure 2.1A**), a HvTrxh2 mutant of C_C (C49S) in the active site motif WC_NGPC_C and BASI mutants C144S and C148S from the target disulfide C144-C148 were used (**Figure 2.1B**). Briefly, the single cysteines $C148_{BASI}$ and $C144_{BASI}$ in C144S and C148S respectively, were conjugated to 2-nitro-5-thiobenzoate (TNB) and subsequently incubated with HvTrxh2 C49S to substitute TNB with $C46_{HvTrxh2}$ (**Figure 2.1B**). To determine whether $C144_{BASI}$ or $C148_{BASI}$ are accessible to nucleophilic attack from $C46_{HvTrxh2}$, the rate of the reaction was monitored spectrophotometrically by following the release of TNB (**Figure 2.1B**). The reaction progressed rapidly with C144S, whereas almost no substitution was observed for C148S (**Figure 2.2A**). The results suggest that essentially only $C148_{BASI}$ is accessible to $C46_{HvTrxh2}$. This is in agreement with the Sγ atom of $C148_{BASI}$ being surface-exposed and covering the Sγ atom of $C144_{BASI}$ in the crystal structure of BASI in complex with barley α-amylase 2 (AMY2/BASI) (PDB entry 1AVA; Vallée et al., 1998) (**Figure 2.2B**).

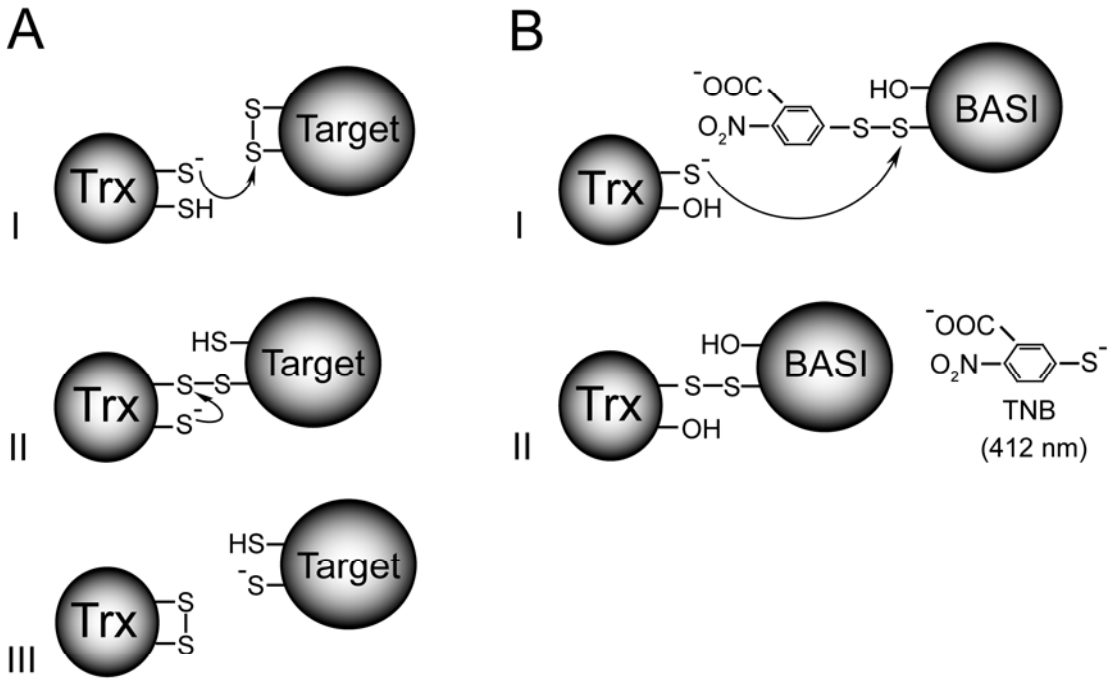

Figure 2.1 Mechanisms of Trx disulfide reductase activity and the strategy used here to form a kinetically stable mixed disulfide. (A) The N-terminal, exposed cysteine (C_N) in the Trx active motif $WC_NG(P)PC_C$ makes a nucleophilic attack on the target disulfide bond (I) to form an intermolecular mixed disulfide intermediate (II), which is subjected to intramolecular attack from the C-terminal, buried cysteine (C_C) to release the reduced target protein and oxidized Trx (III) (B) Activated disulfides formed by conjugation of TNB to single cysteines $C148_{BASI}$ and $C144_{BASI}$ in the BASI target disulfide mutants C144S and C148S are attacked by C_N (C46) in a HvTrxh2 mutant that lacks C_C (C49S) (I), to form stable mixed disulfides between BASI and HvTrxh2 (II). The reaction is monitored spectrophotometrically by following the release of TNB at 412 nm.

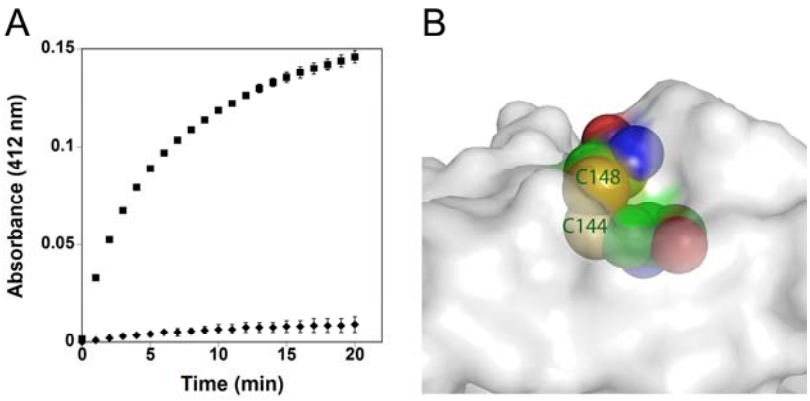

Figure 2.2 Accessibility of the cysteines in the BASI C144-C148 disulfide bond. (A) The time course of the reaction between C49S HvTrxh2 (11.9 μM) and TNB-conjugated C144S ■ (16.4 μM) and C148S BASI ♦ (16.4 μM) is monitored by the liberation of TNB at 412 nm. (B) Close-up view of the disulfide C144-C148 in the crystal structure of BASI in complex with barley α-amylase 2 (PDB entry 1AVA, molecule D; Vallée et al., 1998) showing that C148 Sγ is exposed and shields C144 Sγ. The exposed surface is shown in white except for C144 and C148. For C144 and C148, carbon, oxygen, nitrogen and sulfur atoms are shown as van der Waals spheres and colored green, red, blue and yellow, respectively.

According to the mechanism of bimolecular nucleophilic substitution, the thiolate anion of $C46_{HvTrxh2}$ must perform the nucleophilic attack on an Sγ atom of a disulfide from a direction 180° away from the other Sγ atom that acts as a leaving group. Thus, the relative accessibilities of the two Sγ atoms permit $C46_{HvTrxh2}$ to only attack on C148 of disulfide C144-C148 of BASI. $C148_{BASI}$ was therefore concluded to form an intermolecular disulfide bond in the Trx reaction intermediate, and the $C46_{HvTrxh2}$-$C148_{BASI}$ mixed disulfide (HvTrxh2-S-S-BASI) was prepared in large scale for crystallization.

2.3.2 Architecture of HvTrxh2-S-S-BASI

The final electron density map of HvTrxh2-S-S-BASI at 2.3 Å resolution (PDB entry 2IWT) unambiguously displays the covalent and non-covalent contacts between Trx and BASI in the single mixed-disulfide complex present in the asymmetric unit (**Figure 2.3A**). The structural model comprises residues 13 to 120 of HvTrxh2 (122 amino acids), while the 12 residue N-terminal segment is not visible in the final 1σ 2*Fo-Fc* electron density map, presumably due to high flexibility. Residues 59-64, 94-101 and 112-120 of HvTrxh2, located distant from the BASI interface, exhibit relatively high *B*-factors presumably due to the small number of contacts with symmetry related molecules (in total 214 for HvTrxh2 *versus* 818 for BASI). HvTrxh2 has the typical fold of Trx with a five-stranded β-sheet surrounded by four α-helices in a βαβαβββα topology. The overall structure of HvTrxh2 is representative for Trxs, as the Cα atoms can be superimposed on the crystal structures of oxidized Trxs from *Escherichia coli* (PDB entry 2TRX, molecule A; Katti et al., 1990), *Homo sapiens* (PDB entry 1ERU; Weichsel et al., 1996) and the green alga *C. reinhardtii* (h-type) (PDB entry 1EP7, molecule A; Menchise et al., 2001) with root-mean-square difference (rmsd) values of 0.9 Å, 1.1 Å and 0.8 Å, respectively (70, 86 and 102 Cα atoms are used, respectively). Major deviations are observed for residues at the most N- and C-terminal ends and around α1, which in HvTrxh2 (residues 20-32) is particularly extended in comparison to Trxs from *E. coli* (residues 12-15, molecule A) or *H. sapiens* (residues 8-17). The β-trefoil topology of BASI could be traced in the structure except for an alanine residue at the C-terminus. The global structure of the BASI mutant in HvTrxh2-S-S-BASI is superimposable on the wild-type in AMY2/BASI (molecule D) with rmsd of 0.5 Å using 161 Cα atoms (PDB entry 1AVA; Vallée et al., 1998). The intermolecular disulfide bond is as expected formed between $C46_{HvTrxh2}$ and $C148_{BASI}$.

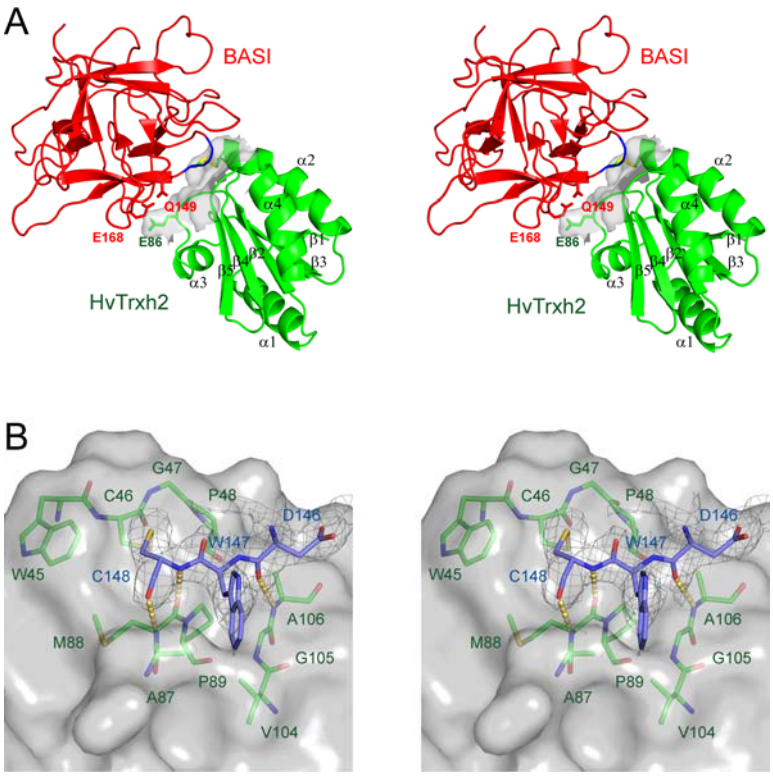

Figure 2.3 The crystal structure of HvTrxh2-S-S-BASI. (A) Stereo view of the overall structure of HvTrxh2-S-S-BASI in cartoon display. HvTrxh2 and BASI are colored green and red, respectively. Secondary structure elements in HvTrxh2 are labeled. The segment $_{146}$DWC$_{148}$ in BASI is blue. The side chains of the disulfide bound C46$_{HvTrxh2}$ and C148$_{BASI}$, and the residues Q149$_{BASI}$, E168$_{BASI}$ and E86$_{HvTrxh2}$ are shown in stick representation. Q149$_{BASI}$ and E168$_{BASI}$ are colored and labeled in red and E86$_{HvTrxh2}$ in green. In C46$_{HvTrxh2}$ and C148$_{BASI}$, the carbon and sulfur atoms are colored green and yellow, respectively. The solvent accessible surface is shown in transparent grey for the residues of HvTrxh2 that are in contact with BASI. (B) Close up stereo view of the interaction between HvTrxh2 and BASI. The solvent accessible surface of HvTrxh2 is colored grey and shown transparent. Segment $_{146}$DWC$_{148}$ of BASI and the substrate recognition loop motif composed of $_{45}$WCGP$_{48}$, $_{87}$AMP$_{89}$ and $_{104}$VGA$_{106}$ of HvTrxh2 are shown in stick representation. Oxygen, nitrogen and sulfur are in red, blue and yellow, respectively. Carbon atoms are in green and blue for HvTrxh2 and BASI, respectively. Intermolecular hydrogen bonds are shown as dashed yellow lines. The 2*Fo-Fc* electron density map is presented as a dark grey isosurface-mesh at the 1.0σ level to a distance of 1.0 Å from $_{146}$DWC$_{148}$ of BASI. Labels on residues from BASI and HvTrxh2 are in blue and green, respectively.

Neither of the bonded cysteines are in a strained conformation as the $\chi 1$ angle of $C46_{HvTrxh2}$ is 175º, close to the values reported in reduced Trxs from other species, *e.g.* human Trx ($\chi 1$=192º, C32) (PDB entry 1ERT; Weichsel et al., 1996), while the $\chi 1$ angle of $C148_{BASI}$ is -60º and comparable to that of C148 from the intact disulfide in wild-type BASI (PDB entry 1AVA; Vallée et al., 1998) ($\chi 1$=-71º in molecule C and $\chi 1$=-64º in molecule D). The intermolecular disulfide bond displays an architecture common to right-handed disulfide bonds (Petersen et al., 1999) with dihedral angles defined by $C\alpha_i$-$C\beta_i$-$S\gamma_i$-$S\gamma_j$, $C\alpha_j$-$C\beta_j$-$S\gamma_j$-$S\gamma_i$ and $C\beta_i$-$S\gamma_i$-$S\gamma_j$-$C\beta_j$ (i=$C46_{HvTrxh2}$ and j=$C148_{BASI}$) of 71º, 112º and 95º, respectively.

2.3.3 The protein-protein interface of HvTrxh2-S-S-BASI

In total, 762 $Å^2$ of accessible surface area is buried in the protein interface of HvTrxh2-S-S-BASI. This value is smaller than the reported average interface area of 1906 $Å^2$ in 70 assemblies of proteins or the interface area of 1140 $Å^2$ in a well-characterized example of an electron transfer complex between cytochrome c peroxidase and cytochrome c (Pelletier and Kraut, 1992; Chakrabarti and Janin, 2002). The structure of HvTrxh2-S-S-BASI shows that BASI is recognized by HvTrxh2 primarily through $C148_{BASI}$ and two immediately preceding residues. This $_{146}DWC_{148}$ segment is stabilized by a spatially defined motif on the HvTrxh2 surface composed of $_{45}WCGP_{48}$, $_{87}AMP_{89}$ and $_{104}VGA_{106}$ (referred to in the following as the substrate recognition loop motif) from three neighboring loops between $\beta 2$-$\alpha 2$, $\alpha 3$-$\beta 4$ and $\beta 5$-$\alpha 4$ and the adjacent $\alpha 2$ and $\beta 5$, all belonging to the core of the Trx-fold (**Figures 2.3A, B**). The substrate recognition loop motif constitutes a hydrophobic groove along which the backbone atoms of $_{146}DWC_{148}$ from BASI are positioned and form van der Waals interactions and backbone-backbone hydrogen bonds (**Figure 2.3B**). Although the conserved *cis* proline,

$P89_{HvTrxh2}$, is buried and has no direct contact with BASI, it plays an essential structural role in this protein-protein interaction. The conformation of the *cis* peptide bond determines the direction of the main chain at the N-terminus of β4. Thereby the backbone amino and carbonyl groups of the adjacent $M88_{HvTrxh2}$ are exposed on the surface, where they make two intermolecular backbone-backbone hydrogen bonds in an anti-parallel fashion to $C148_{BASI}$ (**Figure 2.3B**). In an adjacent loop between β5-α4, the backbone amino group of $A106_{HvTrxh2}$ stabilizes the backbone carbonyl group of $D146_{BASI}$ through a hydrogen bond. The side chain of $P48_{HvTrxh2}$ in the conserved active site sequence motif, WCGPC, further stabilizes the main chain of BASI by van der Waals contacts to five backbone atoms of $D146_{BASI}$ and $W147_{BASI}$. The indole ring of $W147_{BASI}$ is accommodated between the two segments $_{87}AMP_{89}$ and $_{104}VGA_{106}$ of HvTrxh2 and makes hydrophobic interactions with the side chains of $A87_{HvTrxh2}$ and $V104_{HvTrxh2}$ (**Figure 2.3B**). Finally, the side chain of $C148_{BASI}$ fits in a shallow groove between the hydrophobic side chains of $W45_{HvTrxh2}$ and $P48_{HvTrxh2}$. In addition to the segment $_{146}DWC_{148}$, $E168_{BASI}$ and $Q149_{BASI}$ make van der Waals interactions with $E86_{HvTrxh2}$ (**Figure 2.3A**).

2.3.4 Conservation of the substrate recognition loop motif among Trx-fold proteins

The coordinates of the main chain atoms of $_{45}WCGP_{48}$, $_{87}AMP_{89}$ and $_{104}VGA_{106}$ from HvTrxh2 that constitute the substrate recognition loop motif, interacting with $_{146}DWC_{148}$ of BASI were used to search for similar motifs in the existing PDB entries using the SPASM server (http://portray.bmc.uu.se/cgi-bin/spasm/scripts/spasm.pl; Kleywegt, 1999). The result shows that the main chain structure and a major part of the sequence in this motif is conserved among Trxs from diverse species (**Table 2.1**; maximum rmsd set to 1.0 Å for the initial search). For example, the corresponding

motifs in Trxs from *H. sapiens* (PDB entry 1ERT, reduced form) and *E. coli* (PDB entry 2TRX, oxidized form) are superimposed on that of HvTrxh2 with rmsd values of 0.39 Å and 0.48 Å, respectively. Motifs with highly similar main chain structures are also identified in PDIs from *E. coli* (DsbC, PDB entry 1EEJ; DsbG, PDB entry 1V58) that catalyze formation and isomerization of disulfides in proteins, and in glutathione transferases (GSTs) of classes delta (PDB entries 1V2A and 1R5A), kappa (PDB entries 1R4W and 1YZX) and tau (PDB entry 1GWC) that catalyze transfer of the cysteine thiol group in glutathione (**Table 2.1**). The other matched proteins have various functions, overall structures and sequences – nevertheless they all contain the Trx-fold (**Table 2.1**). The conservation of the substrate recognition loop motif in these proteins might therefore only reflect the conserved domain structure. To test this, the conservation of the overall Trx-fold in the identified proteins was examined by searching in the SPASM server using spatially defined fingerprint motifs from secondary structure elements in the Trx-fold of HvTrxh2. The fingerprint motifs β2α2α3, β2α3α4 and β2α2α4 were formed by combining the main chain atoms of segments 38-41 (β2), 53-55 (α2), 78-80 (α3) and 112-114 (α4). A majority of the Trxs that matched the substrate recognition loop motif also superimposed well with the fingerprint motifs from HvTrxh2, whereas most other Trx-fold proteins were either not identified or superimposed poorly with the fingerprint motifs (**Table 2.1**). Thus, the spatially-defined substrate recognition loop motif of HvTrxh2 is more conserved than the overall Trx-fold, supporting its functional significance proposed here.

Table 2.1. Proteins with motifs superimposable to the substrate recognition loop motif in HvTrxh2 identified using the SPASM server

PDB	Protein	Sequence	rmsd[b] (Å)			
		WCGP-AMP-VGA[a]	Loop motif[c]	β2α2α3[d]	β2α3α4[d]	β2α2α4[d]
	Trxs					
1ERT	*H. sapiens*	WCGP-CMP-SGA	0.39	0.64	0.56	0.81
1XWA	*Drosophila melanogaster*	WCGP-SMP-AGA	0.40	0.56	0.57	0.62
2CVK	*Thermus thermophilus*	WCAP-SIP-VGA	0.45	0.41	0.78	-
1SYR	*Plasmodium falciparum*	WCGP-SMP-LGA	0.46	0.59	0.55	0.67
1EP7	*C. reinhardtii*	WCGP-AMP-VGA	0.47	0.63	0.60	0.60
1R26	*Trypanosoma brucei brucei*	WCGP-QLP-IGA	0.47	-	0.60	-
1T00	*Streptomyces coelicolor*	WCGP-SIP-VGA	0.47	0.52	0.85	0.91
2TRX	*E. coli*	WCGP-GIP-VGA	0.48	0.52	0.93	-
1V98	*Thermus thermophilus*	WCGP-SVP-VGA	0.55	0.55	0.92	0.98
1FB6	*Spinacia oleracea*	WCGP-SIP-IGA	0.59	0.42	0.88	-
2F51	*Trichomonas vaginalis*	WCGP-SIP-VGA	0.60	1.22	1.04	-
1THX	*Anabaena sp.*	WCGP-GVP-EGV	0.67	0.48	0.92	-
1W4V	*H. sapiens*	WCGP-AVP-VGI	0.69	-	-	-
1DBY	*C. reinhardtii*	WCGP-SIP-IGA	0.78	0.62	-	0.95
	GSTs					
1R4W	Class kappa, *Rattus norvegicus*	LSPY-GLP-FGS	0.40	-	-	-
1YZX	Class kappa, *H. sapiens*	LSPY-GLP-FGS	0.45	-	-	-
1V2A	Class delta, *Anopheles dirus*	ISPP-TIP-WES	0.78	-	-	-
1GWC	Class tau, *Aegilops tauschii*	PSPF-KIP-CES	0.82	-	-	-
1R5A	Class delta, *Anopheles dirus*	ASPP-CIP-WES	0.87	-	-	-
	PDIs					
1EEJ	DsbC, *E. coli*	TCGY-GTP-PGY	0.65	-	1.27	-
1V58	DsbG, *E. coli*	FCPY-VTP-VGL	0.76	-	-	-
	Other proteins					
1ST9	Cytochrome c biosynthesis protein	WCEP-PLP-TGT	0.43	0.85	-	-
1J08	Glutaredoxin-like protein	TCPY-AVP-EGA	0.46	-	0.97	-
1GH2	Trx-like protein	GCGP-ATP-QGA	0.50	0.50	0.51	0.63
1VRS	Electron transfer protein DsbD	WCVA-GLP-TGF	0.52	-	-	-
1HYU	Alkyl hydroperoxide reductase	SCHN-GVP-QGR	0.66	-	-	-
1JFU	Trx-like protein	WCVP-GMP-AGP	0.67	0.84	-	-
1A8L	Protein disulfide oxidoreductase	TCPY-AVP-EGA	0.78	-	1.00	-
1Z3E	Transcriptional regulator	SCTS-RRP-VGY	0.80	-	-	-
1G7O	Glutaredoxin-2	HCPY-QVP-PES	0.84	-	-	-
1RW1	Hypothetical protein	ACDT-KRP-VGF	0.91	-	-	-
1Z6N	Hypothetical protein	WCPD-AIP-VER	1.11	-	-	-

[a]Sequence of the three segments constituting the substrate recognition loop motif of HvTrxh2. [b]Rmsd values for the superimposition of 40 matched main chain atoms. [c]Main chain atoms for the substrate recognition loop motif of HvTrxh2 constituted of residues 45-48, 87-89 and 104-106 used as a search model. [d]Coordinates for the main chain atoms of residues in secondary structure elements β2 (residues 38-41), α2 (residues 53-55), α3 (residues 78-80) and α4 (residues 112-114) constituted finger print motifs β2α2α3, β2α3α4 and β2α2α4, used as search models to track fold conservation. Proteins not identified using the finger print motifs are marked -.

2.3.5 Comparison with the glutathione recognition mechanisms of GST and Grx

The motif comprised of residues $_{15}$LSPY$_{18}$, $_{182}$GLP$_{184}$ and $_{198}$FGS$_{200}$ in rat mitochondrial class kappa GST (PDB entry 1R4W; Ladner et al., 2004) superimposed with the substrate recognition loop motif of HvTrxh2 (**Table 2.1**). This motif plays a central part in the interaction with the substrate glutathione (Ladner et al., 2004). Visual inspection of the aligned structural motifs reveals remarkable similarities as well as differences in the interactions that stabilize their respective substrate complexes (**Figure 2.4A**; aligned using Cα atoms only). Segment $_{182}$GLP$_{184}$ in rat class kappa GST has a function analogous to the structural counterpart $_{87}$AMP$_{89}$ of HvTrxh2. It binds the cysteine residue of glutathione through backbone-backbone hydrogen bonds from the residue preceding a *cis* proline in an anti-parallel fashion. The cysteine thiol group of glutathione is thereby situated at the catalytic hydroxyl group of S16 in GST (Ladner et al., 2004), superimposed on C46 in HvTrxh2 in the alignment. Segment $_{198}$FGS$_{200}$ in rat class kappa GST involved in the specific recognition of glutathione corresponds to $_{104}$VGA$_{106}$ of HvTrxh2. The side chain and the backbone amino group of the conserved serine (S200, superimposed on A106$_{HvTrxh2}$) in this segment form hydrogen bonds to the γ-glutamate group of glutathione (**Figure 2.4A**). The search in the SPASM server using the substrate recognition loop motif of HvTrxh2 only identified a single Grx, Grx-2 from *E. coli* with an unusual C-terminal helical domain and overall structural similarity to mammalian GST (Xia et al., 2001) (**Table 2.1**). The absence of typical Grxs with a βαβαββα topology among the matched structures reveals that the region corresponding to the substrate recognition loop motif of HvTrxh2 differs in typical Grxs in spite of the high functional and structural similarity to Trx (Eklund et al., 1984). The substrate recognition loop motif of HvTrxh2 is aligned with the motif comprised of residues

$_{36}$SCSY$_{39}$, $_{80}$TVP$_{82}$ and $_{92}$GGA$_{94}$ from the crystal structure of human Grx in complex with glutathione (**Figure 2.4B**; PDB entry 2FLS).

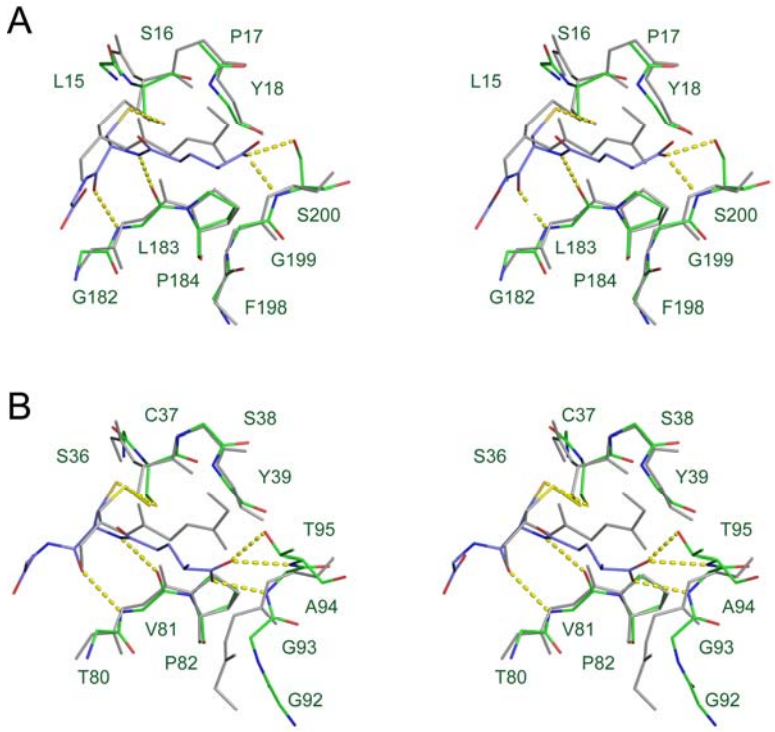

Figure 2.4 Comparison with the glutathione recognition mechanisms of GST and Grx. Stereo views showing the alignment of Cα atoms in the substrate recognition loop motif of HvTrxh2 composed of $_{45}$WCGP$_{48}$, $_{87}$AMP$_{89}$ and $_{104}$VGA$_{106}$ with Cα atoms in (A) residues $_{15}$LSPY$_{18}$, $_{182}$GLP$_{184}$ and $_{198}$FGS$_{200}$ of rat mitochondrial GST (PDB entry 1R4W; Ladner et al., 2004) and (B) residues $_{36}$SCSY$_{39}$, $_{80}$TVP$_{82}$ and $_{92}$GGA$_{94}$ of human Grx (PDB entry 2FLS) in complex with glutathione. HvTrxh2 and $_{146}$DWC$_{148}$ of BASI are in grey except for the cysteine Sγ atoms in yellow. For GST and Grx, carbon, oxygen, nitrogen and sulfur atoms are colored green, red, blue and yellow, respectively. Side chains are not shown except for glutathione, *cis* proline and the catalytic cysteine and serine residues. For rat GST (A), the side chain of S200 is also shown. For human Grx (B), the main chain and the side chain of T95 is also shown. Intermolecular hydrogen bonds are shown as dashed yellow lines.

The main chain Cα atoms of segments $_{36}$SCSY$_{39}$ and $_{80}$TVP$_{82}$ of human Grx superimpose well on the corresponding segments $_{45}$WCGP$_{48}$ and $_{87}$AMP$_{89}$ from HvTrxh2 and stabilize the substrate cysteine residue in a the same manner as observed in rat mitochondrial class kappa GST and in HvTrxh2-S-S-BASI (**Figures 2.4A, B**). In contrast, the position and orientation of the main chain Cα atoms of segment $_{92}$GGA$_{94}$ in human Grx and the corresponding segment $_{104}$VGA$_{106}$ in HvTrxh2 clearly diverge. Whereas segment $_{104}$VGA$_{106}$ constitutes a section of the elongated substrate binding groove in HvTrxh2 (**Figure 2.3B**), segment $_{92}$GGA$_{94}$ and the side chain of the succeeding residue T95 block the corresponding groove section in human Grx and form hydrogen bonds with the γ-glutamate group of glutathione (**Figure 2.4B**). Moreover, whereas A106$_{HvTrxh2}$ and D146$_{BASI}$ are in an antiparallel-like orientation appropriate for backbone-backbone hydrogen bond formation (**Figure 2.3B**), the main chain of A94 in human Grx is oriented almost perpendicularly to the substrate binding surface (**Figure 2.4B**).

2.4 Discussion

The involvement of protein-protein interactions in the disulfide reductase activity of Trx towards a broad range of protein substrates has been the subject of extensive discussions (Holmgren, 1984; Meyer et al., 2002a; Buchanan and Balmer, 2005). In the present study, van der Waals contacts and three intermolecular backbone-backbone hydrogen bonds involving a structural motif created by the $_{45}$WCGP$_{48}$, $_{87}$AMP$_{89}$ and $_{104}$VGA$_{106}$ loops of HvTrxh2 are shown to stabilize the HvTrxh2-S-S-BASI reaction intermediate. HvTrxh2-S-S-BASI has a small interface area and differs largely in the overall interaction features from the two NMR structures of Trx-peptide mixed disulfides, in which at least nine residues of the 13 residues long synthetic peptides interact with

extended surface areas of human Trx (Qin et al., 1995; Qin et al., 1996). The larger number of residues involved in these Trx-peptide interactions most likely reflects the higher conformational freedom of a short peptide compared to a folded protein. Nevertheless, the intermolecular hydrogen bonding pattern observed in the present study is in accordance with the NMR structure of human Trx in complex with a peptide from Ref-1 (Qin et al., 1996). Moreover, a pattern of intermolecular backbone-backbone hydrogen bonds, essentially identical to that in HvTrxh2-S-S-BASI, is also observed in the crystal structure of a mixed disulfide protein-protein complex between the N- and C-terminal domains of the electron transfer protein DsbD from *E. coli* (PDB entry 1VRS; Rozhkova et al., 2004; included in **Table 2.1**). The C-terminal domain of DsbD displays disulfide reductase activity, and is structurally similar to Trx with a βαβααβαβαβα topology and an active site sequence motif WCVAC. We postulate that the mode of interaction observed in HvTrxh2-S-S-BASI is a general feature of Trx-target protein complexes since the essential parts of the identified substrate recognition loop motif are conserved among Trxs from different species. In the NMR structure of human Trx in complex with a peptide from NF-κB, the parts of Trx forming intermolecular backbone-backbone hydrogen bonds agree with the present study, but the direction of the bound peptide is reversed (Qin et al., 1995), suggesting that multiple patterns of Trx-target interactions may exist.

The conserved *cis* proline is present in various Trx-fold proteins (Martin, 1995) and structural studies have suggested its importance for peptide binding in Trx (Qin et al., 1995; Qin et al., 1996) and glutathione binding in Grx (Nordstrand et al., 1999) and in GST (Reinemer et al., 1991). In addition, the functional importance of the *cis* proline for Grx, GST and DsbA activity has been demonstrated by site-directed mutagenesis (Nikkola et al., 1991; Charbonnier et al, 1999; Nathaniel et al., 2003; Kadokura et al.,

2004). The residue preceding the *cis* proline P89 in HvTrxh2 is shown here for the first time to stabilize the target cysteine residue of an intact target protein, supporting that this *cis* peptide bond is also important in Trx for correct positioning of the disulfide from the substrate at the catalytic site. On the other hand, the $_{104}$VGA$_{106}$ segment of the substrate recognition loop motif from HvTrxh2 is shown here to contribute to the unique specificity of Trx. Accordingly, conserved polar and charged residues at the corresponding segments in structures of the diverse classes of GSTs are found to be crucial for the interactions with glutathione (reviewed in Oakley, 2005). The absence of polar or charged residues in Trxs at positions corresponding to $_{104}$VGA$_{106}$ in HvTrxh2 most likely impairs glutathione recognition. An NMR study of an *E. coli* Grx-glutathione mixed disulfide has suggested that Trx with its hydrophobic active site surface is deficient in groups that complement the charged and polar groups of glutathione (Nordstrand et al., 1999). The present study, however, emphasizes the genuine structure-based specificity of Trx that cannot solely be explained by this inability to match with glutathione. The structurally conserved segment $_{104}$VGA$_{106}$ of HvTrxh2 creates a hydrophobic and elongated groove that specifically interacts with a continuous peptide chain from a protein substrate. In contrast, this part of the Grx structure has an alternative main chain conformation and seems to be inappropriate for the recognition of protein substrates.

Trx also shares the redox active sequence motif CXXC and the *cis* proline with prokaryotic Trx-fold proteins DsbA, DsbC and DsbG, responsible for the formation of correct disulfide bonds in periplasmic proteins (reviewed in Kadokura et al., 2003). However, in the structures of DsbC and DsbG from *E. coli* (both included in Table 2.1; McCarthy et al., 2000; Heras et al., 2004) tyrosine and leucine residues, respectively, substitute A106 of HvTrxh2. In *E. coli* DsbA, conserved uncharged and hydrophobic

residues present around the loop corresponding to β5-α4 (residues 105-107) of HvTrxh2 are proposed to participate in interactions with unfolded and misfolded protein substrates (Guddat et al., 1997).

The small interface area that HvTrxh2 forms with a target protein in HvTrxh2-S-S-BASI could account for the broad specificity of Trx towards protein disulfides. The interactions observed in HvTrxh2-S-S-BASI also provide, however, a structural basis to explain protein substrate discrimination by Trx. One of the cysteines in a target protein disulfide should ideally fulfill three structural criteria for optimal interaction with Trx: (1) The backbone amino and carbonyl groups of the cysteine residue, and the carbonyl group of the residue positioned two residues towards the N-terminus, should be solvent-exposed and free of intramolecular contacts (such as backbone-backbone hydrogen bond arrangements in secondary structure elements), to allow the formation of backbone-backbone hydrogen bonds with Trx. (2) The peptide chain between the cysteine and the other residue forming intermolecular hydrogen bonds to Trx should have an extended main chain conformation without a turn or a bend to allow the best fit into the substrate binding groove in Trx. (3) The Sγ atom of the cysteine residue must be solvent-exposed in order to receive the nucleophilic attack from C_N in Trx. There are only a few well-established Trx target proteins for which 3D structures have been solved and the redox active disulfide bond has been identified. Nevertheless, visual inspection of the structures shows that the proposed three criteria are fulfilled for the redox active intramolecular disulfide of oxidized *E. coli* 2-Cys peroxiredoxin (PDB entry 1QXH; Choi et al., 2003), the redox active intermolecular disulfide formed between subunits of rat 2-Cys peroxiredoxin in a homodimer (PDB entry 1QQ2; Hirotsu et al., 1999) and for the C-terminal regulatory disulfide in the oxidized sorghum malate dehydrogenase (PDB entry 7MDH; Johansson et al., 1999). Insulin is widely

used as a substrate to assay Trx activity (Holmgren, 1979b). C7 in chain B of insulin (involved in one of the two interchain disulfides) fulfills all the proposed criteria except that the backbone amino group of H10 in the subsequent α-helical region donates a hydrogen bond to the solvent-exposed carbonyl group of C7 (PDB entry 1APH; Gursky et al., 1992). Also in support of these propositions, a disulfide bond in a mutant of green fluorescent protein that connects two β-strands in the β-barrel structure is susceptible to reduction by reduced glutathione but not by Trx (Østergaard et al., 2001), presumably because the backbone atoms are unavailable for hydrogen bonding to Trx and thus criterion (1) is not fulfilled. In addition to the proposed criteria, the van der Waals interactions with $W147_{BASI}$ observed in HvTrxh2-S-S-BASI indicate that a hydrophobic side chain at this position interacting with A87 and V104 may promote the recognition. This is in agreement with our previous observation that hydrophobic residues are overrepresented in the sequences adjacent to the disulfides in barley seed proteins efficiently reduced by barley Trx h (Maeda et al., 2005). A87 and V104 of HvTrxh2, however, are not conserved among Trxs; these positions are occupied respectively by cysteine and serine in human Trx (PDB entry 1ERT) and by glycine and valine in *E. coli* Trx (PDB entry 2TRX). Thus, amino acid residues at these positions may contribute to the variation in target specificity among Trxs.

The surface charge distribution patterns also differ greatly among the Trx structures reported so far. Even though no charge-charge interactions are observed in HvTrxh2-S-S-BASI, the Trx-target interaction suggests that charge distribution could affect the specificity of Trxs by favoring or disfavoring Trx-target complex formation. In HvTrxh2-S-S-BASI, $E86_{HvTrxh2}$ is within van der Waals distance from $E168_{BASI}$ (**Figure 2.3A**) and one may speculate that substitution by a basic amino acid would favor complex formation. In the crystal structures of the oxidized form of pea

chloroplastic fructose-1,6-bisphosphatase (PDB entries 1DCU and 1D9Q; Chiadmi et al., 1999), C173 in the regulatory disulfide C153-C173 has a solvent-exposed Sγ-atom with exposed backbone amino and carbonyl groups, but is situated in an α-helix and thus does not fulfill criteria (1) and (2) for target disulfide bonds of Trx proposed here. Indeed, most Trxs poorly reduce plant fructose-1,6-bisphosphatase (Meyer et al., 2002a). On the other hand, chloroplastic f-type Trx, which uniquely possesses several surface-exposed basic residues at positions surrounding the substrate recognition loop motif defined in the present work, interacts with a cluster of acidic residues in fructose-1,6-bisphosphatase and efficiently reduces this disulfide bond (de Lamotte-Guery et al., 1991; Geck et al., 1996; Mora-García et al., 1998).

In conclusion, the present study reveals for the first time that structural features around disulfides in proteins are recognized by Trx. This insight is of great importance for understanding the target specificity of Trx. An array of proteomics techniques developed in recent years has been applied for identification of Trx target proteins (Verdoucq et al., 1999; Yano et al., 2001; Maeda et al., 2004), and Trx target disulfide bonds (Maeda et al., 2005). The structural information provided here can be applied for validation of identified target disulfides and prediction of novel redox regulatory pathways. Finally, the detailed knowledge about the structure/function relationship of Trx obtained here opens possibilities for manipulation of protein-protein interactions involving Trx and contributes to the characterization of the numerous other Trx-fold proteins with unresolved functions and specificities.

2.5 Experimental Procedures

2.5.1 Construction of mutants

Mutagenesis was performed using the QuikChange® Site-Directed Mutagenesis Kit (Stratagene, La Jolla, CA, USA). The genes encoding HvTrxh2 inserted into plasmid pET15b (contains a plasmid-encoded thrombin-cleavable N-terminal His-tag) and His-tagged BASI (Bønsager et al., 2003) inserted into plasmid pET11a were used as templates. The following primers were used for mutagenesis; HvTrxh2 mutant C49S: 5'-TGCATCATGGTGCGGACCATCGAGAATCATGGCTCCAGTTTTCG-3' and 5'-CGAAAACTGGAGCCATGATTCTCGATGGTCCGCACCATGATGCA-3', BASI mutant C144S: 5'-GTACAAGCTGATGTCCTCAGGGGACTGGTGCCAGG-3' and 5'-CCTGGCACCAGTCCCCTGAGGACATCAGCTTGTAC-3', BASI mutant C148S: 5'-GCGGGGACTGGTCTCAGGACCTCGGCG-3' and 5'-CGCCGAGGTCCTGAG-ACCAGTCCCCGC-3'. The PCR products were treated with *Dpn*I (Invitrogen, San Diego, CA, USA) to hydrolyze the template plasmid, and transformed into *Escherichia coli* DH5α. All mutations were confirmed by DNA sequencing at MWG Biotech (Ebersberg, Germany).

2.5.2 Protein expression and purification

His-tagged C49S HvTrxh2 mutant was expressed in *E. coli* Rosetta cells at 37°C for 3 h after induction with 100 μM isopropyl β-D-1-thiogalactopyranoside (IPTG). His-tagged BASI mutants C144S and C148S were expressed as described previously for wild-type BASI with minor modifications (Bønsager et al., 2003). Proteins were extracted with Bugbuster® Protein Extraction Reagent including Benzonase Nuclease (Novagen) and the supernatants were applied onto His-Trap HP columns (Amersham Biosciences) pre-equilibrated with loading buffer (10 mM imidazole, 500 mM NaCl, 30 mM Tris/HCl pH

8.0), and eluted in a gradient of 10-200 mM imidazole. Fractions containing C49S HvTrxh2 were dialyzed against 30 mM Tris pH 8.0. For thiol-conjugation to TNB, the fractions containing BASI mutants C144S and C148S were incubated with an excess of 5,5'-dithiobis(2-nitrobenzoic acid) (DTNB) for 1 h at RT. TNB-conjugated BASI mutants were purified using HiLoad™ 16/60 Superdex™ 75 prep grade gel filtration column (Amersham Biosciences) equilibrated with 30 mM Tris pH 8.0. TNB-conjugation of the BASI mutants C144S and C148S was confirmed by adding DTT (10 mM) and quantifying the released TNB spectrophotometrically at 412 nm. Protein concentrations were deduced by aid of amino acid analysis.

2.5.3 Trx-complex formation

Analytical scale formation of mixed disulfides between TNB-conjugated C144S or C148S BASI mutants (11.9 μM) and C49S HvTrxh2 (16.4 μM) in a reaction volume of 126 μl was monitored spectrophotometrically at 412 nm by the release of TNB. For production in preparative scale of HvTrxh2-S-S-BASI, C49S HvTrxh2 (44.7 μM) was incubated with TNB-conjugated C144S BASI (32.5 μM) in a reaction volume of 15 ml for 1 h at RT and purified using HiLoad™ 26/60 Superdex™ 75 prep grade gel filtration column (Amersham Biosciences) equilibrated with 50 mM ammonium acetate pH 6.0, 200 mM NaCl. Fractions containing HvTrxh2-S-S-BASI were treated with immobilized thrombin (Calbiochem) in a 1:100 enzyme:substrate molar ratio for approximately 40 h to remove the N-terminal His-Tag from C49S HvTrxh2. Subsequently, HvTrxh2-S-S-BASI was purified on a His-Trap HP column as described above.

2.5.4 Crystallization and X-ray crystallography

HvTrxh2-S-S-BASI was dialyzed against 10 mM ammonium acetate pH 6.0 and concentrated to 8 $mg \cdot ml^{-1}$ using Centricon 10 (Millipore) filter units. Crystals of HvTrxh2-S-S-BASI were obtained using the hanging drop vapor diffusion method at room temperature with 2 μl each of protein solution and a reservoir solution containing 0.1 M citric acid pH 5.0, 12 (w/v)% polyethylene glycol (PEG) 6000. All attempts to cryo-protect the crystals by soaking in cryo- protectants resulted in loss of resolution and the crystals suffered from radiation damage when data was collected at room temperature. The best data (present study) was obtained by flash freezing the crystals directly from the crystallization drop. Diffraction data were collected on a Rigaku RU-H3RHB rotating Cu anode X-ray generator equipped with an R-AXIS IV++ imaging plate detector, a 700 series Cryostream cooler from Oxford Cryosystems operated at –160 °C and MSC/Confocal Max-Flux mirrors. Reflections were indexed, integrated and scaled with MOSFLM (Leslie, 1994) and SCALA (Kabsch, 1988). A high Wilson *B*-factor (48.3 $Å^2$) is presumably due to the relatively high crystal mosaicity (estimated to 0.6-0.8° in MOSFLM) and incomplete cryo-protection of the crystal. A minor ice-ring at ~3.7 Å is observed in collected diffraction data. The crystal structures of AMY2/BASI (Vallée et al., 1998) and the oxidized HvTrxh2 (Maeda et al., unpublished data) were used as search models for molecular replacement (MR) of HvTrxh2-S-S-BASI in Molrep (Vagin and Teplyakov, 1997). The refinement was carried out with the program CNS (Brünger et al., 1998). Using the simulated annealing protocol against the MLF target function, individual, but restrained *B*-factors were refined after building the protein model. The xray/geometry weight was optimized by the automated CNS procedure. A non-uniform electron density quality with quite poor electron density contrast in some parts of the Trx molecule probably made the assignment of one overall

xray/geometry weight insufficient. To solve this problem by using a less restricted *B*-factor refinement was judged inappropriate bearing the intermediate resolution of the data (2.3 Å) in mind. Water molecules and ions were added in the graphic program Coot (Emsley and Cowtan, 2004), also used for manual model rebuilding. The geometries of the refined structure were checked with PROCHECK (Laskowski et al., 1993). The resultant Ramachandran plot has a relative low (compared to better than 2Å resolution structures with *R*-factors < 20%) proportion of residues in the most favored areas of the plot, but 99.6% of residues are within the allowed regions and none in the disallowed regions. The coordinates and the structure factors of HvTrxh2-S-S-BASI have been deposited with PDB accession code 2IWT. The protein-protein interface in HvTrxh2-S-S-BASI was analyzed using AREAIMOL (Lee and Richards, 1971) and NCONT (Collaborative Computational Project, Number 4, 1994). The numbers of contacts HvTrxh2 and BASI make with symmetry related atoms were determined by CONTACT (Collaborative Computational Project, Number 4, 1994) with cut-off distance of 5.0 Å. Figures of protein structures were made in Pymol (http://pymol.sourceforge.net/; DeLano, 2002). The statistics are listed in **Table 2.2**.

2.5.5 Search for structural motifs in PDB entries

The searches were performed in the SPASM server (http://portray.bmc.uu.se/cgi-bin/spasm/scripts/spasm.pl; Kleywegt, 1999) with standard settings except that Cα-atoms and main chain atoms only were used for the first and finer screenings, respectively. The minimum number of matched atom was set to 40 and maximum superimposing rmsd was set to 1 Å (when the substrate recognition loop motif was used as a template) and 1.3 Å (when the finger print motifs were used as templates). Matched PDB entries of mutant proteins were excluded from **Table 2.1** except for 1VRS. The

substrate recognition loop motif was constituted of residues 45-48, 87-89 and 104-106 of HvTrxh2. Residues 38-41, 53-55, 78-80 and 112-114 situated in the central parts of β2, α2, α3 and α4, respectively, were combined to constitute finger print motifs β2α2α3, β2α3α4 and β2α2α4.

Table 2.2 Crystallographic data and refinement statistics

	HvTrxh2-S-S-BASI
Data collection	
Space group	$P\,4_12_12$
Cell dimensions	
a, *b*, *c* (Å)	76.1, 76.1, 129.4
Resolution (Å)	65.7–2.3
R_{sym}	0.079 (0.429)[a]
$I / \sigma I$	6.6 (1.7)[a]
Completeness (%)	99.3 (99.7)[a]
Redundancy	4.4 (4.6)[a]
Wilson *B*-factor (Å^2)	48.3
Refinement	
Resolution (Å)	24.9–2.3
No. reflections	17,377
R_{work} / R_{free}	22.4 (32.5)[b] / 26.4 (38.0)[b]
No. atoms	
HvTrxh2	841
BASI	1401
Ligand/ion	26
Water	125
B-factors (Å^2)	
HvTrxh2	59.7
BASI	43.0
Ligand/ion	57.5
Water	45.4
Rmsd	
Bond lengths (Å)	0.009
Bond angles (°)	1.4
Ramachandran plot regions	
Most favored	86.5
Additional allowed	13.1
Generously allowed	0.4
Disallowed	0.0

[a]Highest-resolution data shell 2.4–2.3. [b]Highest-resolution data shell 2.4–2.3.

Chapter 3

Crystal structures of two barley thioredoxin h isoforms reveal features involved in protein recognition and possibly discriminating the isoform specificity

3.1 Summary

H-type thioredoxins (Trxs) constitute a particularly large Trx sub-group in higher plants. The crystal structures of the two barley Trx h isoforms HvTrxh1 and HvTrxh2 have been determined in the partially radiation-reduced state to resolutions of 1.7 Å and 1.6 Å, respectively. Additionally, the structure of HvTrxh2 in the oxidized state has been determined to 2.0 Å. The two Trxs are well conserved in overall fold considering their sequence identity of only 51%, and show the typical active site architecture of Trxs. Interestingly, the four independent HvTrxh1 molecules are found as two crystal dimers (AD and BC). The crystal interfaces serve as an excellent model for Trx substrate recognition, as the putative substrate recognition motif of molecules A and B, shaped as a hydrophobic groove, binds equivalent loop segments from the D and C molecules, respectively. In accordance with Trx-substrate protein interactions previously observed in engineered disulfide-linked reaction intermediate mimics, the HvTrxh1 pairs interact *via* numerous van der Waals contacts and three intermolecular hydrogen bonds resembling an anti-parallel β-sheet. The occurrence of these protein-protein interactions in the absence of an engineered disulfide-linkage suggests that Trx has affinity and specificity towards disulfides located on certain protein motifs. Moreover, Glu80 of the bound loop motif in molecules D and C forms a salt-bridge with Arg101 contiguous to the putative substrate recognition motif of molecules A and B, respectively. This arginine is replaced by an isoleucine in HvTrxh2, highlighting a potential for specificity differences between these two Trx isoforms.

3.2 Introduction

Although Trx has a broad specificity, 3D-structures of disulfide-linked Trx-substrate reaction intermediate mimics provided evidence for recognition of structural elements in target protein motifs by Trxs (Qin et al., 1995; Qin et al., 1996; Maeda et al., 2006b (Chapter 2)). Previously, NMR and X-ray structures were determined for Trx h from *C. reinhardtii* (PDB entries 1TOF and 1EP7; Mittard et al., 1997; Menchise et al., 2001). Among higher plants, NMR structures have been reported for Trx h from *A. thaliana* (PBD entry 1XFL; Peterson et al., 2005) and *Populus tremula* (PDB entry 1TI3; Coudevylle et al., 2005). We recently reported the crystal structure of a barley Trx h isoform 2 (HvTrxh2) in a mixed disulfide-linked complex with a substrate protein, BASI (Maeda et al., 2006b (Chapter 2)). The crystal structures of the two barley Trx h isoforms, HvTrxh1 and HvTrxh2, determined in the present study allow the first 3D-structure comparison of two Trx h isoforms.

3.3 Results and Discussion

3.3.1 Protein crystallization, data collection and structure determination

Diffraction data was collected for HvTrxh1 crystals obtained from two different reservoir solutions; (1) 0.1 M MES pH 6.0, 2.4 M ammonium sulfate ($HvTrxh1_{AS}$) and (2) 0.2 M ammonium acetate, 0.1 M sodium acetate trihydrate, 30% (w/v) PEG 4000 ($HvTrxh1_{PEG}$). For HvTrxh2, crystals were obtained in non-buffered 30% (w/v) PEG 1500 ($HvTrxh2_{PEG}$). The $HvTrxh1_{PEG}$ structure was solved by MR using the available crystal structure of *C. reinhardtii* Trx h as a search model (PDB entry 1EP7; Menchise et al., 2001). The $HvTrxh1_{PEG}$ structure was subsequently used for MR of $HvTrxh1_{AS}$ and $HvTrxh2_{PEG}$. $HvTrxh1_{PEG}$ and $HvTrxh1_{AS}$ are both in the C2 space group, having nearly identical unit cell dimensions and crystal packing with four HvTrxh1 molecules

(A-D) per asymmetric unit, while HvTrxh2 has space group p2(1) and includes two HvTrxh2 molecules (A and B) per asymmetric unit.

For the initial refinement of Trxs, the redox cysteine pairs were fixed in disulfide bonds, as neither Trx samples had been treated with disulfide reductant and were thus presumed to be in the oxidized state. However, the resultant *Fo-Fc* electron density maps had significant negative electron density at the center of the disulfide bonds. A revised model refinement without fixing the cysteine pairs in disulfide bonds resulted in disappearance of the negative electron density in *Fo-Fc* maps, giving Trx structures displaying various Sγ-Sγ distances of up to 3.0 Å, greatly exceeding the ideal disulfide bonded Sγ-Sγ distance of 2.03 Å. Disulfide bonds are in general highly radiation-sensitive (Ravelli and McSweeney, 2000) and radiation disruption of redox-active disulfide bonds in Trxs and related proteins during X-ray data collection has often been observed (Friemann et al., 2003; Stirnimann et al., 2006). To confirm that the exposure of crystals to X-ray radiation was the cause of the enlarged Sγ-Sγ distances, the HvTrxh2 structure was independently refined against the dataset partitioned into the initial half ($HvTrxh2_{RED1}$) and the final half ($HvTrxh2_{RED2}$) of data collection, each containing an equal number of images. The two time- and space-averaged HvTrxh2 structures confirmed the progressive disruption of the disulfide during data collection, as the averaged Sγ-Sγ distances for the two independent HvTrxh2 molecules increased from 2.7 Å in $HvTrxh2_{RED1}$ to 3.2 Å in $HvTrxh2_{RED2}$.

To study structural consequences of Trx oxidoreduction, the structure of oxidized HvTrxh2 ($HvTrxh2_{OX}$) was determined. Partially overlapping fractional datasets were collected from three isomorphous HvTrxh2 crystals in order to diminish the radiation-damaged portion of the diffraction data. The HvTrxh2 structure was refined against the merged fractional datasets with the redox cysteine pairs fixed in

disulfide bonds. The absence of negative electron density at the center of disulfide bonds in the resultant 1σ *Fo-Fc* electron density map confirmed that radiation damage was limited. The data collection and refinement statistics are listed in **Table 3.1**. The statistics for $HvTrxh1_{AS}$ are superior to those for $HvTrxh1_{PEG}$, and unless otherwise specified the following characterization is based on the $HvTrxh1_{AS}$ structure. Likewise, $HvTrxh2_{RED1}$ is used to describe the HvTrxh2 structure unless otherwise specified.

3.3.2 The fold of HvTrxh1 and HvTrxh2

The primary structures of Trxs vary greatly both between species and between different isoforms within the same species. For instance, spinach chloroplastic Trxs categorized as f- and m-types share only 29% sequence identity (Capitani et al., 2000). Large variations are indeed observed in amino acid sequences of h-type Trxs (**Figure 3.1A**). 3D structures of various Trxs nevertheless show little deviation in the overall fold. Accordingly, HvTrxh1 and HvTrxh2 have the typical fold of Trx consisting of a five stranded central β-sheet surrounded by four α-helices in a βαβαβββα topology (**Figures 3B, C**). While the vast majority of residues in the folded regions of Trxs were modeled, the N-terminal regions preceding β1 in HvTrxh1 and HvTrxh2 displayed poorly interpretable electron densities for approximately eight and fourteen residues, respectively, and were not modeled.

Table 3.1 Data collection and refinement statistics

	$HvTrxh1_{AS}$	$HvTrxh1_{PEG}$	$HvTrxh2_{OX}$	$HvTrxh2_{RED1}$	$HvTrxh2_{RED2}$
Data Collection					
Space group	C2	C2	$P2_1$	$P2_1$	$P2_1$
Unit cell dimensions	a = 120.9 Å	a = 121.7 Å	a = 47.3 Å	a = 49.3 Å	a = 49.3 Å
	b = 33.5 Å	b = 33.7 Å	b = 38.4 Å	b = 38.6 Å	b = 38.6 Å
	c = 131.0 Å	c = 132.2 Å	c = 56.6 Å	c = 57.3 Å	c = 57.3 Å
	β = 112.3°	β = 112.5°	β = 109.8°	β = 105.8°	β = 105.8°
T (K)	100	100	100	100	100
Resolution (Å)	20.5 - 1.70	20.6 - 1.80	23.6 - 2.00	24.6 - 1.62	24.6 -1.62
R_{sym}	0.073 (0.479)[a]	0.070 (0.348)[a]	0.147 (0.257)[a]	0.036 (0.226)[a]	0.035 (0.341)[a]
Completeness (%)	99.0 (96.0)[a]	99.3 (99.8)[a]	92.3 (94.7)[a]	89.3 (55.0)[a]	89.2 (54.8)[a]
$I/\sigma I$	9.0 (1.6)[a]	6.5 (2.1)[a]	2.9 (2.3)[a]	12.3 (3.3)[a]	12.0 (2.2)[a]
Redundancy	4.8 (4.6)[a]	2.9 (2.8)[a]	2.5 (2.4)[a]	3.3 (2.3)[a]	3.3 (2.3)[a]
Wilson *B* factor[b] ($Å^2$)	18.3	23.4	17.7	24.8	26.5
Refinement					
No. of non-H protein atoms	3504	3391	1730	1832	1810
No. of water molecules	468	545	131	257	253
No. ions	4	0	0	0	0
R_{work}	0.18 (0.30)[d]	0.20 (0.31)[d]	0.20 (0.23)[d]	0.20 (0.44)[d]	0.19 (0.42)[d]
R_{free}	0.22 (0.36)[d]	0.25 (0.40)[d]	0.27 (0.22)[d]	0.24 (0.54)[d]	0.24 (0.65)[d]
Rmsd. from ideality[e]					
Bond length (Å)	0.012	0.016	0.010	0.013	0.029
Bond angle (°)	1.2	1.3	1.3	1.4	2.1
Estimated overall coordinate error based on R_{free}[f] (Å)	0.1	0.1	0.2	0.1	0.1
B factors					
Protein ($Å^2$)	15.8	23.8	15.2	24.1	28.2
Solvent ($Å^2$)	28.0	29.9	19.2	31.0	34.9
Ramachandran plot[g]					
Most favored regions (%)	95.1	94.5	90.5	92.1	92.6
Disallowed regions (%)	0	0	0	0	0

Numbers in parenthesis refer to the outer resolution shell. [a]Outer resolution shell; $HvTrxh1_{AS}$ = 1.79 - 1.70 Å, $HvTrxh1_{PEG}$ = 1.90 - 1.80 Å, $HvTrxh2_{RED1}$ = 1.72 - 1.62 Å, $HvTrxh2_{RED2}$ = 1.72 - 1.62 Å, $HvTrxh2_{OX}$ = 2.11 - 2.00 Å. [b]Calculated using TRUNCATE from the CCP4 suite. [c]R_{free} is equal to R_{work} but calculated using 5% of the reflections, which were not included in the refinement procedure. [d]Outer resolution shell $HvTrxh1_{AS}$ = 1.74 - 1.70 Å, $HvTrxh1_{PEG}$ = 1.85 - 1.80 Å, $HvTrxh2_{RED1}$ = 1.66 - 1.62 Å, $HvTrxh2_{RED2}$ = 1.66 - 1.62 Å, $HvTrxh2_{OX}$ = 2.05 - 2.00 Å. [e]As defined by (Engh and Huber, 1991). [f]Calculated in PROCHECK as implemented in the CCP4 suite.

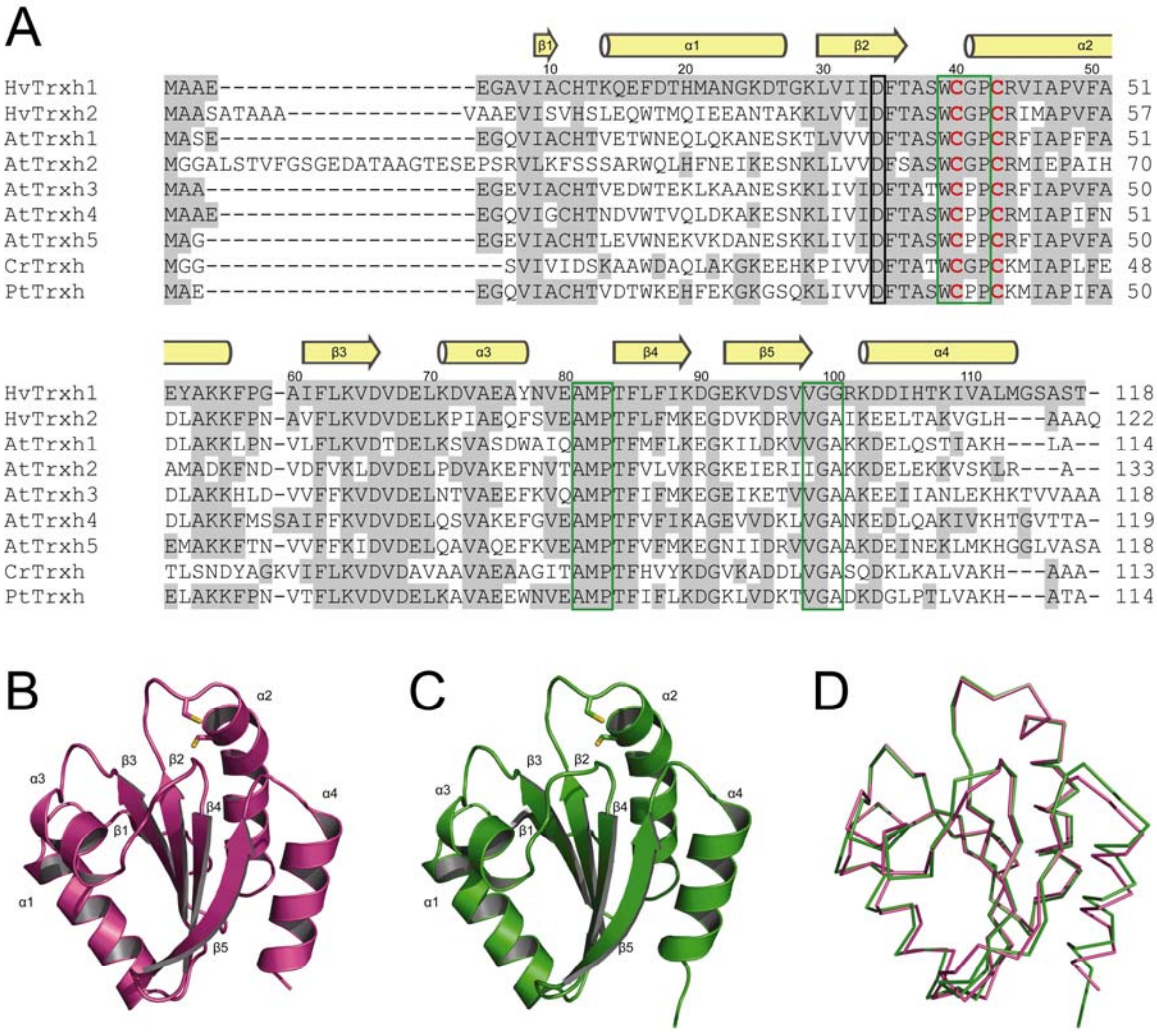

Figure 3.1 Amino acid sequences and crystal structures of HvTrxh1 and HvTrxh2. (A) Multiple sequence alignment of HvTrxh1, HvTrxh2, five *Arabidopsis* Trx h isoforms (AtTrxh1-5), *C. reinhardtii* Trx h (CrTrxh) and *P. tremula* Trx h (PtTrxh). HvTrxh1 (Q7XZK3), HvTrxh2 (Q7XZK2), AtTrxh1 (*A. thaliana* Trx H-type 1, P29448), AtTrxh2 (*A. thaliana* Trx H-type 2, Q38879), AtTrxh3 (*A. thaliana* Trx H-type 3, Q42403), AtTrxh4 (*A. thaliana* Trx H-type 4, Q39239) AtTrxh5 (*A. thaliana* Trx H-type 5, Q39241), CrTrxh (*C. reinhardtii* Trx-H, P80028), PtTrxh (*P. tremula* Trx H, Q8S3L3) were aligned using ClustalW at the European Bioinformatics Institute (http://www.ebi.ac.uk/clustalw/). The redox active cysteine pair is indicated with bold red letters. Positions of the HvTrxh1 loop segments, Trp39-Pro42, Ala81-Pro83 and Val98-Gly100 are indicated with green boxes, and the position of Asp34 (Asp_C) in HvTrxh1 is indicated with a black box. Amino acids identical to those in HvTrxh1 are indicated with grey background. The indicated secondary structure elements are based on the structure of HvTrxh1 molecule A. (B, C) Cartoon display of the crystal structures of HvTrxh1 (B) and HvTrxh2 (C) colored magenta and

green, respectively. Stick representation shows the redox active cysteine pairs, Cys40/Cys43 (HvTrxh1) and Cys46/Cys49 (HvTrxh2), and sulfur atoms are colored yellow. (D) Structural alignment of HvTrxh1 and HvTrxh2 shown as Cα traces colored in accordance with **Figures 3.1B, C**.

The same region of HvTrxh2 was also distorted in the crystal structure of HvTrxh2 in complex with BASI (Maeda et al., 2006b (Chapter 2). This region did not form any secondary structure in the NMR structures of h-type Trxs from *A. thaliana* (PDB entry 1XFL, Peterson et al., 2005) or *P. tremula* (PDB entry 1TI3, Coudevylle et al., 2005). The N-terminal HvTrxh1 motif Met-Ala-Ala-Glu-Glu (**Figure 3.1A**), is essential for phloem trafficking of the closely related rice phloem Trx h (Ishiwatari et al., 1998). The longer and more hydrophobic N-terminal region present in HvTrxh2 was speculated to be involved in membrane association of wheat Trx h (Gautier et al., 1998).

HvTrxh1 molecule A can be superimposed on the three other HvTrxh1 molecules in the asymmetric unit with rmsd of up to 0.4 Å using 92 Cα atoms. The two HvTrxh2 molecules in the asymmetric unit superimpose on one another with rmsd of 0.2 Å using 102 Cα atoms. This excellent superimposition of independent molecules shows that the structures of HvTrxh1 and HvTrxh2 are rigid. Despite having only 56% sequence identity in the folded regions, HvTrxh1 molecule A aligns with HvTrxh2 molecule A with an rmsd of 0.6 Å using 90 Cα atoms (**Figure 3.1D**). Significant deviation is nevertheless seen at the C-terminal end of loop α3-β4, but this difference is most likely due to the influence of tight crystal packing of HvTrxh1 in this region, as discussed later.

The structure of HvTrxh1 (molecule A) superimposes on the crystal structure of *C. reinhardtii* Trx h (PDB entry 1EP7, molecule A; Menchise et al., 2001) with an rmsd of 0.7 Å using 91 Cα atoms, showing that the structures of h-type Trxs are well

conserved among species. In contrast, HvTrxh1 (molecule A) only superimposes on Trxs from *E. coli* (PDB entry 2TRX, molecule A; Katti et al., 1990) and human (PDB entry 1ERU; Weichsel, et al., 1996) with rmsd of 1.0 Å and 0.5 Å over a region of 68 and 72 Cα atoms, respectively. The most N-terminal ~30 residues including β1 and α1 (HvTrxh1 sequence) which show poor sequence conservation (**Figure 3.1A**) show as expected the largest variation in 3D-structure. While 14 residues constitute α1 in HvTrxh1, HvTrxh2 and *C. reinhardtii* Trx h (PDB entry 1EP7), 13 in *A. thaliana* Trx h1 (PDB entry 1XFL) and 11 in *P. tremula* Trx h (PDB entry 1TI3), only four residues form α1 in *E. coli* Trx (PDB entry 2TRX) and in spinach Trx m (PDB entry 1FB6).

3.3.3 The catalytic mechanism of HvTrxh1 and HvTrxh2

An aspartic acid (Asp26) in the hydrophobic interior of *E. coli* Trx acts as a general acid/base catalyst for the protonation/deprotonation of the buried Cys_C thiol group during the oxidoreduction (Chivers and Raines, 1997). The equivalent aspartic acid residues occur in HvTrxh1 and HvTrxh2 at positions 34 and 40 with the carboxyl groups at distances of 5.6 Å and 5.5 Å from the Cys_C Sγ atom, respectively (**Figures 3.1A, 3.2**).

The carboxyl group is surrounded by hydrophobic residues, but slightly exposed to solvent in the narrow internal cavity separating it from the Cys_C Sγ atom, as typically seen for Trx structures (Katti et al., 1990). While the residues in contact with the thiol groups of the redox active cysteines are all conserved, the Asp carboxyl group seems more desolvated in HvTrxh1 than in HvTrxh2. The side chain of Ile46 at position +3 from Cys_C in HvTrxh1 occupies more space in the internal cavity in the proximity of the Asp carboxyl group (**Figure 3.2A**) in comparison with Met52 at the equivalent position in HvTrxh2 (**Figure 3.2B**).

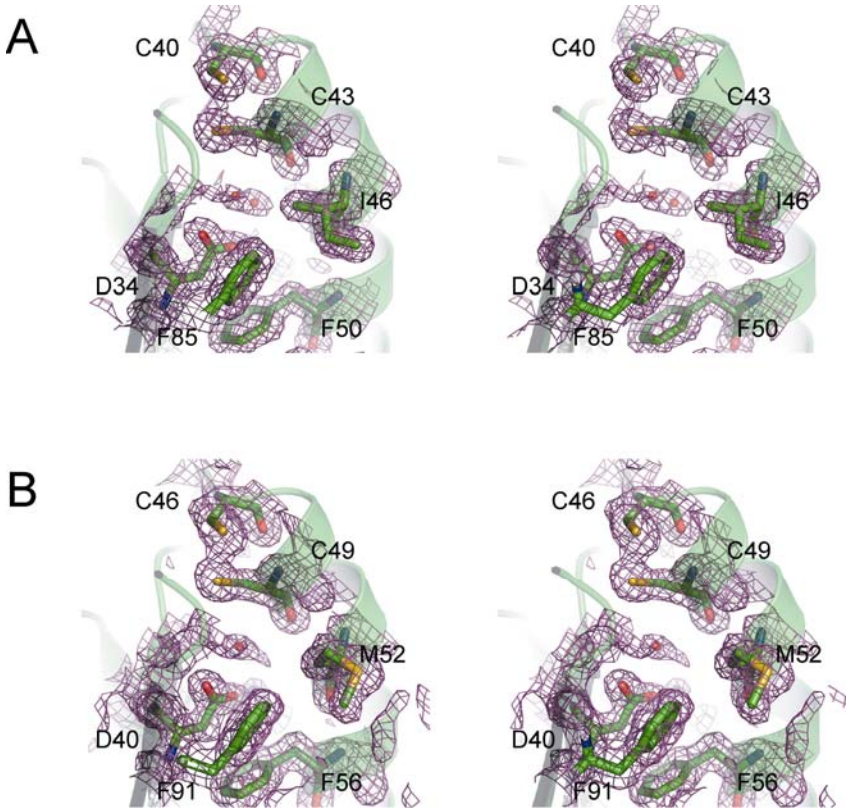

Figure 3.2 Stereo images of the active site architecture in HvTrxh1 (A) and HvTrxh2 (B). Carbon, nitrogen, oxygen and sulfur atoms are colored green, blue, red and yellow, respectively. Trxs are shown in transparent ribbon display and key residues are shown in stick representation. Water molecules in the Trx interior are shown as red spheres (a single water molecule was modeled at two alternative positions for HvTrxh1). The 2*Fo–Fc* electron density maps are presented as grey isosurface-mesh at the 1.0σ level.

The HvTrxh2 crystal structures in oxidized ($HvTrxh2_{OX}$) and partially disulfide-disrupted states ($HvTrxh2_{RED2}$) enable a detailed description of structural changes following the Trx oxidoreduction (**Figure 3.3**). The active site of HvTrxh2 is loosely packed in the crystals and therefore suited for such analysis.

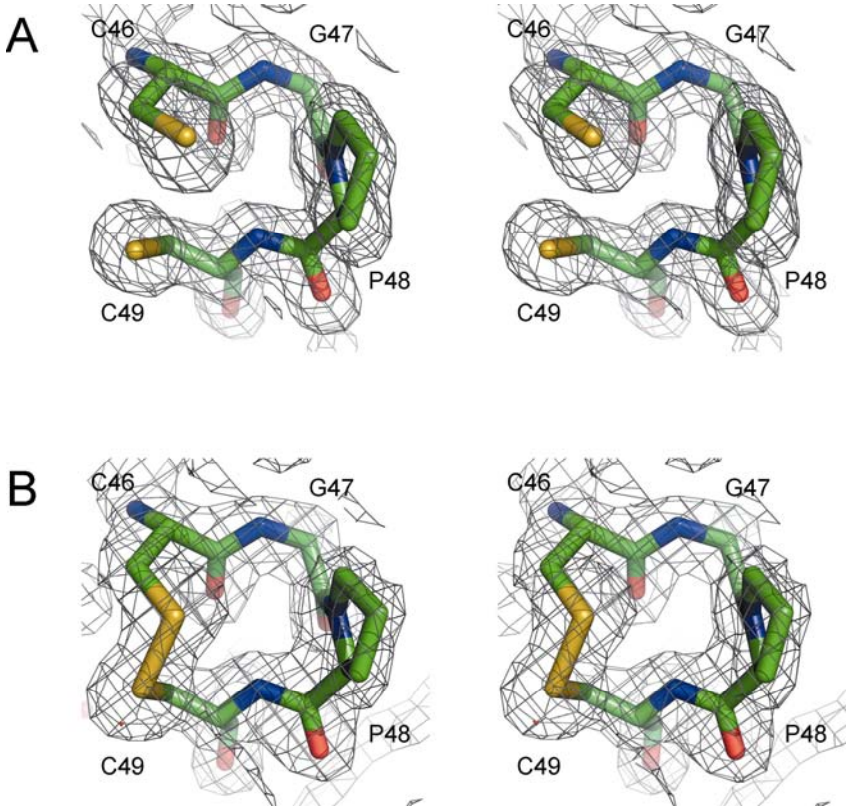

Figure 3.3 Stereo images of segment Cys46–Cys49 in HvTrxh2$_{RED2}$ (A) and HvTrxh2$_{OX}$ (B) shown in stick representation. Carbon, nitrogen, oxygen and sulfur atoms are colored green, blue, red and yellow, respectively. The 2*Fo–Fc* electron density maps are presented as grey isosurface-mesh at the 1.0σ level. The *Fo–Fc* maps are shown as isosurface-mesh and colored red (at the 3.0σ level) and green (at the -3.0σ level).

The Cys$_N$ Sγ–Cys$_C$ Sγ distance increases from 2.0 Å in HvTrxh2$_{OX}$ to 3.2 Å in HvTrxh2$_{RED2}$, in association with the shifts in Cys$_N$ χ1 angle from 166° to –179° and Cys$_C$ χ1 angle from –61° to –72° (**Figure 3.3**). Since the corresponding Sγ–Sγ distance is 3.9 Å in the NMR structure of the reduced human Trx (Weichsel et al., 1996), a major portion of HvTrxh2 was most likely in the reduced state during data collection for HvTrxh2$_{RED2}$. Disulfide reduction does not alter the main chain conformation of HvTrxh2 to a significant extent at this resolution, in accordance with studies on Trxs from *E. coli* (Jeng et al., 1994), human (Weichsel et al., 1996) and spinach (Capitani et al., 2000). Neither is any major change in position observed for the catalytic aspartic

acid nor for the water molecules buried in the cavity. The distance between the Asp40 carboxyl group and Cys_C Sγ atom is 5.7 and 5.4 Å in $HvTrxh2_{OX}$ and $HvTrxh2_{RED2}$, respectively.

The Coulombic interaction between the proximate Cys_N thiolate anion and the Asp26 carboxylate anion in the reduced *E. coli* Trx creates negative cooperativity and *microscopic* pK_as of 7.5 and 9.2 for the respective ionizing groups (Chivers et al., 1997). Cys_N and Asp40 in $HvTrxh2_{RED2}$ are at a distance of 7.8 Å, close to the corresponding distance of ~8.0 Å in the NMR structure of reduced *E. coli* Trx (Jeng et al., 1994).

3.3.4 A hydrophobic groove on HvTrxh1 and HvTrxh2 implicated for protein recognition

Solvent-exposed hydrophobic and non-charged residues constitute an elongated shallow groove at the redox active cysteines of HvTrxh1 and HvTrxh2 (**Figure 3.4**). We refer to this conserved feature in Trx structures as the substrate-binding loop motif, since it is proposed to play a central role in the binding of substrate proteins (Qin et al., 1995; Qin et al., 1996; Maeda et al., 2006b (Chapter 2); Chartron et al., 2007). This motif involves three loop segments, Trp39-Cys40(Cys_N)-Gly41-Pro42, Ala81-Met82-Pro83 and Val98-Gly99-Gly100 of HvTrxh1 (**Figure 3.4A**). The Gly100 is substituted with an alanine in HvTrxh2 (**Figure 3.4B**) that is more commonly present at this position in Trxs (**Figure 3.1A**). The equivalent loop regions in glutaredoxin and glutathione transferase, which share the Trx-fold, are involved in their glutathione affinity (Reinemer et al., 1991; Nordstrand et al., 1999).

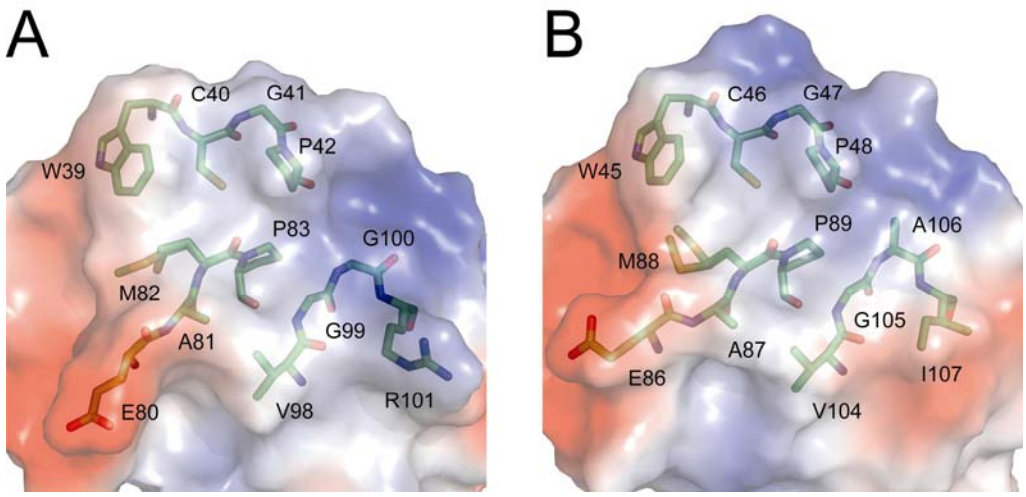

Figure 3.4 The vacuum electrostatic potential surfaces of HvTrxh1 (A) and HvTrxh2 (B). The surfaces are shown transparently. Sticks are shown for HvTrxh1 segments Trp39–Pro42, Glu80–Pro83 and Val98–Arg101 and for the equivalent residues in HvTrxh2. Carbon, nitrogen, oxygen and sulfur atoms are colored green, blue, red and yellow, respectively. Met82 of HvTrxh1 and Met88 of HvTrxh2 are modeled in two alternative conformations.

In the HvTrxH1 structure, the substrate binding loop motif is largely buried in the two protein-protein interfaces formed between molecules A and D in the same asymmetric unit and between molecules B and C in two translationally related units (**Figure 3.5A**). The residues in the three loop segments account for >85% of the total buried accessible surface area (ASA) (902 $Å^2$ (AD) and 989 $Å^2$ (BC)). The two interfaces display essentially identical protein-protein interactions, as the two HvTrxh1 molecular pairs AD and BC can be aligned with an rmsd of 1.1 Å using 199 Cα atoms (**Figure 3.5B**). The HvTrxh1 crystal dimers do not lie on crystallographic two-fold axes as often seen in protein homodimers, and no evidence suggests that the dimer represents the *in vivo* quaternary structure of HvTrxh1. The interface areas in the HvTrxh1 crystals are in accordance with those found in crystals of monomeric proteins, typically burying 200-1200 $Å^2$ ASA (Janin and Rodier, 1995) and are smaller than protein dimer

interfaces that generally bury >2000 Å^2 ASA (Bahadur et al., 2003). Nevertheless the HvTrxh1 crystal dimers must either be formed in solution under crystallization conditions or be strongly favored to form during crystal growth. The residues in the AD interface have well defined electron density both in the HvTrxh1$_{AS}$ and HvTrxh1$_{PEG}$ crystals. A few residues around the BC interface of HvTrxh1$_{PEG}$ crystals have high *B* factors or not modeled. In both crystal forms, molecule C seems to be forced into a slightly constrained conformation during crystal packing, as the helical structure is deformed at the most N-terminal part of α2, which is in contact with molecule B.

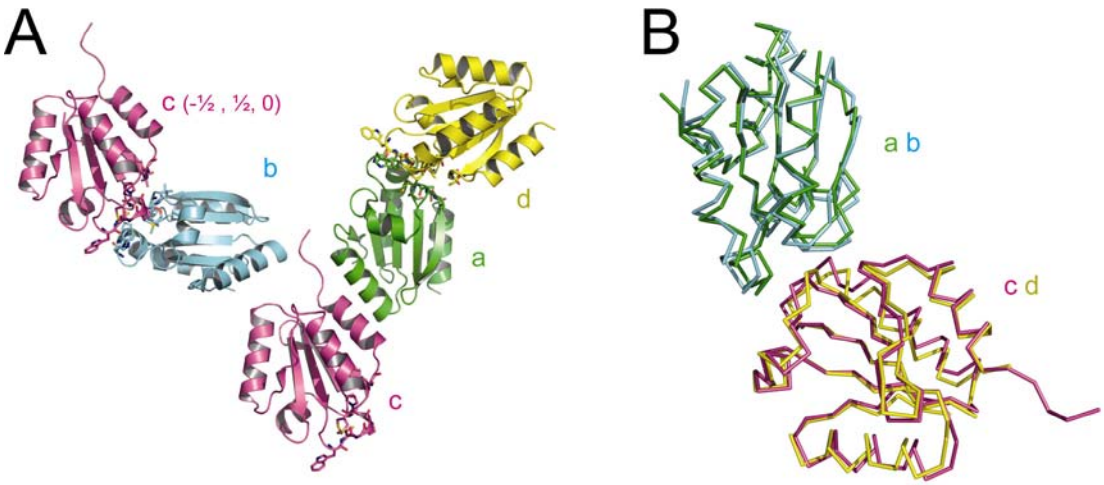

Figure 3.5 The two HvTrxh1 crystal dimers. (A) Cartoon display shows the four crystallographically independent HvTrxh1 molecules A, B, C and D in the same asymmetric unit, colored green, cyan, magenta and yellow, respectively. Molecule C from a translationally (-½,½,0) related asymmetric unit is also shown and colored magenta. Sticks are shown for residues Trp39–Pro42, Ala81–Pro83 and Val98–G100 that constitute the substrate binding loop motif. Sulfur, nitrogen, oxygen are colored yellow, blue and red, respectively. (B) Cα traces of two crystal dimers of HvTrxh1 molecules AD and BC. HvTrxh1 molecules are colored in accordance with **Figure 3.5A**.

3.3.5 Features of HvTrxh1 dimer interfaces

For simplicity, the following descriptions of the dimer interfaces are based on the AD interface unless specified. The indole group of Trp39 in A is positioned close to the Cys_N thiol group of the same molecule as seen in most other Trx structures and greatly contributes to the buried ASA (**Figures 3.6A, B**). In contrast, the indole group in the molecule D is 'flipped out' and located distantly from Cys_N. The equivalent tryptophan residue is also observed in both conformations in crystal structures of Trx from spinach (Capitani et al., 2000) and *Trypanosoma brucei brucei* (Friemann et al., 2003). The loop segment α3-β4 of molecule D (Glu80-Ala81-Met82) has extended main chain conformation and is bound along the hydrophobic groove formed by the substrate-binding loop motif on the surface of molecule A (**Figures 3.6A, B**). This contact includes several van der Waals interactions and three intermolecular backbone-backbone hydrogen bonds, resembling an anti-parallel β-sheet. Of particular importance, this mode of binding brings the Met82 side chain Cγ of the bound molecule D loop α3-β4 to a distance of 4.1 Å from the Cys_N thiol group Sγ of molecule A (**Figures 3.6A, B**). The dithiol/disulfide exchange reaction between Trx and a substrate protein requires the approximation of the Cys_N thiol group and a cysteine Sγ atom (positionally equivalent to the Met Cγ atom) of the substrate protein in the disulfide form. Therefore, the protein-protein interaction features of the HvTrxh1 dimer interfaces could represent a model for the Trx-substrate interaction.

The pattern of intermolecular hydrogen bonds observed in the HvTrxh1 dimer interfaces was previously seen in structures of disulfide-linked Trx-substrate complexes mimicking reaction intermediates as determined by NMR (Qin et al., 1996) and X-ray crystallography (Maeda et al., 2006b (Chapter 2)). **Figures 3.6E and F** show the crystal structure of a HvTrxh2 mutant disulfide-linked *via* Cys_N with Cys148 of a BASI mutant

(HvTrxh2-S-S-BASI; Maeda et al., 2006b (Chapter 2)) representing an outcome of initial nucleophilic attack from HvTrxh2 Cys_N on BASI disulfide Cys144-Cys148. Both the main chain and side chain orientations of the disulfide-linked BASI segment, Asp146-Trp147-Cys148, on the HvTrxh2 surface resemble those of the loop segment Glu80-Ala81-Met82 of the HvTrxh1 molecule D on molecule A. Most recently, the crystal structure of the 3′-phosphoadenosine-5′-phosphosulfate reductase in a disulfide-linked complex with *E. coli* Trx showed a similar mode of binding except that one of the hydrogen bonds is absent (Chartron et al., 2007). The equivalent Trx moieties are also shown to bind a disulfide-linked peptide in the parallel direction (Qin et al., 1995). A pattern of intermolecular hydrogen bonding, essentially identical to that observed here, is present in a crystal structure of the N-terminal domain of *E. coli* DsbD, with Trx-like structure and activity, in a disulfide-linked complex with DsbD C-terminal domain (Rozhkova et al., 2004). We previously proposed that this mode of intermolecular hydrogen bond formation plays an essential role in substrate recognition by Trx (Maeda et al., 2006b (Chapter 2)). Nevertheless this manner of interactions between Trx and its substrates has until now only been demonstrated using covalently-bound complexes (Qin et al., 1996; Maeda et al., 2006b (Chapter 2); Chartron et al., 2007). Non-covalent association of Trx with substrate proteins was considered to be weak and thus unfeasible for structural analysis either by NMR or X-ray crystallography. The present study, however, provides remarkable structural evidence for selective binding of a protein loop motif to the active site of HvTrxh1 in the absence of an engineered disulfide-linkage. This pattern of intermolecular backbone-backbone hydrogen bonds is also involved in the crystal structure of *E. coli* Trx in a non-covalent complex with bacteriophage T7 DNA polymerase (PDB entry 1T7P; Doublié et al., 1998).

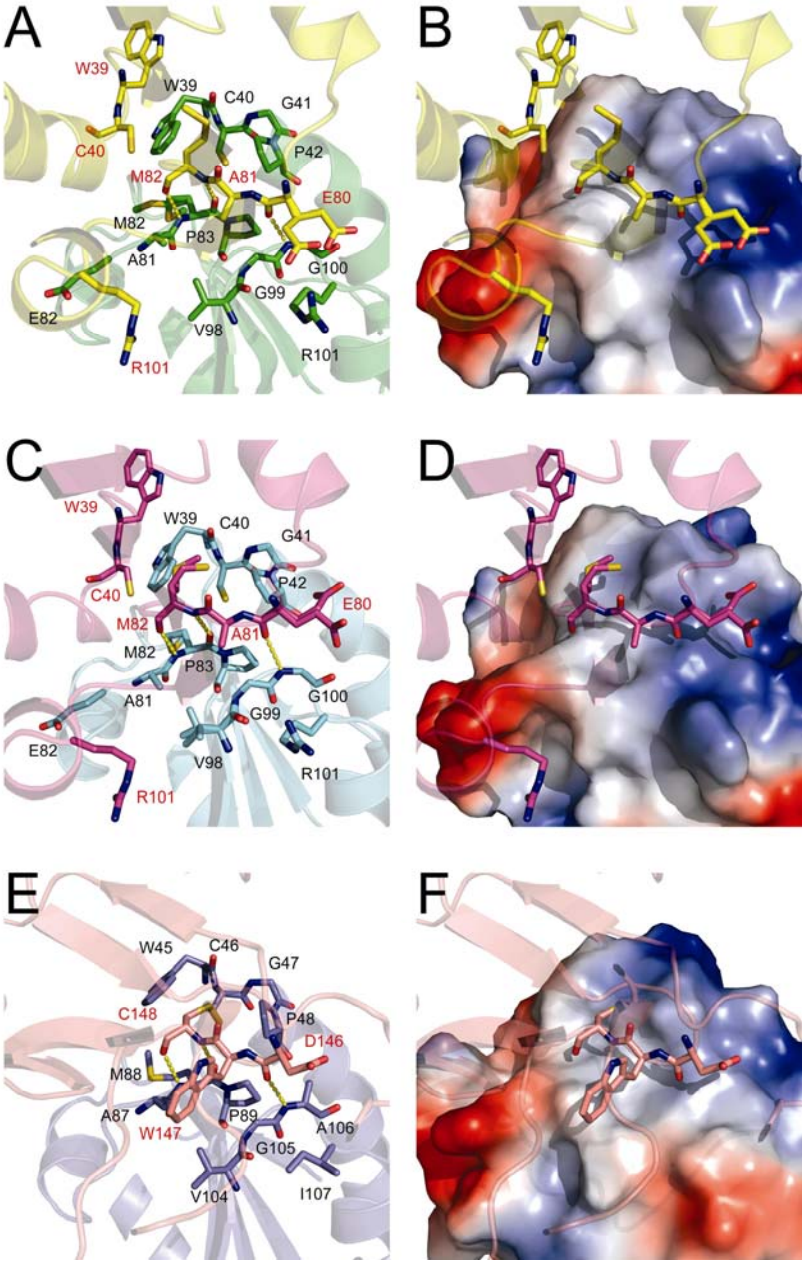

Figure 3.6 Cartoon display of protein–protein interfaces formed in HvTrxh1 crystal dimers of molecules AD (A, B) and BC (C, D) and in HvTrxh2-S-S-BASI (E, F) (Maeda et al., 2006b (Chapter 2)). Key residues are shown in stick representation. Residue labels for HvTrxh1 molecules C and D and BASI are colored red. HvTrxh1 molecules A, B, C and D are colored green, cyan, magenta and yellow, respectively. HvTrxh2 and BASI are colored blue and pink, respectively. Sulfur, nitrogen, oxygen atoms are colored yellow, blue, red respectively. Hydrogen bonds are shown as dashed yellow lines. The vacuum electrostatic potential surfaces are shown for HvTrxh1 molecule A (B), HvTrxh1 molecule B (D) and HvTrxh2 (F). Met82 (molecules A, B and C), Glu80 (molecules C and D) and Val98 (molecule B) of HvTrxh1 are modeled in two alternative conformations.

3.3.6 The involvement of electrostatic interactions in HvTrxh1 crystal dimer formations

The protein-protein interactions found in HvTrxh1 are absent in the HvTrxh2 crystal. A brief inspection of the existing PDB entries has not revealed such interaction patterns among Trx structures, although two-fold symmetry-related dimerization is reported in crystals of a *C. reinhardtii* Trx h mutant (Menchise et al., 2001) and for *Drosophila melanogaster* Trx (Wahl et al., 2005). Hence the HvTrxh1 crystal complex formation may signify structural self-complementarity. Whilst the hydrophobicity of the substrate-binding loop motif is well-conserved among Trxs, surrounding solvent-exposed residues are more divergent in the electrostatic features. For instance, the substitution of HvTrxh1 Arg101 with an isoleucine (Ile107) in HvTrxh2 changes the electrostatic properties of the surface contiguous to the substrate-binding loop motif (**Figure 3.4**). At the opposite edge of the substrate-binding loop motif, Glu80 (HvTrxh1 numbering) is present in both Trxs. Close to the HvTrxh1 crystal interfaces, the Arg101 guanidinium cation from molecule A forms an electrostatic interaction with the Glu80 carboxylate anion of the bound molecule D loop segment (**Figures 3.6A, B**). This interaction is evident in the AD interface where the distances between the Arg101 guanidinium and Glu80 carboxylate (two alternative confirmations are modeled for Glu80 in both molecules C and D) are 2.7 Å and 3.9 Å, while the groups are 6.7 Å and 10.2 Å apart in the BC interface. The other pair of Glu80 carboxylate (of molecule A) and Arg101 guanidinium (of molecule D) in HvTrxh1 dimers at a distance of 7.2 Å, and the HvTrxh1 interfaces involve no obvious conflicting contacts of charged groups.

Electrostatic complementarity is a major driving force for the rapid association of electron donors and acceptor proteins into complexes (Crowley and Carrondo, 2004). Accordingly, a charge mutation of *E. coli* Trx at the position equivalent to HvTrxh1

Arg101 affects its reactivity towards fructose-1,6-bisphosphatase (Mora-Garcia et al., 1998). The features of the HvTrxh1 crystal complex support that electrostatic interactions are involved in the Trx substrate recognition mechanism, and suggest that the substitution of HvTrxh1 Arg101 to the uncharged isoleucine in HvTrxh2 may give rise to differential interaction with some redox partners.

3.4 Experimental procedures

3.4.1 X-ray crystallography

Recombinant HvTrxh1 and HvTrxh2 were expressed in *E. coli* and purified as described previously (Maeda et al., 2003). Purified Trxs were dialyzed against water and concentrated using Centricon 10 (Millipore). Crystals of HvTrxh1 and HvTrxh2 were obtained using the hanging drop vapor diffusion method at room temperature with 2 μL each of reservoir and protein solutions. HvTrxh1 solutions of 10 mg/mL and 20 mg/mL were used for the crystallization in 0.1 M Mes pH 6.0, 2.4 M ammonium sulfate and in 0.2 M ammonium acetate, 0.1 M tri-sodium citrate pH 5.6, 30% (w/v) PEG 4000, respectively. A HvTrxh2 solution of 20 mg/mL was used for crystallization in non-buffered 30% (w/v) PEG 1500. All diffraction data were collected on a Rigaku RU–H3RHB rotating Cu anode X–ray generator equipped with an R–AXIS IV++ imaging plate detector and a 700 series Cryostream cooler (Oxford Cryosystems) at –160 °C. To generate a structural model for oxidized HvTrxh2, diffraction data was collected from three isomorphous HvTrxh2 crystals through 40° rotation (80 diffraction images) each. Reflections were indexed, integrated and scaled with MOSFLM (Leslie et al., 1992) and SCALA (Collaborative Computational Project, Number 4, 1994). MR was performed in Phaser (Collaborative Computational Project, Number 4, 1994; Storoni et al., 2004). The refinement was carried out with the program CNS (Brünger et

al., 1998) and Refmac 5 (Collaborative Computational Project, Number 4, 1994; Murshudov et al., 1997). The electron density maps of HvTrxh1 and HvTrxh2 allowed manual building of the models in O (Jones et al., 1991) and Coot (Emsley et al., 2004). The final refinements were performed in Refmac 5 and CNS. The geometries of the refined structures were checked with PROCHECK (Laskowski et al., 1993). Secondary structures were assigned in Stride (http://webclu.bio.wzw.tum.de/cgi-bin/stride/stridecgi.py/ ; Frishman and Argos, 1995). The protein-protein interfaces were analyzed in the Protein-Protein Interaction Server (V1.5) (http://www.biochem.ucl.ac.uk/bsm/PP/server/; Jones and Thornton, 1996). Figures of protein structures are made in Pymol (http://pymol.sourceforge.net/; DeLano, 2002).

Chapter 4

Differentiated reactivity of the redox active cysteines in barley thioredoxin h isoforms, HvTrxh1 and HvTrxh2

4.1 Summary

Thioredoxin (Trx) is a protein disulfide reductase possessing two redox active cysteines in the active site motif, Trp–Cys_N–Gly/Pro–Pro–Cys_C. The redox properties of two h-type barley Trxs, HvTrxh1 and HvTrxh2, were here compared. For determination of standard redox potentials ($E°'$), the reaction constants were fluorometrically determined for the bidirectional redox reactions between the barley Trxs and a reference, *E. coli* Trx (EcTrx; $E°'$ = –270 mV). The $E°'$ values for HvTrxh1 (–268 mV) and HvTrxh2 (–270 mV) assigned by this novel approach were similar, but the oxidoreduction rates of HvTrxh1 were higher than those of HvTrxh2 in both directions. Moreover, even though the primary nucleophile Cys_N of both Trxs was alkylated in the pH interval 5.5–9.4 with rate constants (k) that excellently fit with a pK_a of 7.7, Cys_N in HvTrxh1 approached ~70% higher k_{max} value (at high pH) than in HvTrxh2 and was more nucleophilic. The conserved aspartic acid (Asp_C) in EcTrx is previously shown to titrate at a perturbed and slightly basic pK_a value and create for Cys_N a heterogeneous electrostatic milieu and two microscopic pK_as. Considering this, the pK_a assigned here most likely represents Cys_N titration in the Asp_C–protonated Trx fractions, while the distinct nucleophilicity of Cys_N in the two Trxs indicates that Asp_C in HvTrxh1 has a higher pK_a value than in HvTrxh2. Accordingly, Cys_N was almost equally nucleophilic in Cys_C to Ser variants of HvTrxh1 and HvTrxh2, in which Cys_N was decreased in pK_a and therefore presumed to titrate predominantly under Asp_C-protonated state.

4.2 Introduction

H-type Trxs are yet poorly characterized in terms of biological roles, 3D structures and biophysical properties, in comparison with EcTrx or chloroplastic Trxs. The present study reports biophysical comparison of two barley Trx h isoforms, HvTrxh1 and HvTrxh2 (Maeda et al., 2003).

4.3 Results

4.3.1 Trx-Trx redox reaction kinetics for *E*°′ determination of HvTrxh1 and HvTrxh2

The calculation of standard redox potential (*E*°′) for a given substance by the Nernst equation requires an experimentally assigned equilibrium constant (*K*) for the redox reaction between the substance and any reference with known *E*°′. The well-characterized EcTrx was chosen as the reference (–270 mV) (Åslund et al., 1997) for the present *E*°′ assignment for HvTrxh1 and HvTrxh2, because the *K* values of redox reactions involving pairs of Trxs were presumed to be close to unity and thereby easy to precisely determine experimentally.

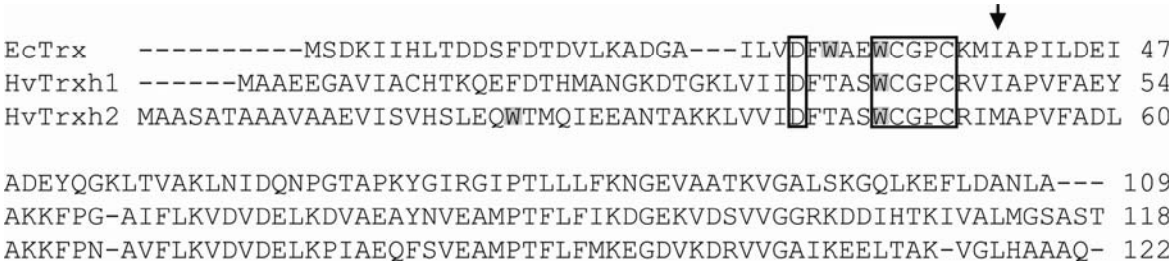

Figure 4.1 Sequence alignment of EcTrx (P0AA27), HvTrxh1 (AAP72290) and HvTrxh2 (AAP72291). The positions of the conserved active site sequence motif, Trp-Cys_N-Gly/Pro-Pro-Cys_C and Asp_C are indicated with black boxes. Tryptophan residues are indicated with gray background.

The fluorescence emission of EcTrx intensifies ~6 folds upon reduction of the active site disulfide bond (Holmgren, 1972). This redox dependency chiefly stems from the unique tryptophan residue at position −3 from Cys_N, and not from the conserved tryptophan in the Trx active site at the immediate N-terminus of Cys_N (**Figure 4.1**) (Holmgren, 1972). Whilst HvTrxh1 possesses only the conserved tryptophan in the active site, an additional tryptophan is present in HvTrxh2 at position 23 (**Figure 4.1**). **Figure 4.2** shows fluorescence emission spectra at 300–400 nm (excitation at 280 nm) for the oxidized and reduced forms of EcTrx, HvTrxh1 and HvTrxh2 at pH 7.0. The oxidized forms of HvTrxh1 and EcTrx exhibit emission maxima at ~310 nm and ~350 nm, respectively. In comparison, the overall intensity for the emission spectrum of the oxidized HvTrxh2 with a maximum at ~340 nm is several folds higher, presumably due to the presence of Trp23.

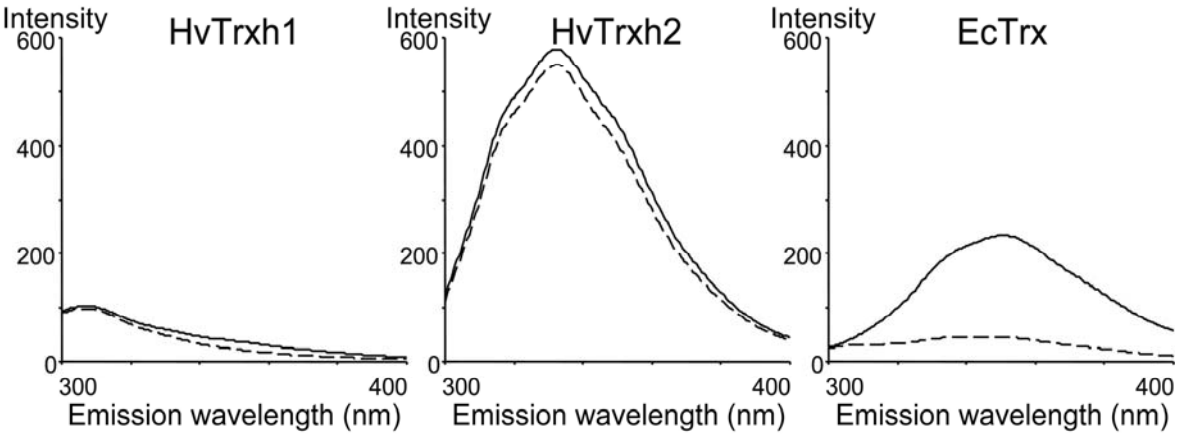

Figure 4.2 Fluorescence emission spectra for HvTrxh1, HvTrxh2 and EcTrx1 in the oxidized and reduced forms. The excitation is at 280 nm and the emission spectra cover 300–400 nm. The spectra for the reduced forms are shown with black lines, while those for the oxidized forms are shown with dashed line.

Upon complete disulfide reduction by a large excess of the disulfide reductant Tris(2-carboxyethyl)phosphine (TCEP), the emission intensity substantially increases for EcTrx (>5 folds) but remains nearly unchanged for the two barley Trxs (**Figure 4.2**). We take advantage of this unique redox dependency of the emission intensity for EcTrx to fluormetrically determine the rates of redox reactions between Trx pairs, EcTrx–HvTrxh1 and EcTrx–EcTrxh2. The second orders reaction constants (k) are determined for the bidirectional reactions between the Trxs, and used for the calculation of K ($K=k_2/k_1$), and $E°'$ for HvTrxh1 and HvTrxh2.

4.3.2 $E°'$ values for HvTrxh1 and HvTrxh2

The fluorescence emission was measured at 380 nm (excitation at 280 nm) throughout the analysis of Trx–Trx redox reactions. At this wavelength, the reduction of the active site disulfide bond increased the emission intensity of EcTrx1, HvTrxh1 and HvTrxh2 with 28, 2 and 4 units/μM, respectively. Accordingly, completion of the redox reaction between 1.0 μM each of oxidized EcTrx and reduced HvTrxh1 alters the emission intensity with +26 units (–26 units for the reversed reaction). The corresponding values are +24 and –24 units for the redox reactions between EcTrx and HvTrxh2.

6.0 μM oxidized EcTrx was mixed with an equimolar concentration of the reduced HvTrxh1 or HvTrxh2, and the fluorescence emission intensity was monitored (**Figure 4.3A**). For both reactions an increase in intensity was observed in accordance with the reduction of EcTrx. The increase in intensity continued for ~5 and ~10 hours for the reaction mixtures containing HvTrxh1 and HvTrxh2, respectively, followed by a slow decrease, presumably due to Trx oxidation by dissolved oxygen or precipitation (**Figure 3.3A**).

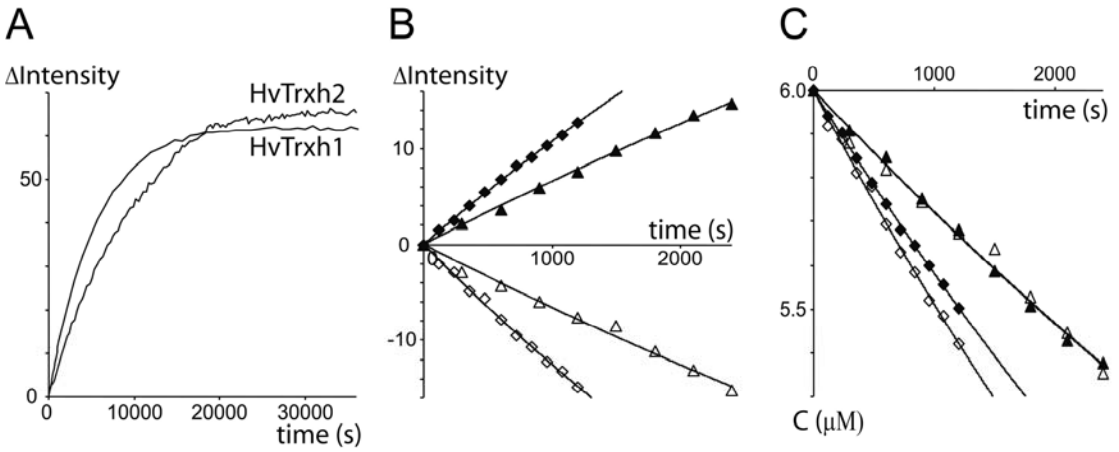

Figure 4.3 The redox reactions between Trxs followed fluorimetrically. (A) The time courses of change in emission intensity for the reaction mixture containing 6.0 μM each of the oxidized EcTrx and the reduced forms of HvTrxh1 or HvTrxh2 followed for ten hours. (B) The initial time courses of change in emission intensity for Trx-Trx redox reactions. The reaction mixtures contain following Trxs (6.0 μM each); (1) oxidized EcTrx and reduced HvTrxh1 (filled diamonds) (2) oxidized EcTrx and reduced HvTrxh2 (filled triangles), (3) reduced EcTrx and oxidized HvTrxh1 (unfilled diamonds), (4) reduced EcTrx and oxidized HvTrxh2 (unfilled triangles). All measuring results represent the mean values for the duplicated measurements (C) Time courses of decrease in the molar concentrations of the individual reactants calculated for the same reaction mixtures as in **Figure 4.3B**.

Determination of *k* values was based on fluorescence measurements recorded during the initial 20 and 40 minutes for HvTrxh1 and HvTrxh2, respectively (**Figure 4.3B**). The molar concentrations of the remaining individual reactants at different time point were calculated for each reaction mixture based on the measured change in emission intensity (**Figure 4.3C**). The reactions between the products were here ignored, as less than 15 % of the initial reactants were converted into the products in these time intervals. By using curve fitting, the second orders reaction constants for the redox reaction between the oxidized

EcTrx1 and reduced HvTrxh1 (k_1), and the reverse reaction (k_2) were determined to 13 $M^{-1}s^{-1}$ and 15 $M^{-1}s^{-1}$, respectively, while the corresponding values were 8.1 $M^{-1}s^{-1}$ and 8.1 $M^{-1}s^{-1}$ for the redox reactions involving HvTrxh2. The equilibrium constants (k_2/k_1) for redox reactions between the two Trx pairs, EcTrx–HvTrxh1 and EcTrx–HvTrxh2, were thereby calculated to 1.2 and 1.0, respectively, and finally the $E°'$ values for HvTrxh1 and HvTrxh2 were determined to –268 mV and –270 mV, respectively, using the $E°'$ value of –270 mV for EcTrx (Åslund et al., 1997). The standard deviations of the duplicated $E°'$ determinations for HvTrxh1 and HvTrxh2 were 0.5 mV and 1.1 mV, respectively.

The two barley Trx h isoforms thus appear to be analogous in the redox properties in terms of thermodynamics. Nevertheless, the faster oxidoreduction rates of HvTrxh1 in comparison with HvTrxh2 indicate distinct reactivities of the active site cysteines in the two barley Trxs, in agreement with the previously reported superior insulin reduction efficiency of HvTrxh1 (Maeda et al., 2003).

4.3.3 pH-titration of Cys_N in HvTrxh1 and HvTrxh2

The pH dependency of Cys_N ionization in HvTrxh1 and HvTrxh2 was analyzed here based on kinetics of the reaction between Cys_N thiolate anion and iodoacetamide (IAM). Studies on EcTrx have shown that Cys_N but not Cys_C is alkylated by IAM (Takahashi and Creighton, 1996). The same pattern was expected for HvTrxh1 and HvTrxh2, as only the Cys_N thiol group is solvent exposed (**Figure 4.4**; Chapter 3).

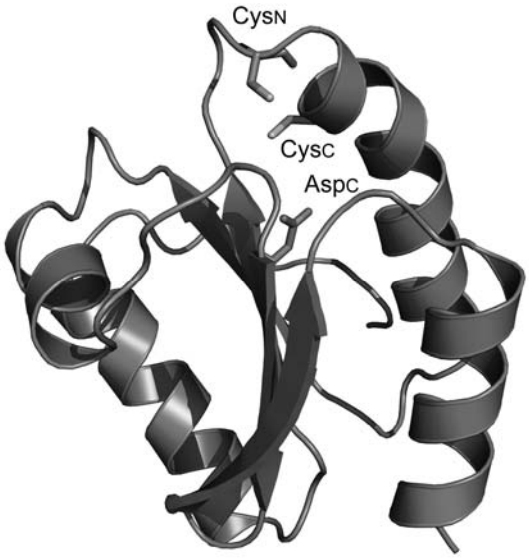

Figure 4.4 Crystal structure of HvTrxh1 in the partially radiation-reduced form. The overall structure is shown in cartoon display with regions of helices, sheets and loops colored yellow, red and green, respectively. Cys40 (Cys_N), Cys46 (Cys_C) and Asp36 (Asp_C) are displayed in stick representation.

The analysis was performed for pH 5.5–9.4, while conditions of higher pH values seemed to either damage the Trxs or cause modification on unspecified protein moieties. The reactions were quenched at different time points by addition of acetic acid to 10% (v/v), and the unmodified and Cys_N-carbamidomethylated forms of Trxs were separated and relatively quantified on a reversed-phase HPLC column. The resultant chromatograms for the two Trxs showed resolved peaks for the unmodified Trxs and the Cys_N-carbamidomethylated Trxs (**Figure 4.5A**). The Cys_N-carbamidomethylation of HvTrxh2 in the peak of shorter retention time was confirmed by trypsin digestion followed by tandem mass spectrometry of the relevant peptide (data not shown). The second order reaction constants at each pH value were calculated for HvTrxh1 and HvTrxh2 (**Figure 4.5B**). Curve fitting of the pH-titration data to the Henderson-Hasselbalch equation, which does not account for cooperativity between proximity ionizing groups, assigned an identical

Cys_N pK_a value of 7.7 for both barley Trxs (**Figure 4.5B**). On contrary, the k_{max} values (k at high pH) of 0.82 and 0.48 $nM^{-1} \cdot s^{-1}$ determined for HvTrxh1 and HvTrxh2, respectively, considerably diverged.

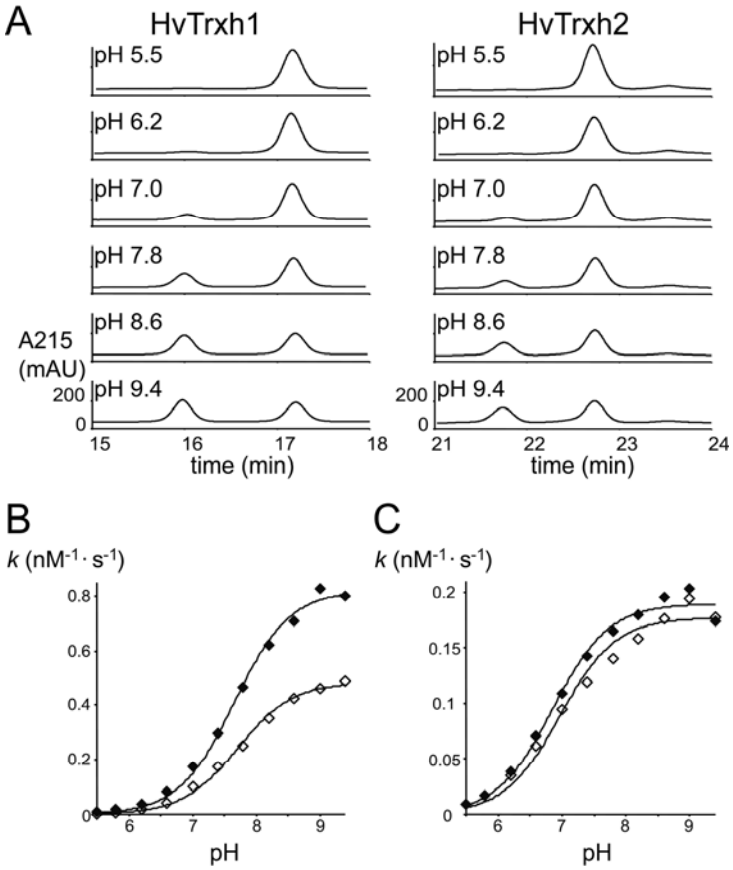

Figure 4.5 Alkylation rates of Cys_N in HvTrxh1, HvTrxh2 and in their Cys_C to Ser variants. (A) Chromatograms showing the pH-dependency of Cys_N alkylation rates in HvTrxh1 and in HvTrxh2. Trxs (4.0 μM) are incubated for 40 seconds with 20 μM IAM under conditions of various pH values. The reactions are quenched with addition of acetic acid to 10% (v/v), and the unmodified and Cys_N-carbamidomethylated Trxs are separated with on a reverse phase HPLC column. (B) The determined second orders reaction constants for HvTrxh1 (filled diamond) and HvTrxh2 (unfilled diamonds). (C) The determined second orders reaction constants for HvTrxh1 Cys43Ser (filled diamond) and HvTrxh2 Cys49Ser (unfilled diamonds). All measuring results in **Figure 4.5B**, C represent the mean values for the duplicated measurements.

The conserved Asp_C in the active site of Trx has been shown to a have strongly perturbed pK_a (7.5 in EcTrx) (Langsetmo et al., 1991; Chivers et al., 1997). The proximity of the Asp_C carboxyl and Cys_N thiol in HvTrxh1 and HvTrxh2 (~8 Å; Chapter 3) necessitates the consideration that the ionization of the two residues are interdependent. It may therefore be postulated that the assigned Cys_N pK_a of 7.7 only represent fractional ionization in the Asp_C-protonated Trx populations, while the remaining fractions of Cys_N ionizes with a more basic pK_a value (>9.4). In view of this hypothesis, the observed difference in the k_{max} values signifies that a larger fraction of the Cys_N population in HvTrxh1 ionizes with the pK_a of 7.7 relative to that in HvTrxh2. This implies that the Asp_C must have a higher pK_a value and be less ionized in HvTrxh1 than in HvTrxh2. The Asp_C pK_a values in the two barley Trxs must moreover be close to that of Cys_N for the creation of microscopic Cys_N pK_as. Alternatively, the observed difference in k_{max} values can be due to distinctly different accessibility of the Cys_N thiolate anion in the two Trxs. The later is however unlikely in view of the superimposable active site structures (Chapter 3) and the equivalent pK_a values assigned here for both Trxs, since solvent accessibility in general affects pK_a values of protein ionizable groups (Li et al., 2005).

To further investigate the ionization of Cys_N, pK_a values were determined for Cys_C to Ser mutants of HvTrxh1 (Cys43Ser) and HvTrxh2 (Cys49Ser). The pH-dependent titration of Cys43Ser and Cys49Ser resulted in pK_a values of 6.9 and 7.0, respectively, in accordance with the replacement of Cys_C sulfhydryl, in van der Waals contact with that of Cys_N, with the more hydrophilic serine hydroxyl group (**Figure 4.5C**). The decrease in Cys_N pK_a values in the mutants were accompanied by diminution and almost complete equalization of k_{max} values, determined to 0.19 and 0.18 $nM^{-1}\cdot s^{-1}$ for the HvTrxh1 and HvTrxh2 mutants, respectively (**Figure 4.5C**). Firstly, the decrease in k_{max} values for the

mutants occurring in association with the decrease in Cys_N pK_a values is in accordance with the Brønsted relationship for thiol/disulfide exchange reactions (Szajewski and Whitesides, 1980). Secondly, the equalized k_{max} values in the mutants of HvTrxh1 and HvTrxh2 exclude the possibility that the Cys_N thiol group has differentiated accessibility in the two wild type Trxs, since Cys_C to Ser mutations does not largely alter the Trx active site architecture (Dyson et al., 1994; Maeda et al., 2006b (Chapter 2)). On the contrary, this behavior supports our hypothesis that the different k_{max} values observed for the wildtype HvTrxh1 and HvTrxh2 reflects the influence of Asp_C ionization. At the lowered Cys_N pK_a values determined for the mutants, larger fractions of Cys_N will titrate while Asp_C is protonated and the interference of the Asp_C carboxylate anion will be diminished.

4.4 Discussion

4.4.1 Thermodynamics of HvTrxh1 and HvTrxh2

The application of Trx superfamily proteins for redox potential measurements as alternatives to the more traditionally used low-Mw references such as NADPH or glutathione has been proposed by Åslund et al. (1997). These authors assigned the $E°'$ values for Grxs through direct protein-protein equilibrium with the reference, EcTrx, and chromatographic quantification of the reduced and oxidized species.

EcTrx is likewise used as a reference here, nevertheless, the novel approach introduced for $E°'$ assignment of the two barley Trxs has advantageously provided information regarding the redox kinetics of the two proteins. In addition to comparative studies on Trxs, this approach can be used in mutagenesis studies on Trxs and other redox proteins, since it can reveal thermodynamic and kinetic consequences of mutations in a straightforward manner. Remarkably, the redox dependent behavior of the fluorescence

emission of EcTrx has been demonstrated to be transferable to another Trx superfamily protein, DsbD, by simply introducing tryptophan at position –3 from Cys_N (Rozhkova and Glockshuber, 2007).

The $E°'$ values of –268 mV and –270 mV assigned here for HvTrxh1 and HvTrxh2, respectively, show that the redox properties of the barley Trxs are analogous to that of EcTrx in terms of thermodynamics. $E°'$ values of –290 mV and –300 mV has been assigned for *C. reinhardtii* Trx h using an approach that employs DTT as the reference (Krimm et al., 1998; Setterdahl et al., 2003). Since a $E°'$ value of –285 mV has been assigned for EcTrx using this approach (Setterdahl et al., 2003) compared to –270 mV adopted here (Åslund et al., 1997), this deviation is chiefly due to the difference in the experimental procedures.

4.4.2 Thiol-pK_a of Cys_N in HvTrxh1 and HvTrxh2

The thiol-pK_a of Cys_N influences the reaction kinetics and thermodynamics of Trx superfamily proteins (Chivers et al., 1996). In general, a shift in pK_a is associated with two counteracting effects on the reactivity of the thiol group, as thiol of lower pK_a is more ionized but the corresponding thiolate anion is intrinsically less nucleophilic (Gilbert, 1990). The crystal structures of HvTrxh1 and HvTrxh2 previously showed active site architectures typical for Trxs and of high similarity to that in the well-characterized EcTrx (Maeda et al., 2006b (Chapter 2); Chapter 3). It was thereby indicated that the active site residues in the two barley Trxs have ionization features analogous to those of the equivalent residues in EcTrx. Firstly, this indication was in part confirmed in the present study by the assignment of Cys_N pK_a of 7.7 for HvTrxh1 and HvTrxh2, a value close to 7.5 for EcTrx determined by NMR spectroscopy (Chivers et al., 1997). Secondly, the results of

pH titrations of Cys_N in the wild type barley Trxs and their Cys_C to Ser variants are in consistence with the existence of negative cooperativity between the ionization of Cys_N and Asp_C. Moreover, these results are best explained by proposing that the value of Asp_C pK_a is higher in HvTrxh1 than in HvTrxh2, even though the assignment of Asp_C pK_a requiring NMR spectroscopy has not been carried out here. This proposal does not only fit with the results of the pH titrations, but also provides explanation for the superior oxidoreduction rates that HvTrxh1 has exhibited in the redox reactions with EcTrx. Since the Sγ atom of Cys_C is buried in both the oxidized and reduced forms of Trxs (Chapter 3), the Trx-Trx redox reactions are most likely initiated by the Cys_N thiolate anion of the reduced Trx performing a nucleophilic attack on the Cys_N Sγ atom of the oxidized Trx (**Figure 4.6A**). In the transition state, a single negative charge is shared between the Cys_N Sγ atoms of the reduced Trx and the Cys_C Sγ atom of the oxidized Trx (**Figure 4.6B**). Firstly, a higher Asp_C pK_a value decreases the fraction of Asp_C in the anionic state that disfavors the partial charge on Cys_C Sγ atom in the transition state, and thereby enhances the rate of HvTrxh1 reduction by EcTrx in comparison with that of HvTrxh2. Secondly, a higher Asp_C pK_a value diminishes the negative influence on the formation of Cys_N thiolate anion in the reduced form of Trx and explains that HvTrxh1 reduces EcTrx faster than HvTrxh2. Furthermore, such a proposal is in accordance with the previously observed structural variation around the Asp_C carboxyl group between the two barley Trxs (Chapter 3). The Asp_C carboxyl group is situated in the hydrophobic core of Trxs, disfavoring the formation of carboxylate anion and explains its pK_a around neutral pH. Nevertheless, the Asp_C carboxyl group is slightly exposed to the solvent in the narrow cavity that separates it from the Cys_C thiol group with a distance of ~5.5 Å. Whilst the majority of the surrounding residues are conserved, the substitution of isoleucine at position +3 from Cys_C in HvTrxh1

with methionine in HvTrxh2 differentiates the local environment of the Asp_C carboxyl group. The branched side chain of isoleucine exposed to the internal cavity makes the Asp_C carboxyl group more desolvated in HvTrxh1, in accordance with our proposal of a higher Asp_C pK_a in HvTrxh1.

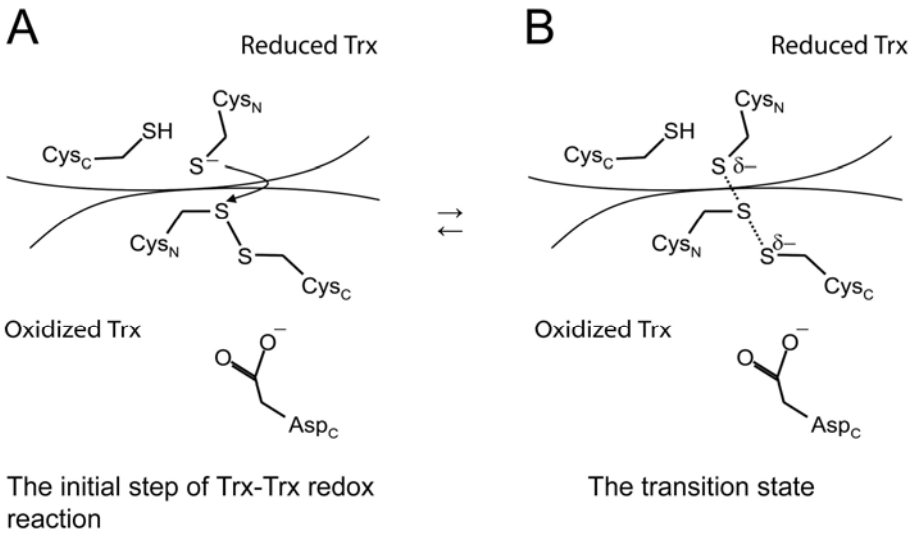

Figure 4.6 Putative mechanism of Trx-Trx redox reaction showing the reaction initiation (A) and the transition state (B).

4.4.3 Biological roles of the h-type Trxs

As described in the Introduction, the two barley Trxs have distinct patterns of appearance in barley seeds (Maeda et al., 2003). While both Trx isoforms are abundant in the embryo, HvTrxh1 is predominantly present in the endosperm. A study on transgenic barley overexpressing wheat Trx h has shown that the Trx h in the endosperm has a positive influence on the germination process (Wong et al., 2002). Moreover, proteomics-based studies have demonstrated the ability of h-type Trxs to reduce various endospermic proteins *in vitro* (Wong et al., 2004; Maeda et al., 2004, 2005). The endosperm of

germinating cereal grain is acidified to pH ~5 (Mikola and Virtanen, 1980) and therefore represents a distinctly different environment from the cytoplasm where Trxs primarily exist. The biophysical properties of both HvTrxh1 and HvTrxh2 revealed here are nevertheless typical for Trxs. Further studies are required to understand the molecular basis for the suggested roles of Trx h in the germination process, as the acidic environment in the endosperm of germinating cereal seeds presumably almost entirely protonates the Cys_N and suppress the Trx activity.

In conclusion, the present study has unveiled a detailed biophysical characterization of two h-type Trxs from barley. This information is of fundamental importance for interpreting the structures of these proteins (Maeda et al., 2006b (Chapter 2); Chapter 3), and is essential for understanding the biological importance of h-type Trxs in germinating seeds.

4.5 Experimental Procedures

4.5.1 Construction of mutants

The expression systems for the N-terminal His-tagged forms of HvTrxh1 and HvTrxh2 were constructed by inserting the encoding genes (Maeda et al., 2003) into the plasmid pET15b. Construction of the Cys49Ser mutant of HvTrxh2 was described previously (Maeda et al., 2006b (Chapter 2)). A Cys43Ser mutation of HvTrxh1 was constructed using the QuikChange® Site-Directed Mutagenesis Kit (Stratagene, La Jolla, CA, USA). The gene encoding HvTrxh1 inserted into plasmid pET15b was used as template and the primers were 5'- CCTGGTGCGGTCCATCACGTGTCATAGCCCC -3' and 5'- GGGGCTATGACACGTGATGGACCGCACCAGG -3'. The PCR products were treated with *Dpn*I (Invitrogen, San Diego, CA, USA) to hydrolyze the template plasmid, and

transformed into *Escherichia coli* DH5α. The mutations were confirmed by DNA sequencing at MWG Biotech (Ebersberg, Germany).

4.5.2 Protein production

Non-tagged HvTrxh1 and HvTrxh2 were produced in *E. coli* and purified using heat treatment, anion exchanging chromatography and gel filtration chromatography as previously described (Maeda et al., 2003). The N-terminal His-tagged HvTrxh1, HvTrxh2, Cys43Ser and Cys49Ser were produced in *E. coli* Rosetta cells at 37°C for 3 h after induction with 100 μM IPTG. Proteins were extracted with Bugbuster® Protein Extraction Reagent including Benzonase Nuclease (Novagen) and the supernatants were applied onto His-Trap HP columns (Amersham Biosciences) pre-equilibrated with loading buffer (10 mM imidazole, 500 mM NaCl, 30 mM Tris/HCl pH 8.0), and eluted by a gradient of 10-200 mM imidazole.

4.5.3 Emission spectra of HvTrxh1, HvTrxh2 and EcTrx

Non-tagged HvTrxh1 and HvTrxh2 were used for all fluorimetric measurements. EcTrx was from Promega (Madison, WI , USA). Fluorescence spectra of Trxs were acquired on a Perkin-Elmer Luminescence Spectrometer LS55 with a thermostated single-cell. The excitation wavelength was 280 nm (5 nm slit width) and the emission covered wavelengths of 300–400 nm (8 nm slit width). Measurements were performed on 12.0 μM Trx in 100 mM Hepes buffer at pH 7.0 and 1 mM EDTA at 25 °C. The spectra of Trxs in the reduced forms were obtained under the same conditions except the addition of 100 μM TCEP and incubated for at least one hour at room temperature (22 °C) to achieve complete disulfide reduction.

4.5.4 Redox potential assignment for HvTrxh1 and HvTrxh2 based on Trx-Trx redox kinetics

Prior to all experiments, the buffer was thoroughly purged with argon to prevent Trx oxidation by dissolved molecular oxygen. Trxs (60 μM) were reduced by 1.0 mM TCEP in 100 μL 100 mM HEPES pH 7.0 and 1 mM EDTA for at least one hour at room temperature. Reduced Trxs were purified by gel filtration chromatography using NAP-5 columns (GE Healthcare) pre-equilibrated with 100 mM HEPES pH 7.0 and 1 mM EDTA to final volume of ~500 μL and concentrations of ~12 μM. The precise concentrations were determined based on the fluorescence emission intensity at excitation and emission wavelengths of 280 nm and 380 nm (8 nm slit widths), respectively. For determination of Trx-Trx redox reaction rates, the oxidized and reduced Trxs were mixed to final concentrations of 6.0 μM each in final volumes of ~150 μL 100 mM HEPES pH 7.0 and 1 mM EDTA, and the reactions were followed at 25 °C with excitation and emission wavelengths at 280 nm and 380 nm (8 nm slit widths), respectively. Since changes in emission intensities that accompanies the small temperature adjustment at the insertion of the reaction cell into the fluorimeter can obscure the kinetic measurements, the first measurements (time 0) were performed four minutes after the reaction initiation. This dead time was ignored in the present calculations of reaction constants as only <3% of reactants were estimated to be consumed in this time length based on the determined reaction rates. The $E°'$ values were calculated using the Nernst equation, $E°' = E°'_{EcTrx} - (R \cdot T/n \cdot F)\ln(k_2/k_1)$, in which $E°'_{EcTrx}$ is the $E°'$ value of –270 mV for EcTrx (Åslund et al., 1997).

4.5.5 Alkylation kinetics for HvTrxh1, HvTrxh2 and their Cys_C to Ser variants

Cys_N thiol-p*K*a values in the barley Trxs and their variants were determined based on the second orders reaction constants between the Trxs and IAM in the pH interval of 5.5-9.4. To ensure the fully reduction of cysteine residues, 12 μM Trxs were pre-incubated for at least one hour with 0.50 mM TCEP in 1.0 mM HEPES buffer pH 7.0 at room temperature. The alkylation reactions were performed with 4.0 μM reduced Trxs and 20 μM IAM in 150 μL solutions of 30 mM buffers of different pH values, 1 mM EDTA and 200 mM NaCl at room temperature. The buffers used were MES for pH 5.5–6.6, HEPES for pH 7.0–7.8, Tris-HCl for pH 8.0–9.0 and glycine for pH 9.4. After incubation for various time lengths, the reactions were quenched with 1/3 volume of 40% acetic acid. Trxs in the unmodified and carbamidomethylated forms were separated and quantified using a C18 reversed-phase HPLC column on an ICS-3000 Ion Chromatography System (Dionex, Sunnyvale, CA, USA) at 30 °C. The column was pre-equilibrated with solution A (0.1% trifluoroacetic acid (TFA)), and the proteins were eluted with a linear gradient of solution B (0.1% TFA and 90% acetonitrile) 37–54% in 25 min at a flow rate of 1.0 mL/min. The elution of proteins was followed at 215 nm. The determined reaction rate constants at different pH values were fitted to the Henderson-Hasselbalch equation, $k' = k'_{max}/[1 + 10^{(pKa-pH)}]$, using CurveExpert v. 1.3 (D.G. Hyams, Hixson, TN, USA).

4.5.6 Mass spectrometric analysis of carbamidomethylation site in Trxs

Trxs in collected chromatographic fractions were subjected to digestion by ~1:100 (w/w) of trypsin in 50 mM NH_4HCO_3 pH 8.8 for 3 h. The resultant tryptic peptides were desalted and concentrated on a home-made 5 mm nano-column (Gobom et al., 1999) as described previously (Finnie et al., 2002). Peptides were eluted with 0.8 μL matrix (20 mg/ml α-

cyano 4-hydroxycinnamic acid in 70% acetonitrile/ 0.1% TFA) and deposited directly on to the MALDI target. A Bruker ultraflex II TOF/TOF (Bruker-Daltonics, Bremen, Germany) in positive-ion reflector mode was used to analyze tryptic peptides.

Concluding remarks and perspectives

The present Ph.D. project has provided the first reported structure of a protein-protein complex of Trx and a substrate. The structure of HvTrxh2-S-S-BASI, together with that of HvTrxh1 crystal dimers, has provided evidence for that Trx is able to recognize protein substrates *via* interaction with specific structural features around protein disulfides. Our studies suggest that Trx-catalyzed disulfide reduction is dependent on protein-protein interactions and targeted towards specific interaction partners, and thereby challenges the commonly accepted view of Trx as a general protein disulfide reductase. The achieved knowledge in Trx specificity will enable structure-based prediction and validation of Trx-substrate interactions and a more complete mapping of redox regulatory pathways involving Trx. Moreover, the novel insight into the structure/function relationship of Trx will support characterization of numerous Trx-fold proteins with still unresolved functions, specificities and biological roles. Additional studies are however required to verify that the suggested mode of target recognition truly plays a central role for the disulfide reductase activity and specificity of Trx. These studies can include *e.g.* site-directed mutagenesis of some key residues in the putative substrate binding motif.

Besides knowledge in substrate recognition mechanism relevant for Trx in all species, the present Ph.D. project has achieved detailed structural and biophysical characterizations of the barley Trxs, HvTrxh1 and HvTrxh2. While a number of studies have comparatively characterized h-type Trx isoforms from different plants for biological aspects, few studies have compared them at the protein chemistry level. The two barley Trxs are shown here to be similar in the overall structures and in redox properties in terms of thermodynamics, but to vary in the biophysical properties and in the charge distribution

patterns around the putative substrate recognition motif, indicating specificity differentiation among coexisting Trx h isoforms.

Finally, the knowledge achieved in the present Ph.D. project is not exclusively valuable for the field of research, but also of pharmacological science. The Trx system and redox homeostasis play roles in diverse human diseases (Burke-Gaffney et al., 2005). For instance, the level of Trx increases under malignant disease and harms the patients, because the anti-apoptotic effect of Trx enhances tumor growth (Lincoln et al., 2003). Firstly, the attained information regarding the Trx-substrate interactions supplies structural basis for the assignment of precise molecular mechanisms for Trx roles in diseases. Secondly, it can support the ongoing efforts for acquiring control of the physiological Trx activity, for instance by the development of Trx inhibitors which can be beneficial as anti-cancer therapeutic agents (Pallis et al., 2003; Welsh et al., 2003).

References

Arnér, E.S.J., and Holmgren, A. (2000). Physiological functions of thioredoxin and thioredoxin reductase. Eur. J. Biochem. *267*, 6102–6109.

Åslund, F., and Beckwith, J. (1999). The thioredoxin superfamily: redundancy, specificity, and gray-area genomics. J. Bacteriol. *181*, 1375–1379.

Åslund, F., Berndt, K.D., and Holmgren, A. (1997). Redox potentials of glutaredoxins and other thiol-disulfide oxidoreductases of the thioredoxin superfamily determined by direct protein-protein redox equilibria. J. Biol. Chem. *272*, 30780–30786.

Åslund, F., Zheng, M., Beckwith, J., and Storz, G. (1999). Regulation of the OxyR transcription factor by hydrogen peroxide and the cellular thiol-disulfide status. Proc. Natl. Acad. Sci. USA *96*, 6161–6165.

Bahadur, R.P., Chakrabarti, P., Rodier, F., and Janin, J. (2003). Dissecting subunit interfaces in homodimeric proteins. Proteins *53*, 708–719.

Bailly, C. (2004). Active oxygen species and antioxidants in seed biology. Seed Sci. Res. *14*, 93–107.

Bhattacharyya, R., Pal, D., and Chakrabarti, P. (2004). Disulfide bonds, their stereospecific environment and conservation in protein structures. Protein Eng. Des. Sel. *17*, 795–808.

Biteau, B., Labarre, J., and Toledano, M.B. (2003). ATP-dependent reduction of cysteine-sulphinic acid by *S. cerevisiae* sulphiredoxin. Nature *425*, 980–984.

Bønsager, B.C., Praetorius-Ibba, M., Nielsen, P.K., and Svensson, B. (2003). Purification and characterization of the beta-trefoil fold protein barley alpha-amylase/subtilisin inhibitor overexpressed in *Escherichia coli*. Protein Expr. Purif. *30*, 185–193.

Brünger, A.T., Adams, P.D., Clore, G.M., DeLano, W.L., Gros, P., Grosse-Kunstleve, R.W., Jiang, J.S., Kuszewski, J. Nilges, M., Pannu, N.S., et al. (1998). Crystallography and NMR system: A new software suite for macromolecular structure determination. Acta Crystallogr. D Biol. Crystallogr. *54*, 905–921.

Buchanan, B.B., and Balmer, Y. (2005). Redox regulation: a broadening horizon. Annu. Rev. Plant Biol. *56*, 187–220.

Burke-Gaffney, A., Callister, M.E., and Nakamura, H. (2005). Thioredoxin: friend or foe in human disease? Trends Pharmacol. Sci. *26*, 398–404.

Capitani, G., Markovic-Housley, Z., DelVal, G., Morris, M., Jansonius, J.N., and Schurmann, P. (2000). Crystal structures of two functionally different thioredoxins in spinach chloroplasts. J. Mol. Biol. *302*, 135–154.

Chakrabarti, P., and Janin, J. (2002). Dissecting protein-protein recognition sites. Proteins *47*, 334–343.

Charbonnier, J.B., Belin, P., Moutiez, M., Stura, E.A., and Quéméneur, E. (1999). On the role of the cis-proline residue in the active site of DsbA. Protein Sci. *8*, 96–105.

Chartron, J., Shiau, C., Stout, C.D., and Carroll, K.S. (2007). 3'-Phosphoadenosine-5'-phosphosulfate reductase in complex with thioredoxin: A structural snapshot in the catalytic cycle. Biochemistry *46*, 3942–3951.

Chiadmi, M., Navaza, A., Miginiac-Maslow, M., Jacquot, J.P., and Cherfils, J. (1999). Redox signalling in the chloroplast: structure of oxidized pea fructose-1,6-bisphosphate phosphatase. EMBO J. *18*, 6809–6815.

Chivers, P.T, Laboissiere, M.C., and Raines, R.T. (1996). The CXXC motif: imperatives for the formation of native disulfide bonds in the cell. EMBO J. *15*, 2659–2667.

Chivers, P.T., and Raines, R.T. (1997). General acid/base catalysis in the active site of *Escherichia coli* thioredoxin. Biochemistry *36*, 15810–15816.

Chivers, P.T., Prehoda, K.E., Volkman, B.F., Kim, B.M., Markley, J.L., and Raines, R.T. (1997). Microscopic pK_a values of *E. coli* thioredoxin. Biochemistry *36*, 14985–14991.

Choi, J., Choi, S., Choi, J., Cha, M.K., Kim, I.H., and Shin, W. (2003). Crystal structure of *Escherichia coli* thiol peroxidase in the oxidized state: insights into intramolecular disulfide formation and substrate binding in atypical 2-Cys peroxiredoxins. J. Biol. Chem. *278*, 49478–49486.

Chrestensen, C.A., Starke, D.W., and Mieyal, J.J. (2000). Acute cadmium exposure inactivates thioltransferase (Glutaredoxin), inhibits intracellular reduction of protein-glutathionyl-mixed disulfides, and initiates apoptosis. J. Biol. Chem. *275*, 26556–26565.

Collaborative Computational Project, Number 4. (1994). Acta Crystallogr. D Biol. Crystallogr. *50*, 760–763.

Coudevylle, N., Thureau, A., Hemmerlin, C., Gelhaye, E., Jacquot, J.P., and Cung, M.T. (2005). Solution structure of a natural CPPC active site variant, the reduced form of thioredoxin h1 from poplar. Biochemistry *44*, 2001–2008.

Crowley, P.B., and Carrondo, M.A. (2004). The architecture of the binding site in redox protein complexes: implications for fast dissociation. Proteins *55*, 603–612.

de Lamotte-Guery, F., Miginiac-Maslow, M., Decottignies, P., Stein, M., Minard, P., and Jacquot, J.P. (1991). Mutation of a negatively charged amino acid in thioredoxin modifies its reactivity with chloroplastic enzymes. Eur. J. Biochem. *196*, 287–294.

DeLano, W.L. (2002). The Pymol Molecular Graphics System. (San Carlos, CA, USA, DeLano Scientific).

Delaunay, A., Isnard, A.D., and Toledano, M.B. (2000). H_2O_2 sensing through oxidation of the Yap1 transcription factor. EMBO J. 19, 5157–5166.

Delaunay, A., Pflieger, D., Barrault, M.B., Vinh, J., and Toledano, M.B. (2002). A thiol peroxidase is an H_2O_2 receptor and redox-transducer in gene activation. Cell *111*, 471–481.

Doublié, S., Tabor, S., Long, A.M., Richardson, C.C., and Ellenberger, T. (1998). Crystal structure of a bacteriophage T7 DNA replication complex at 2.2 Å resolution. Nature *391*, 251–258.

Dyson, H.J., Jeng, M.F., Model, P., and Holmgren, A. (1994). Characterization by ^{1}H NMR of a C32S,C35S double mutant of *Escherichia coli* thioredoxin confirms its resemblance to the reduced wild-type protein. FEBS Lett. *339*, 11–17.

Eklund, H., Cambillau, C., Sjöberg, B.M., Holmgren, A., Jörnvall, H., Höög, J.O., and Brändén, C.I. (1984). Conformational and functional similarities between glutaredoxin and thioredoxins. EMBO J. *3*, 1443–1449.

Emsley, P., and Cowtan, K. (2004). Coot: model-building tools for molecular graphics. Acta Crystallogr. D Biol. Crystallogr. *60*, 2126–2132.

Engh, R.A., and Huber, R. (1991). Accurate bond and angle parameters for X-ray protein structure refinement. Acta Cryst. A. *47*, 392–400.

Fernandes, A.P., and Holmgren, A. (2004). Glutaredoxins: glutathione-dependent redox enzymes with functions far beyond a simple thioredoxin backup system. Antioxid. Redox Signal. *6*, 63–74.

Finnie, C., Melchior, S., Roepstorff, P., and Svensson, B. (2002). Proteome analysis of grain filling and seed maturation in barley. Plant Physiol. *129*, 1308–1319.

Friemann, R., Schmidt, H., Ramaswamy, S., Forstner, M., Krauth-Siegel, R.L., and Eklund, H. (2003). Structure of thioredoxin from *Trypanosoma brucei brucei*. FEBS Lett. *554*, 301–305.

Frishman, D., and Argos, P. (1995). Knowledge-based protein secondary structure assignment. Proteins *23*, 566–579.

Gamaley, I. A., and Klyubin, I. V. (1999). Roles of reactive oxygen species: Signaling and regulation of cellular functions. Int. Rev. Cytol. *188*, 203–255.

Gan, Z.R., Sardana, M.K., Jacobs, J.W., and Polokoff, M.A. (1990). Yeast thioltransferase – the active site cysteines display differential reactivity. Arch. Biochem. Biophys. 282, 110–115.

Gautier, M.F., Lullien-Pellerin, V., de Lamotte-Guery, F., Guirao, A., and Joudrier, P. (1998) Characterization of wheat thioredoxin h cDNA and production of an active *Triticum aestivum* protein in *Escherichia coli*. Eur. J. Biochem. *252*, 314–324.

Geck, M.K., Larimer, F.K., and Hartman, F.C. (1996). Identification of residues of spinach thioredoxin f that influence interactions with target enzymes. J. Biol. Chem. *271*, 24736–24740.

Gilbert, H.F. (1990). Molecular and cellular aspects of thiol-disulfide exchange. Adv. Enzymol. *63*, 69 –172.

Gobom, J., Nordhoff, E., Mirgorodskaya, E., Ekman, R., and Roepstorff, P. (1999). Sample purification and preparation technique based on nano-scale reversed-phase columns for the sensitive analysis of complex peptide mixtures by matrix-assisted laser desorption/ionization mass spectrometry. J. Mass Spectrom. *34*, 105–116.

Gravina, S.A., and Mieyal, J.J. (1993). Thioltransferase is a specific glutathionyl mixed disulfide oxidoreductase. Biochemistry *32*, 3368–3376.

Guddat, L.W., Bardwell, J.C., Zander, T., and Martin, J.L. (1997). The uncharged surface features surrounding the active site of *Escherichia coli* DsbA are conserved and are implicated in peptide binding. Protein Sci. *6*, 1148–1156.

Gursky, O., Badger, J., Li, Y., and Caspar, D.L. (1992). Conformational changes in cubic insulin crystals in the pH range 7-11. Biophys. J. *63*, 1210–1220.

Heras, B., Edeling, M.A., Schirra, H.J., Raina, S., and Martin, J.L. (2004). Crystal structures of the DsbG disulfide isomerase reveal an unstable disulfide. Proc. Natl. Acad. Sci. USA *101*, 8876–8881.

Hirotsu, S., Abe, Y., Okada, K., Nagahara, N., Hori, H., Nishino, T., and Hakoshima, T. (1999). Crystal structure of a multifunctional 2-Cys peroxiredoxin heme-binding protein 23 kDa/proliferation-associated gene product. Proc. Natl. Acad. Sci. USA *96*, 12333–12338.

Holmgren, A. (1972). Tryptophan fluorescence study of conformational transitions of the oxidized and reduced form of thioredoxin. J. Biol. Chem. *247*, 1992–1998.

Holmgren, A. (1979a). Glutathione-dependent synthesis of deoxyribonucleotides. Purification and characterization of glutaredoxin from *Escherichia coli*. J. Biol. Chem. *254*, 3664–3671.

Holmgren A. (1979b). Thioredoxin catalyzes the reduction of insulin disulfides by dithiothreitol and dihydrolipoamide. J. Biol. Chem. *254*, 9627–9632.

Holmgren, A. (1984). Enzymatic reduction-oxidation of protein disulfides by thioredoxin. Methods in Enzymol. *107*, 295–300.

Holmgren, A., Söderberg, B.O., Eklund, H., and Bränden, C.I. (1975). Three-dimensional structure of *Escherichia coli* thioredoxin-S_2 to 2.8 Å resolution. Proc. Natl. Acad. Sci. USA *72*, 2305–2309.

Hwang, C., Sinskey, A.J., and Lodish, H.F. (1992). Oxidized redox state of glutathione in the endoplasmic reticulum. Science *25*, 1496–1502.

Ishiwatari, Y., Fujiwara, T., McFarland, K.C., Nemoto, K., Hayashi, H., Chino, M., and Lucas, W.J. (1998). Rice phloem thioredoxin h has the capacity to mediate its own cell-to-cell transport through plasmodesmata. Planta *205*, 12–22.

Izawa, S., Maeda, K., Sugiyama, K., Mano, J., Inoue, Y., and Kimura, A. (1999). Thioredoxin deficiency causes the constitutive activation of Yap1, an AP-1-like transcription factor in *Saccharomyces cerevisiae*. J. Biol. Chem. *274*, 28459–28465.

Janin, J., and Rodier, F. (1995). Protein-protein interaction at crystal contacts. Proteins *23*, 580–587.

Jeng, M.F., Campbell, A.P., Begley, T., Holmgren, A., Case, D.A., Wright, P.E., and Dyson, H.J. (1994). High-resolution solution structures of oxidized and reduced *Escherichia coli* thioredoxin. Structure *2*, 853–868.

Johansson, K., Ramaswamy, S., Saarinen, M., Lemaire-Chamley, M., Issakidis-Bourguet, E., Miginiac-Maslow, M., and Eklund, H. (1999). Structural basis for light activation of a chloroplast enzyme: the structure of sorghum NADP-malate dehydrogenase in its oxidized form. Biochemistry *38*, 4319–4326.

Jones, S., and Thornton, J.M. (1996). Principles of protein-protein interactions. Proc. Natl. Acad. Sci. USA *93*, 13–20.

Jones, T.A., Zou, J.Y., Cowan, S.W., and Kjeldgaard, M. (1991). Improved methods for building protein models in electron density maps and the location of errors in these models. Acta Crystallogr. A. *47*, 110–119.

Kadokura, H., Katzen, F., and Beckwith, J. (2003). Protein disulfide bond formation in prokaryotes. Annu. Rev. Biochem. *72*, 111–135.

Kadokura, H., Tian, H., Zander, T., Bardwell, J.C., and Beckwith, J. (2004). Snapshots of DsbA in action: detection of proteins in the process of oxidative folding. Science *303*, 534–537.

Kabsch, W. (1988). Evaluation of single-crystal X-ray-diffraction data from a position-sensitive detector. J. Appl. Cryst. *21*, 916–924.

Kallis, G.B., and Holmgren, A. (1980). Differential reactivity of the functional sulfhydryl groups of cysteine-32 and cysteine-35 present in the reduced form of thioredoxin from *Escherichia coli*. J. Biol. Chem. *255*, 10261–10265.

Katti, S.K., LeMaster, D.M., and Eklund, H. (1990). Crystal structure of thioredoxin from *Escherichia coli* at 1.68 Å resolution. J. Mol. Biol. *212*, 167–184.

Kleywegt, G.J. (1999). Recognition of spatial motifs in protein structures. J. Mol. Biol. *285*, 1887–1897.

Krimm, I., Lemaire, S., Ruelland, E., Miginiac-Maslow, M., Jaquot, J.P., Hirasawa, M., Knaff, D.B., and Lancelin, J.M. (1998). The single mutation Trp35→Ala in the 35-40 redox site of *Chlamydomonas reinhardtii* thioredoxin h affects its biochemical activity and the pH dependence of C36-C39 ^{1}H-^{13}C NMR. Eur. J. Biochem. *255*, 185–195.

Ladner, J.E., Parsons, J.F., Rife, C.L., Gilliland, G.L., and Armstrong, R.N. (2004). Parallel evolutionary pathways for glutathione transferases: structure and mechanism of the mitochondrial class kappa enzyme rGSTK1-1. Biochemistry *43*, 352–361.

Laloi, C., Mestres-Ortega, D., Marco, Y., Meyer, Y., and Reichheld, J.P. (2004). The Arabidopsis cytosolic thioredoxin h5 gene induction by oxidative stress and its W-box-mediated response to pathogen elicitor. Plant Physiol. *134*, 1006–1016.

Langsetmo, K., Fuchs, J.A., and Woodward, C. (1991). The conserved, buried aspartic acid in oxidized *Escherichia coli* thioredoxin has a pK_a of 7.5. Its titration produces a related shift in global stability. Biochemistry *30*, 7603–7609.

Laskowski, R.A., McArthur, M.W., Moss, D.S., and Thornton, J.M. (1993). PROCHECK: A program to check the stereochemical quality of protein structures. J. Appl. Cryst. *26*, 283–291.

Lee, B., and Richards, F.M. (1971). The interpretation of protein structures: estimation of static accessibility. J. Mol. Biol. *55*, 379–400.

LeMaster, D.M. (1996). Structural determinants of the catalytic reactivity of the buried cysteine of *Escherichia coli* thioredoxin. Biochemistry *35*, 14876–14881.

Leslie, A.G.W. (1994). Mosflm User Guide, Mosflm Version 5.30. (Cambridge, UK: MRC Laboratory of Molecular Biology).

Li, H., Robertson, A.D., and Jensen, J.H. (2005). Very fast empirical prediction and rationalization of protein pK_a values. Proteins *61*, 704–721.

Lincoln, D.T., Ali Emadi, E.M., Tonissen, K.F., and Clarke, F.M. (2003). The thioredoxin-thioredoxin reductase system: over-expression in human cancer. Anticancer Res. *23*, 2425–2433.

Liu, H., Nishitoh, H., Ichijo, H., and Kyriakis, J.M. (2000). Activation of apoptosis signal-regulating kinase 1 (ASK1) by tumor necrosis factor receptor-associated factor 2 requires prior dissociation of the ASK1 inhibitor thioredoxin. Mol. Cell. Biol. *20*, 2198–2208.

Maeda, K., Finnie, C., Østergaard, O., and Svensson, B. (2003). Identification, cloning and characterization of two thioredoxin h isoforms, HvTrxh1 and HvTrxh2, from the barley seed proteome. Eur. J. Biochem. *270*, 2633–2643.

Maeda, K., Finnie, C., and Svensson, B. (2004). Cy5 maleimide labelling for sensitive detection of free thiols in native protein extracts: identification of seed proteins targeted by barley thioredoxin h isoforms. Biochem. J. *378*, 497–507.

Maeda, K., Finnie, C., and Svensson, B. (2005). Identification of thioredoxin h-reducible disulphides in proteomes by differential labelling of cysteines: insight into recognition and regulation of proteins in barley seeds by thioredoxin h. Proteomics *5*, 1634–1644.

Maeda, K., Hägglund, P., Finnie, C., and Svensson, B. (2006a). Proteomics of disulphide and cysteine oxidoreduction. In Plant Proteomics, The Annual Plant Reviews, Vol. 28, Finnie, C., ed. (Blackwell Publishing: Oxford, UK), pp. 71-97.

Maeda, K., Hägglund, P., Finnie, C., Svensson, B., and Henriksen, A. (2006b). Structural basis for target protein recognition by the protein disulfide reductase thioredoxin. Structure *14*, 1701–1710.

Martin, J.L. (1995). Thioredoxin – a fold for all reasons. Structure *3*, 245–250.

McCarthy, A.A., Haebel, P.W., Torronen, A., Rybin, V., Baker, E.N., and Metcalf, P. (2000). Crystal structure of the protein disulfide bond isomerase, DsbC, from *Escherichia coli*. Nat. Struct. Biol. *7*, 196–199.

Menchise, V., Corbier, C., Didierjean, C., Saviano, M., Benedetti, E., Jacquot, J.P., and Aubry, A. (2001). Crystal structure of the wild-type and D30A mutant thioredoxin h of *Chlamydomonas reinhardtii* and implications for the catalytic mechanism. Biochem. J. *359*, 65–75.

Meyer, Y., Miginiac-Maslow, M., Schürmann, P., and Jacquot, J.P. (2002a). Protein-protein interactions in plant thioredoxin dependent systems. In Protein-Protein Interactions in Plant Biology, The Annual Plant Reviews, Vol. 7, M.T. McManus, W. Laing and A. Allan, ed. (Sheffield, England: Sheffield Academic Press), pp. 1-29.

Meyer, Y., Vignols, F., and Reichheld, J.P. (2002b). Classification of plant thioredoxins by sequence similarity and intron position. Method Enzymol. *347*, 394–402.

Mikola, L., and Virtanen, M. (1980). Secretion of l-malic acid by barley aleurone layers (abstract no. 783). Plant Physiol. *65*, 142.

Mittard, V., Blackledge, M.J., Stein, M., Jacquot, J.P., Marion, D., and Lancelin, J.M. (1997). NMR solution structure of an oxidised thioredoxin h from the eukaryotic green alga *Chlamydomonas reinhardtii*. Eur. J. Biochem. *243*, 374–383.

Mora-García, S., Rodríguez-Suárez, R., and Wolosiuk, R.A. (1998). Role of electrostatic interactions on the affinity of thioredoxin for target proteins. Recognition of chloroplast fructose-1, 6-bisphosphatase by mutant *Escherichia coli* thioredoxins. J. Biol. Chem. *273*, 16273–16280.

Mouaheb, N., Thomas, D., Verdoucq, L., Monfort, P., and Meyer, Y. (1998). *In vivo* functional discrimination between plant thioredoxins by heterologous expression in the yeast *Saccharomyces cerevisiae*. Proc. Natl. Acad. Sci. USA *95*, 3312–3317.

Murshudov, G.N., Vagin, A.A., and Dodson, E.J. (1997). Refinement of macromolecular structures by the maximum-likelihood method. Acta Crystallogr. D Biol. Crystallogr. *53*, 240–255.

Nakamura, H., Nakamura, K., and Yodoi, J. (1997). Redox regulation of cellular activation. Annu. Rev. Immunol. *15,* 351–369.

Nathaniel, C., Wallace, L.A., Burke, J., and Dirr, H.W. (2003). The role of an evolutionarily conserved *cis*-proline in the thioredoxin-like domain of human class Alpha glutathione transferase A1-1. Biochem. J. *372*, 241–246.

Nikkola, M., Gleason, F.K., Saarinen, M., Joelson, T., Björnberg, O., and Eklund, H. (1991). A putative glutathione-binding site in T4 glutaredoxin investigated by site-directed mutagenesis. J. Biol. Chem. *266*, 16105–16112.

Nordstrand, K., Åslund, F., Holmgren, A., Otting, G., and Berndt, K.D. (1999). NMR structure of *Escherichia coli* glutaredoxin 3-glutathione mixed disulfide complex: implications for the enzymatic mechanism. J. Mol. Biol. *286*, 541–552.

Oakley, A.J. (2005). Glutathione transferases: new functions. Curr. Opin. Struct. Biol. *15*, 716–723.

Østergaard, H., Henriksen, A., Hansen, F.G., and Winther, J.R. (2001). Shedding light on disulfide bond formation: engineering a redox switch in green fluorescent protein. EMBO J. *20*, 5853–5862.

Pallis, M., Bradshaw, T.D., Westwell, A.D., Grundy, M., Stevens, M.F., and Russell, N. (2003). Induction of apoptosis without redox catastrophe by thioredoxin-inhibitory compounds. Biochem. Pharmacol. *66*, 1695–1705.

Pelletier, H., and Kraut, J. (1992). Crystal structure of a complex between electron transfer partners, cytochrome c peroxidase and cytochrome c. Science *258*, 1748–1755.

Peterson, F.C., Lytle, B.L., Sampath, S., Vinarov, D., Tyler, E., Shahan, M., Markley, J.L., and Volkman, B.F. (2005). Solution structure of thioredoxin h1 from *Arabidopsis thaliana*. Protein Sci. *14*, 2195–2200.

Petersen, M.T.N., Jonson, P.H., and Petersen, S.B. (1999). Amino acid neighbours and detailed conformational analysis of cysteines in proteins. Protein Eng. *12*, 535–548.

Potters, G., de Gara, L., Asard, H., and Horemans, N. (2002). Ascorbate and Glutathione: guardians of the cell cycle, partners in crime? Plant Physiol. Biochem. *40*, 537–548.

Qin, J., Clore, G.M., Kennedy, W.M., Huth, J.R., and Gronenborn, A.M. (1995). Solution structure of human thioredoxin in a mixed disulfide intermediate complex with its target peptide from the transcription factor NFκB. Structure *3*, 289–297.

Qin, J., Clore, G.M., Kennedy, W.P., Kuszewski, J., and Gronenborn, A.M. (1996). The solution structure of human thioredoxin complexed with its target from Ref-1 reveals peptide chain reversal. Structure *4*, 613–620.

Ravelli, R.B., and McSweeney, S.M. (2000). The 'fingerprint' that X-rays can leave on structures. Structure *8*, 315–328.

Reichheld, J.P., Mestres-Ortega, D., Laloi, C., and Meyer, Y. (2002). The multigenic family of thioredoxin h in *Arabidopsis thaliana*: specific expression and stress response. Plant Physiol. Biochem. *40*, 685–690.

Reinemer, P., Dirr, H.W., Ladenstein, R., Schäffer, J., Gallay, O., and Huber, R. (1991). The three-dimensional structure of class π glutathione S-transferase in complex with glutathione sulfonate at 2.3 Å resolution. EMBO J. *10*, 1997–2005.

Rouhier, N., Gelhaye, E., and Jacquot, J.P. (2002a). Exploring the active site of plant glutaredoxin by site directed mutagenesis. FEBS Lett. *511*, 145–149.

Rouhier, N., Gelhaye, E., and Jacquot, J.P. (2002b). Glutaredoxin-dependent peroxiredoxin from poplar: protein-protein interaction and catalytic mechanism. J. Biol. Chem. *277*, 13609–13614.

Rouhier, N., Gelhaye, E., and Jacquot, J.P. (2004). Plant glutaredoxins: still mysterious reducing systems. Cell Mol. Life Sci. *61*, 1266–1277.

Rozhkova, A., and Glockshuber, R. (2007). Kinetics of the intramolecular disulfide exchange between the periplasmic domains of DsbD. J. Mol. Biol. *367*, 1162–1170.

Rozhkova, A., Stirnimann, C.U., Frei, P., Grauschopf, U., Brunisholz, R., Grütter, M.G., Capitani, G., and Glockshuber, R. (2004). Structural basis and kinetics of inter- and intramolecular disulfide exchange in the redox catalyst DsbD. EMBO J. *23*, 1709–1719.

Sarkar, N., Lemaire, S., Wu-Scharf, D., Issakidis-Bourguet, E., and Cerutti, H. (2005). Functional specialization of *Chlamydomonas reinhardtii* cytosolic thioredoxin h1 in the response to alkylation-induced DNA damage. Eukaryot. Cell *4*, 262–273.

Setterdahl, A.T., Chivers, P.T., Hirasawa, M., Lemaire, S.D., Keryer, E., Miginiac-Maslow, M., Kim, S.K., Mason, J., Jacquot, J.P., Longbine, C.C., de Lamotte-Guery, F., and Knaff, D.B. (2003). Effect of pH on the oxidation-reduction properties of thioredoxins. Biochemistry *42*, 14877–14884.

Stirnimann, C.U., Rozhkova, A., Grauschopf, U., Bockmann, R.A., Glockshuber, R., Capitani, G., and Grutter, M.G. (2006). High-resolution structures of *Escherichia coli* cDsbD in different redox states: A combined crystallographic, biochemical and computational study. J. Mol. Biol. *358*, 829–845.

Storoni, L.C., McCoy, A.J., and Read, R.J. (2004). Likelihood-enhanced fast rotation functions. Acta Crystallogr. D Biol. Crystallogr. *60*, 432–438.

Szajewski, R. P., and Whitesides, G. M. (1980). Rate constants and equilibrium constants for thiol-disulfide interchange reactions involving oxidized glutathione. J. Am. Chem. Soc. *102*, 2011–2026.

Takahashi, N., and Creighton, T.E. (1996). On the reactivity and ionization of the active site cysteine residues of *E. coli* thioredoxin. Biochemistry *35*, 8342–8353.

Thannickal, V. J., and Fanburg, B. L. (2000). Reactive oxygen species in cell signaling. Am. J. Physiol. Lung Cell. Mol. Physiol. *279,* L1005–L1028.

Toledano, M.B., Delaunay, A., Monceau, L., and Tacnet, F. (2004). Microbial H_2O_2 sensors as archetypical redox signaling modules. Trends Biochem. Sci. *29*, 351–357.

Traverso, J.A., Vignols, F., Cazalis, R., Pulido, A., Sahrawy, M., Cejudo, F.J., Meyer, Y., and Chueca, A. (2007). PsTRXh1 and PsTRXh2, are both pea (*Pisum sativum*) h-type thioredoxins with antagonistic behaviour in redox imbalances. Plant Physiol. *143*, 300–311.

Trebitsh, T., Meiri, E., Ostersetzer, O., Adam, Z., and Danon, A. (2001). The protein disulfide isomerase like RB60 is partitioned between stroma and thylakoids in *Chlamydomonas reinhardtii* chloroplasts. J. Biol. Chem. *276*, 4564–4569.

Vagin, A., and Teplyakov, A. (1997). MOLREP: an automated program for molecular replacement. J. Appl. Cryst. *30*, 1022–1025.

Vallée, F. Kadziola, A., Bourne, Y., Juy, M., Rodenburg, K.W., Svensson, B., and Haser, R. (1998). Barley α-amylase bound to its endogenous protein inhibitor BASI: crystal structure of the complex at 1.9 Å resolution. Structure *6*, 649–659.

Verdoucq, L., Vignols, F., Jacquot, J.P., Chartier, Y., and Meyer, Y. (1999). *In vivo* characterization of a thioredoxin h target protein defines a new peroxiredoxin family. J. Biol .Chem. *274*, 19714–19722.

Wahl, M.C., Irmler, A., Hecker, B., Schirmer, R.H., and Becker, K. (2004). Comparative structural analysis of oxidized and reduced thioredoxin from *Drosophila melanogaster*. J. Mol. Biol. *345*, 1119–1130.

Weichsel, A., Gasdaska, J.R., Powis, G., and Montfort, W.R. (1996). Crystal structures of reduced, oxidized, and mutated human thioredoxins: evidence for a regulatory homodimer. Structure *4*, 735–751.

Welsh, S.J., Williams, R.R., Birmingham, A., Newman, D.J., Kirkpatrick, D.L., and Powis, G. (2003). The thioredoxin redox inhibitors 1-methylpropyl 2-imidazolyl disulfide and pleurotin inhibit hypoxia-induced factor 1α and vascular endothelial growth factor formation. Mol. Cancer Ther. *2*, 235–243.

Wilkinson, B., and Gilbert, H.F. (2004). Protein disulfide isomerase. Biochim. Biophys. Acta *1699*, 35–44.

Wolosiuk, R.A., Crawford, N.A., Yee, B.C., and Buchanan, B.B. (1979). Isolation of three thioredoxins from spinach leaves. J. Biol. Chem. *254*, 1627–1632.

Wong, J.H., Kim, Y.B., Ren, P.H., Cai, N., Cho, M.J., Hedden, P., Lemaux, P.G., and Buchanan, B.B. (2002). Transgenic barley grain overexpressing thioredoxin shows evidence that the starchy endosperm communicates with the embryo and the aleurone. Proc. Natl. Acad. Sci. USA *99*, 16325–16330.

Wong, J.H., Cai, N., Tanaka, C.K., Vensel, W.H., Hurkman, W.J., and Buchanan, B.B. (2004). Thioredoxin reduction alters the solubility of proteins of wheat starchy endosperm: an early event in cereal germination. Plant Cell Physiol. *45*, 407–415.

Xia, B., Vlamis-Gardikas, A., Holmgren, A., Wright, P.E., and Dyson, H.J. (2001). Solution structure of *Escherichia coli* glutaredoxin-2 shows similarity to mammalian glutathione-S-transferases. J. Mol. Biol. *310*, 907–918.

Yang, Y., Jao, S., Nanduri, S., Starke, D.W., Mieyal, J.J., and Qin, J. (1998). Reactivity of the human thioltransferase (glutaredoxin) C7S, C25S, C78S, C82S mutant and NMR solution structure of its glutathionyl mixed disulfide intermediate reflect catalytic specificity. Biochemistry *37*, 17145–17156.

Yano, H., Wong, J.H., Lee, Y.M., Cho, M.J., and Buchanan, B.B. (2001). A strategy for the identification of proteins targeted by thioredoxin. Proc. Natl. Acad. Sci. USA *98*, 4794–4799.

Appendix I

Werhahn, W. and Braun, H.P. (2002) Biochemical dissection of the mitochondrial proteome from *Arabidopsis thaliana* by three-dimensional gel electrophoresis. *Electrophoresis*, **23**, 640–646.

Werhahn, W., Niemeyer, A., Jänsch, L., Kruft, V., Schmitz, U.K. and Braun, H.P. (2001) Purification and characterization of the preprotein translocase of the outer mitochondrial membrane from *Arabidopsis thaliana*: identification of multiple forms of TOM20. *Plant Physiol.*, **125**, 943–954.

Witte, C.P., Noel, L.D., Gielbert, J., Parker, J.E. and Romeis, T. (2004) Rapid one-step protein purification from plant material using the eight-amino acid StrepII epitope. *Plant Mol. Biol.*, **55**, 135–147.

Zerbetto, E., Vergani, L. and Dabbeni-Sala, F. (1997) Quantitation of muscle mitochondrial oxidative phosphorylation enzymes via histochemical staining of blue native polyacrylamide gels. *Electrophoresis*, **18**, 2059–2064.

4 Proteomics of disulphide and cysteine oxidoreduction

Kenji Maeda, Per Hägglund, Christine Finnie and Birte Svensson

4.1 Introduction

The proteome in a given cell, tissue or organelle of an organism is dynamic, changing both in terms of protein composition and post-translational modifications (PTMs) that alter the properties and functions of proteins. PTM of specific amino acid residues is a major regulatory mechanism in diverse physiological processes.

In protein three-dimensional structures, cysteine residues are most commonly observed in the free thiol form or in the oxidized and paired form in which two cysteine side chains are cross-linked via a disulphide bond. The reduced thiol form of cysteine is the most reactive amino acid residue present in proteins apart from the rare selenocysteine, and it is often located in the active sites of enzymes. It can also have a structural role, for example, in iron–sulphur centres of metal proteins. Disulphide bonds are important stabilizing factors of proteins due to the additional covalent bond between two sequentially separated residues. In addition, disulphide bond reduction, formation or isomerization is involved in regulation of the activity of diverse proteins.

Due to the reactive nature of its thiol group, cysteine is susceptible to several other reversible and irreversible oxidative modifications including formation of sulphenic acid (SOH), sulphinic acid (SO_2H), sulphonic acid (SO_3H) and mixed disulphides with low-molecular-weight thiols such as glutathione, cysteine and homocysteine. Cysteine in the thiol form can furthermore react reversibly with nitric oxide (NO) to give a nitrosothiol (SNO). As cysteine often has catalytic or structural roles in proteins, such modifications can profoundly influence protein function.

A wide variety of proteins catalysing cysteine redox modifications modulate an array of regulatory processes in cells. Several of these proteins such as protein disulphide isomerase (PDI) have central roles in protein folding and function and have been studied for several decades (reviewed by Wilkinson and Gilbert, 2004). Others, for example sulphiredoxin (Biteau et al., 2003) that can reduce cysteine SO_2H, have been discovered recently, emphasizing the fact that our knowledge of thiol modification mechanisms is still very incomplete. These proteins in turn are often regulated in response to cellular redox signals, and thus participate in a highly complex network concerned with redox regulation.

In this chapter we discuss the various PTMs of cysteine residues, the redox-regulatory systems in which they belong and the proteomics techniques that have been developed to analyse them.

4.2 Control of cellular redox status

Reactive oxygen/nitrogen species (ROS/RNS) such as hydrogen peroxide (H_2O_2), superoxide, singlet oxygen, NO and the hydroxyl radical can cause damage to lipids, nucleic acids and proteins and are very reactive against protein thiols. In plant tissues, ROS are produced primarily by chloroplasts and peroxisomes. However, some ROS production also takes place in the electron transport chain of the respiratory pathway in the mitochondrion (Bailly, 2004). ROS/RNS moreover have signalling roles (Foyer and Noctor, 2005), and in plants, the production is induced during developmental processes (e.g. seed germination) and by abiotic (e.g. desiccation) or biotic (e.g. pathogen attack) stresses.

A coordinated system for detoxification of ROS is required to remove the different toxic by-products of metabolism and to regulate oxidative signalling. The major control of cellular redox status is the ascorbate–glutathione cycle (Potters et al., 2002; Figure 4.1A). The enzymes of the ascorbate–glutathione cycle in plants occur in the chloroplast, mitochondrion and cytosol. Glutathione, the tripeptide γ–glutamyl–cysteinyl–glycine, is the dominant low-molecular-weight thiol in the cell, present at millimolar concentrations. The ratio of reduced (GSH) to oxidized (GSSG) glutathione is the main control of cellular redox balance including the thiol-disulphide redox status. This ratio is around 100:1 in the cytoplasm of eukaryotic cells (Hwang et al., 1992) and the maintenance of the GSH/GSSG ratio is coupled by glutathione reductase to the availability of NADPH. The reducing environment of the cytosol does not favour disulphide formation. Disulphides formed in cytosolic proteins are therefore likely to be transient and highly sensitive to changes in the redox status of the cell. In contrast to the cytoplasm the GSH/GSSG ratio is around 3:1 in the endoplasmic reticulum (ER). This more oxidizing environment permits stable disulphide bond formation. PDI catalyses disulphide formation and isomerization in the ER, and is responsible for the correct disulphide pairing in nascent secretory proteins. Although PDI has also been identified in chloroplasts of the unicellular green alga *Chlamydomonas reinhardtti* (Trebitsh et al., 2001), disulphide bonds are typically found in proteins that are processed via the secretory pathway and are generally considered to have a structural and stabilizing role. Disulphide bond reduction can be used to regulate these proteins by destabilization and increasing their susceptibility to proteolytic degradation. This mechanism is suggested for the solubilization and breakdown of cereal seed storage proteins during seed germination (Kobrehel et al., 1992). In addition to the role of glutathione in maintenance and regulation of the cellular redox state, glutathionylation of thiol groups in proteins protects them from irreversible oxidation by ROS. The glutaredoxin (Grx) system (Figure 4.1B) is responsible for the subsequent dethiolation, which also requires reducing power from NADPH, supplied via glutathione reductase. Another major system for regulation of protein thiol redox status is the thioredoxin (Trx) system that also uses reducing power from NADPH, via Trx reductases, to reduce disulphide bonds in target proteins (Figure 4.1C). It is noteworthy that several of the proteins known to be regulated by Trxs or Grxs are themselves involved in ROS

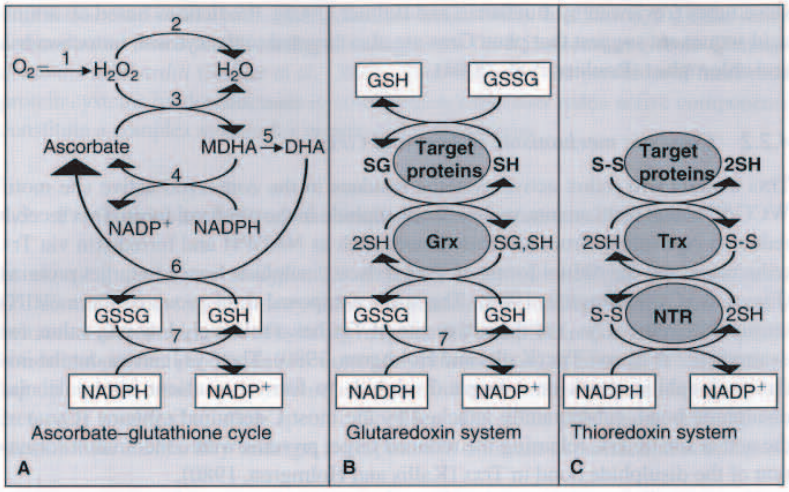

Figure 4.1 Interrelated mechanisms for control of cellular redox status. A: The ascorbate–glutathione cycle for detoxification of ROS. **B:** The glutaredoxin (Grx) system for protein dethiolation. **C:** The thioredoxin (Trx) system for protein disulphide reduction. NTR: NADP-dependent thioredoxin reductase; MDHA: monodehydroascorbate; DHA: dehydroascorbate; SH: free protein thiol group; SG: glutathionylated protein; S—S disulphide bond. Reactions involved: (1) superoxide dismutase; (2) catalase; (3) ascorbate peroxidase; (4) MDHA reductase; (5) non-enzymatic disproportionation of MDHA to DHA (and ascorbate); (6) DHA reductase; (7) glutathione reductase.

metabolism, for example Trx peroxidases are involved in peroxide detoxification (reviewed by Deitz, 2003). Cellular redox control and protein thiol status are intimately linked in a complex regulatory network that is increasingly recognized as central to plant metabolism.

4.2.1 *Sequence and structural features of proteins catalysing cysteine redox modifications*

PDIs, Trxs and Grxs carry out distinct types of oxidoreductions of cysteine residues. All of these proteins have a conserved active site motif, CXXC/S and share Trx-like folds (Martin, 1995). PDIs typically contain two Trx domains, whereas Trxs and Grxs are single domain proteins. The *Arabidopsis thaliana* genome includes at least 19 and 31 genes coding for Trxs and Grxs, respectively, in contrast to human, yeast and *Escherichia coli* (*E. coli*) which contain only a few Trx and Grx encoding genes (Meyer et al., 2002; Rouhier et al., 2004). The numerous isoforms of plant Trxs are grouped in six families based on their amino acid sequences. The f-, m-, x- and y-type are chloroplastic, the o-type is mitochondrial and the h-type is mainly cytosolic although it has also been identified in the nucleus, mitochondria and phloem

sieve tubes (reviewed by Buchanan and Balmer, 2005). Predictions based on amino acid sequences suggest that plant Grxs are also targeted to the cytosol, mitochondria and chloroplast (Rouhier et al., 2004).

4.2.2 *Catalytic mechanisms of Trxs and Grxs*

Trxs contain two redox active cysteine residues in the conserved active site motif WCG/PPC that form an intramolecular disulphide in the oxidized form. Trxs receive reducing equivalents from electron donors such as NADPH and ferredoxin via Trx reductases, and the dithiol forms of Trxs reduce disulphide bonds in target proteins (Figure 4.1C) (Holmgren, 1985). The surface-exposed thiol group of the most N-terminal cysteine (Cys_1) of the active site of Trx has a relatively low pK_a value, for example 6.7 in *E. coli* Trx (Kallis and Holmgren, 1980). The Cys_1 carries out the initial nucleophilic attack on a target disulphide to form a transient intermolecular disulphide bond, subsequently attacked by the most C-terminal cysteine (Cys_2) of the active site of Trx, releasing the reduced target proteins with concomitant formation of the disulphide bond in Trxs (Kallis and Holmgren, 1980).

Grxs typically contain the active site motif CPYC, although this sequence varies in several Grxs from *Arabidopsis*. Grxs accept reducing equivalents either from NADPH via Grx reductase or from GSH (Holmgren, 1979). Grxs are weaker reductants than Trxs, with redox potentials around −200 mV compared to about −270 mV for Trxs (Åslund et al., 1997). The thiol-pK_a value of the Grx Cys_1 is exceptionally low, for example 3.5 in yeast Grx (Gan et al., 1990), and much lower than in Trxs. Grxs preferentially reduce glutathione mixed disulphides (Gravina and Mieyal, 1993) and account for the majority of deglutathionylation activity in human cells (Chrestensen et al., 2000). Whereas both Cys_1 and Cys_2 are essential in reduction of disulphide bonds by Trxs, Cys_1 is sufficient for protein deglutathionylation by Grxs as it can receive the glutathione group from *S*-glutathionylated proteins by a single nucleophilic attack (Yang et al., 1998). In fact Cys_2 in a number of Grxs from *Arabidopsis thaliana* is replaced by serine (Rouhier et al., 2004). Grxs and Grx mutants that lack Cys_2 retain reductase activity towards *S*-glutathionylated proteins (Yang et al., 1998), dehydroascorbate (DHA) and cysteine SOH in peroxiredoxin (Rouhier et al., 2002a, b). Grxs have also been shown to catalyse protein *S*-glutathionylation (Beer et al., 2004).

While it is often possible to predict a role in redox regulation for proteins containing a CXXC/S motif, the target proteins for these reactions have proved to be highly diverse in sequence, structure and function. Currently, it is still a matter of debate to which extent the various enzyme-catalysed thiol-disulphide exchange reactions are governed by specific protein–protein interactions. Moreover, it is not yet possible to predict whether a protein is likely to be a target for one of the redox-regulatory proteins discussed here. However, some of the coexisting Trx isoforms in plants have been demonstrated to have distinct physiological functions. For instance, the two chloroplastic Trxs, Trx f and Trx m, preferentially reduce fructose-1,6-bisphosphatase and NADP-malate dehydrogenase, respectively, *in vitro* (Wolosiuk et al., 1979). *Arabidopsis thaliana* Trx h isoforms differ in their ability to substitute for endogenous

Trxs in *Saccharomyces cerevisiae* (Mouaheb et al., 1998). In addition, a similar study demonstrated functional diversity of endogenous Trx h isoforms *in vivo* in *Chlamydomonas reinhardtti* (Sarkar et al., 2005). Thus in plants, the presence of numerous protein cysteine oxidoreductases in combination with other redox active components constitute a complex system for protein redox regulation.

4.3 Proteomics techniques for analysis of cysteine modifications

In classical proteome analysis, involving two-dimensional gel electrophoresis (2-DE) and/or mass spectrometry (MS), the general approach has been to treat protein extracts with reducing and alkylating reagents for complete reduction of disulphide bonds and prevention of side reactions of cysteines. In order to study PTMs involving disulphide bonds and cysteine residues, the proteomics techniques have been creatively modified to allow specific labelling of cysteine side chains for determination of the PTMs they undergo in response to different experimental conditions.

4.3.1 *Reagents for cysteine labelling*

Reduced cysteines are very reactive and can be covalently labelled with a series of thiol-specific reagents (Table 4.1) many of which are invaluable tools for investigation of cysteine modifications in proteomes. Most of these reagents react irreversibly with cysteine residues either through substitution reactions (e.g. alkyl halides such as iodoacetamide (IAM) and iodoacetic acid (IAA)) or double bond addition reactions (e.g. vinylpyridine and *N*-ethylmaleimide (NEM)) (Figure 4.2A,B). Cysteines can also be reversibly labelled by dithiol reagents such as the Ellman's reagent (5,5′-dithio-bis(2-nitrobenzoic acid) (DTNB)) that form a mixed disulphide and can be released upon reduction (Figure 4.2C). In general, cysteine-reactive reagents act on the thiolate ion form of cysteinyl residues, and thus do not react with oxidized cysteine species such as disulphides, mixed disulphides, SOH, SO_2H and SO_3H. It should be noted that some reagents, especially outside the recommended pH-ranges, at a large excess or during prolonged incubation may also react with histidine, methionine, tyrosine and N-terminal amino groups (Bailey, 1967; Lapko et al., 2000; Boja and Fales, 2001).

A wide array of derivatives of cysteine-reactive reagents have been developed that contain chromophores (e.g. 4-dimethylaminophenylazaphenyl-4′-maleimide (BABMI)), fluorophores (e.g. iodoacetamidofluorescein) and radiolabels (e.g. [^{14}C]IAM) for visualization of proteins after sodium dodecyl sulphate-polyacrylamide gel electrophoresis (SDS-PAGE) or 2-DE or for detection after chromatographic separation (Table 4.1). In addition, high-molecular-weight reagents such as maleimide-conjugated polyethylene glycol polymer (maleimide-PEG), shift protein migration patterns in SDS-PAGE (Xiao et al., 2004). Other reagents are designed for selective enrichment or isolation of proteins and peptides. For example, biotin-conjugated reagents are used for avidin affinity chromatography and some reagents with positively

Table 4.1 Thiol-reactive reagents applied in studies of protein disulphides and cysteine oxidoreduction

Reagent	Description[a]	References
Acrylamide	Regularly used for cysteine alkylation in protocols for 2-DE and MS peptide analysis.	Brune (1992), Sechi and Chait (1998)
[2,3,3′-D_3]acrylamide	Deuterium-labelled reagent used to determine cysteine content of peptides based on the isotopic distributions in MS.	Sechi and Chait (1998)
AMS (4-acetamido-4′-maleimidylstilbene-2,2′-disulphonic acid)	Water-soluble fluorophore (322/411 nm) used in combination with SDS-PAGE and MS peptide analysis.	Kobayashi et al. 1997, Vestweber and Schatz (1988), Tie et al. (2004)
APTA (3-acrylamidopropyl)-trimethylammonium chloride	Acrylamide derivative with quaternary amine tag used for enrichment of cysteine-containing peptides by cation exchange chromatography. Induces characteristic fragmentation patterns in tandem MS.	Ren et al. (2004)
Biotin-HPDP (*N*-[6-(biotinamido)hexyl]-3′-(2′-pyridyldithio)propionamide)	Reagent for reversible labelling. Used for isolation of proteins and peptides by avidin affinity chromatography. The chromophore pyridine-2-thione (343 nm) is released upon reaction with thiol.	Jaffrey et al. (2001), Kuncewicz et al. (2003), Lindermayr et al. (2005)
Biotin-maleimide	Used for isolation of proteins and peptides by avidin affinity chromatography.	Lind et al. (2002), Hamnell-Pamment et al. (2005)
Bromoethylamine	Trypsin cleaves at cysteines aminoethylated with this reagent.	Thevis et al. (2003)
DABMI (4-dimethylaminophenylazaphenyl-4′-maleimide)	Chromophore (515 nm) that provides characteristic fragmentation patterns in MALDI-TOF MS.	Borges and Watson (2003)
DTNB	Reagent for reversible labelling. Regularly used for thiol quantification. Stoichiometrically yields the chromophore, 5-mercapto-2-nitrobenzoic acid (412 nm) upon reaction with thiols.	Laragione et al. (2003), Gevaert et al. (2004)
DTPD (4,4′-dithiopyridine)	Reagent for reversible labelling. Smaller molecule than DTNB and mostly uncharged at neutral pH. Stoichiometrically yields the chromophore, 4-thiopyridone (324 nm) upon reaction with thiols	Riener et al. (2002)
Ethylenimine	Trypsin cleaves at cysteines aminoethylated with this reagent.	Plapp et al. (1967)
IAA (Iodoacetic acid)	Negatively charged reagent regularly used for cysteine alkylation.	Galvani et al. (2001)
[^{14}C]IAA	Used for autoradiography in combination with electrophoretic protein separation.	Lee et al. (1998)
IAM (Iodoacetamide)	Regularly used for cysteine alkylation in protocols for 2-DE and MS peptide analysis.	Shevchenko et al. (1996)
[^{14}C]IAM	Used for autoradiography in combination with 2-DE.	Marchand et al. (2004)
IBTP ((4-iodobutyl)triphenyl-phosphonium)	Hydrophobic and positively charged reagent targeted into mitochondria. Used for *in vivo* labelling of mitochondrial proteins in combination with 2-DE.	Lin et al. (2002)
[D_{15}]IBTP	Stable isotope-labelled IBTP. Potentially useful for quantitative peptide analysis.	Marley et al. (2005)
ICAT reagents	Pairs of stable isotope labelled and unlabelled reagents with IAM group used for quantitative proteomics. Contain a biotin affinity tag for peptide isolation by avidin affinity chromatography.	Gygi et al. (1999), Sethuraman et al. (2004)
5-iodoacetamidofluorescein	Extensively used water-soluble fluorophore (488/530 nm).	Wu et al. (1998), Baty et al. (2002)
Iodoacetyl-biotin	Used for isolation of proteins and peptides by avidin affinity chromatography.	Kim et al. (2000), Laragione et al. (2003)
Iodoacetyl-PEO-biotin	Alternative to iodoacetyl-biotin with water-soluble PEO spacer arm.	Conrads et al. (2001), Borisov et al. (2002)
Iodoacetyl-cyanine dyes	Spectrally distinct fluorophores, Cy3 (532/580 nm) and Cy5 (633/670 nm), used for quantitative proteomics in 2-D DIGE technique.	Chan et al. (2005)
1,5-I-AEDANS (5–{2((iodoacetyl)amino(ethyl)}(amino)naphthalene-1-sulphonic acid)	Potentially useful fluorophore (336/490 nm) for quantitative proteomics based on peptide enrichment by immobilized metal affinity chromatography followed by LC-MS.	Clements et al. (2005)
Maleimide-cyanine dyes	Spectrally distinct fluorophores, Cy3 (532/580 nm) and Cy5 (633/670 nm), used for quantitative proteomics in 2-D DIGE technique.	Shaw et al. (2003), Maeda et al. (2004)
Maleimide-PEG	High-molecular-weight reagent used to shift protein migration patterns in SDS-PAGE	Xiao et al. (2004)
Methyl methanethiosulphonate	Used for reversible methylthiolation.	Jaffrey et al. 2001; Kuncewicz et al. (2003), Lindermayr et al. (2005)
Monobromobimane	Fluorescent (380/490 nm) when conjugated to thiol. Extensively used in combination with SDS-PAGE and 2-DE.	Yano et al. (2001)
NEM	Regularly used for cysteine alkylation.	Yen et al. (2002)
SBD-F (Ammonium 7-fluoro-2,1,3-benzoxadiazole-4-sulphonate)	Water-soluble fluorophore (380/505 nm) used for quantitative proteomics in combination with LC.	Toriumi and Imai (2003)
2-vinylpyridine	Can be used for cysteine alkylation below neutral pH.	Lindorff-Larsen and Winther (2000)
[D_4]2-vinylpyridine	Deuterium-labelled reagent potentially useful for quantitative proteomics.	Sebastiano et al. (2003)
4-vinylpyridine	Regularly used for cysteine alkylation in protocols for 2-DE and MS peptide analysis.	Friedman et al. (1970), Sechi and Chait (1998)

[a]In brackets, the appropriate wavelengths are indicated for chromophores (absorption wavelength) and fluorophores (extinction wavelength/emission wavelength).

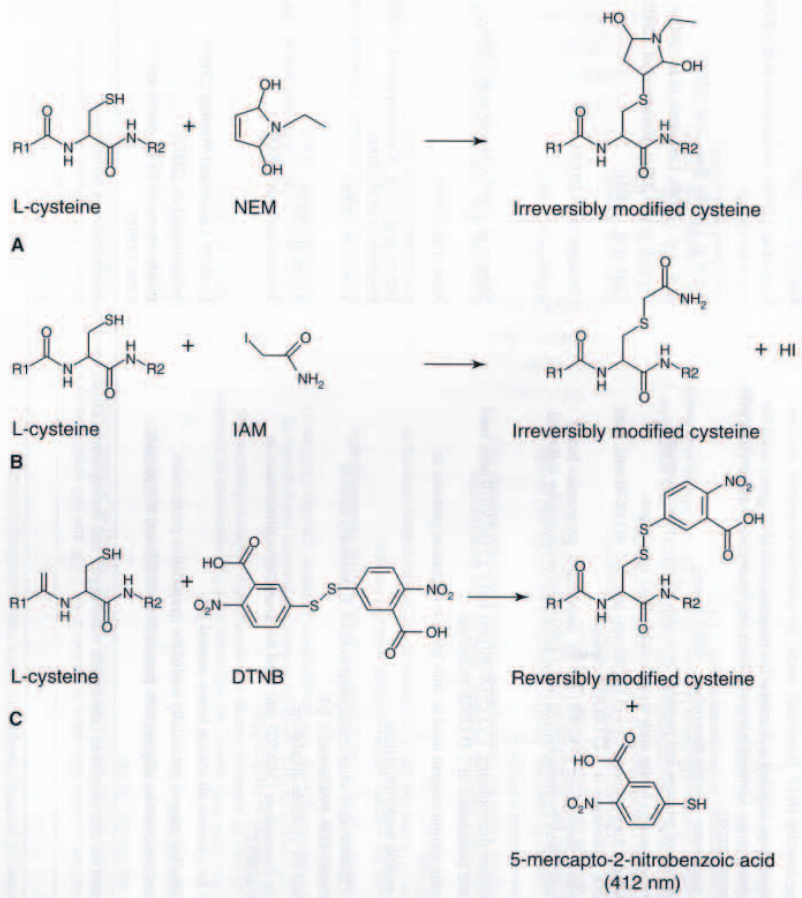

Figure 4.2 Reactions of L-cysteinyl residues with thiol-specific reagents. Examples of reactions between L-cysteinyl residues and thiol-specific reagents. **A:** NEM and other thiol-specific reagents containing reactive double bonds form irreversible conjugates with L-cysteinyl residues through addition reactions. **B:** IAM and other alkyl halides react irreversibly with L-cysteinyl residues through substitution reactions. **C:** Dithiol reagents such as DTNB react reversibly with L-cysteinyl residues to form a mixed disulphide. The released chromophore 5-mercapto-2-nitrobenzoic acid can be monitored spectrophotometrically at 412 nm. R1: N-terminal continuation of the peptide chain; R2: C-terminal continuation of the peptide chain.

charged groups can be used for immobilized metal affinity chromatography and cation exchange chromatography (Laragione et al., 2003; Ren et al., 2004; Clements et al., 2005). Modification of cysteines can also alter protein digestion patterns. Aminoethylation with bromoethylamine converts cysteine into a target for trypsin

digestion, and the N-terminal peptide bond of cysteine residues cyanylated with 1-cyano-4-dimethylamino-pyridinium tetrafluoroborate is cleaved under alkaline conditions (Wu and Watson, 1997; Thevis et al., 2003). Other promising reagents for proteome analysis of cysteine oxidoreduction are isotope-coded thiol-specific reagents such as isotope-coded affinity tags (ICAT) reagents regularly used for quantitative proteomics (Gygi et al., 1999). Sethuraman et al. (2004) introduced a technique to quantify oxidation of individual cysteine residues in complex mixtures of proteins using ICAT reagents. Briefly, a sample of a protein mixture exposed to H_2O_2 was treated with the ^{13}C-isotope-coded 'heavy' ICAT reagent and the control sample treated with the ^{12}C-isotope-coded 'light' ICAT reagent. The two samples were combined and then digested with trypsin. Labelled peptides were isolated by avidin affinity chromatography and analysed by liquid chromatography (LC) coupled to tandem MS (LC-MS/MS). Since only reduced thiol groups react with the ICAT reagents, a peptide containing a cysteine oxidized by H_2O_2 will have a light/heavy ratio higher than one. Deuterium-labelled thiol-specific reagent such as [2,3,3′-D_3]acrylamide, [D_4]2-vinylpyridine and [D_{15}](4-iodobutyl)triphenyl-phosphonium ([D_{15}]IBTP), are also potentially useful for quantification of cysteine oxidation (Sechi and Chait, 1998; Sebastiano et al., 2003; Marley et al., 2005). An alternative approach that can be used for quantitative analysis of cysteine oxidation is two-dimensional difference gel electrophoresis (2-D DIGE). In this method, which is conceptually similar to the ICAT approach, the samples to be compared are each labelled with a spectrally distinct thiol-specific fluorescent reagent, combined and separated by 2-DE. Chan et al. (2005) used iodoacetylated cyanine dyes in a 2-D DIGE approach to analyse the redox status of proteins under conditions of oxidative stress.

The chemical structure of cysteine-reactive compounds can influence their applicability for proteome research. Some reagents have been shown to provide increased ionization efficiency in MS analysis (Ren et al., 2004). Furthermore, it has been shown that certain reagents elicit specific fragmentation patterns that are useful for identification of modified peptides by MS/MS (Borisov et al., 2002; Borges and Watson, 2003). When applied to 2-DE, the choice of cysteine reagent can influence streaking (Luche et al., 2004) and charged reagents may cause migration shifts in isoelectric focusing (Shaw et al., 2003).

4.3.2 Disulphide mapping

In spite of the importance of disulphide bonds in structure and regulation, it is still not possible to predict the disulphide bond patterns of proteins from the amino acid sequence, or even to predict whether or not disulphide bonds are likely to be formed. Analysis of protein disulphide bond patterns is often very challenging. For example, the complex inter- and intramolecular disulphide bonding in seed storage proteins is still not well characterized despite considerable effort (Cunsolo et al., 2004). For purified proteins, an established and widely used approach for determination of intramolecular disulphide pairing consists in proteolytic digestion of non-reduced proteins followed by chromatographic peptide separation in reducing and non-reducing

conditions. Disulphide paired peptides, which display changed retention times after reduction, are selected for identification by MS (Gorman et al., 2002). Mildly acidic digestion conditions are preferable, since thiol-disulphide exchange reactions are known to occur at neutral, alkaline and strongly acidic pH (Bailey, 1967). Pepsin has often been used for this purpose (Gorman et al., 2002) and its broad specificity is an advantage in disulphide mapping, since peptide fragments containing a single cysteine residue are often generated. However, protein digestion with pepsin often results in a complex mixture of overlapping peptides which may complicate identification by peptide mass fingerprinting. To overcome these problems, Wallis et al. (2001) developed a method adding ^{18}O-labelled water to the digestion mixtures. Briefly, ^{18}O is incorporated in the released C-termini of the produced peptides, and disulphide-bound peptic fragments will thus contain two ^{18}O provided that neither of the fragments contain the C-terminus of the intact protein. In contrast, single chain fragments, regardless of whether they contain a disulphide bond, incorporate only one ^{18}O. MS analysis of the isotope distribution of ^{18}O-labelled peptic fragments can thus distinguish disulphide-paired peptides from other peptides. If proteolytic digestions are carried out at non-acidic pH, the free cysteines are blocked first, to avoid thiol-disulphide exchange (Yen et al., 2000).

Disulphide bonds in digested peptides are commonly validated by comparing mass spectra acquired before and after *in vitro* chemical reduction (e.g. using dithiothreitol (DTT)). Under some circumstances this reduction can be carried out directly in a matrix spot on a matrix-assisted laser desorption/ionization (MALDI) MS target (Fischer et al., 1993). Information about disulphide bond linkages may also be obtained *in situ* in the mass spectrometer. For example, fragmentation of disulphide bonds by in-source or post-source decay has been demonstrated in MALDI time-of-flight (TOF) MS and MALDI ion trap MS (Patterson and Katta, 1994; Qin and Chait, 1997; Jones et al., 1998). Furthermore, cleavage of disulphide bonds is particularly pronounced in the electron capture dissociation MS/MS fragmentation technique that is used in conjunction with Fourier transform ion cyclotron MS (Zubarev et al., 1999).

In the complex protein mixtures that are subject to proteome analysis, it is very difficult to determine the complete disulphide bond connectivity. A simpler objective may be to identify proteins linked by intermolecular disulphide bonds. Such proteins can be identified using 2-D diagonal electrophoresis, a concept originally developed by Sommer and Traut (1974). In the first dimension, proteins are separated by non-reducing SDS-PAGE and in the second dimension – at right angles to the initial direction – by reducing SDS-PAGE. Thus, proteins not linked by intermolecular disulphide bonds will line up on the diagonal, whereas protein partners in intermolecular disulphide bonds will dissociate from each other in the second dimension and migrate below the diagonal. This method combined with MS has been used to identify proteins forming intermolecular disulphide bonds in human myocytes during conditions of oxidative stress (Brennan et al., 2004).

In extracts from stem and leaf of *Arabidopsis thaliana*, Lee et al. (2004) used a novel proteomics approach to identify 65 proteins forming disulphide bonds *in vivo*.

In the first step of this procedure free thiol groups in the extracted proteins were blocked by a combination of IAM and NEM under denaturating conditions. The proteins were treated with tributylphosphine to reduce disulphides and then subjected to a thiol-affinity chromatography with sepharose-bound glutathione 2-pyridyl disulphide as the active group. In the control experiment, treatment with tributylphosphine was omitted. Using this procedure, the proteins containing disulphides *in vivo* were trapped on the affinity resin, subsequently eluted by DTT, separated by SDS-PAGE and identified by MALDI-TOF MS after tryptic digestion. The identified proteins included cytosolic proteins, proteins processed via the secretory pathway, membrane proteins and chloroplastic proteins including four known Trx targets. Also identified was ADP-glucose pyrophosphorylase (AGPase) involved in starch synthesis. In potato, AGPase forms an inactive dimer that is activated by *in vitro* treatment with DTT (Tiessen et al., 2002). Taken together, these studies support a role for redox regulation in the control of starch synthesis.

4.3.3 S-*glutathionylation*

In studies of plants and plant cells with suppressed glutathione synthesis, a requirement for GSH has been suggested for many developmental processes, for example flowering (Ogawa et al., 2001) and transition from the vegetative to the reproductive growth stage (Yanagida et al., 2004). This emphasizes the vital importance of glutathione for maintenance of the cellular redox state and protection against irreversible oxidation of cysteines.

One of the best characterized examples of the involvement of *S*-glutathionylation in regulatory signalling is the redox regulation of mammalian protein tyrosine phosphatases (PTPs). Growth factors and cytokines that stimulate cell differentiation and proliferation induce a slight increase in intracellular ROS concentration (Meier et al., 1989; Bae et al., 1997). When treated with ROS *in vitro*, PTPs are inactivated by oxidation and *S*-glutathionylation of the active site cysteine (Denu and Tanner, 1998; Lee et al., 1998; Barrett et al., 1999a). Moreover, in a cell culture treated with epidermal growth factor (EGF), the amount of the reduced form of PTP decreased (Lee et al., 1998), and the glutathionylated active site cysteine in PTP was detected by immunoprecipitation and MS (Barrett et al., 1999b). Tyrosine phosphorylation is involved in various processes in plants such as pollen development (Gupta et al., 2002) and stomatal closure (MacRobbie, 2002). Redox regulation of PTPs is likely also to occur in plants, as inhibition of two PTPs from *Arabidopsis thaliana* by H_2O_2 (Meinhard and Grill, 2001; Gupta and Luan, 2003), and *S*-glutathionylation of a soybean PTP (Dixon et al., 2005a) have been demonstrated *in vitro*. Some transcription factors are also regulated by reversible oxidations and *S*-glutathionylation of cysteine residues. Reversible *S*-glutathionylation of the transcription factor, nuclear factor I, has been suggested *in vitro* and *in vivo* to result in loss of DNA-binding activity (Bandyopadhyay et al., 1998).

Immobilized glutathione or nitrosoglutathione have been used for isolation of proteins susceptible to *in vitro S*-glutathionylation from a mixture of proteins (Klatt et al., 2000; Eaton and Shattock 2002). Proteins that are *in vivo S*-glutathionylated

under conditions of oxidative stress have been identified from human cells using a strategy for radiolabelling of cellular glutathione (Fratelli et al., 2002; Ghezzi and Bonetto, 2003). Protein synthesis was blocked by cycloheximide and [^{35}S]-labelled L-cysteine was added to cell cultures to allow selective incorporation of ^{35}S into glutathione. The cells were then exposed to oxidants, diamide (*N,N,N′,N′*-tetramethylazodicarboxamide) and H_2O_2, to induce *S*-glutathionylation and the *S*-glutathionylated proteins were detected by 2-DE and autoradiography. Alternatively, *in vivo S*-glutathionylated proteins can be detected by western blotting using anti-GSH antibodies (Wang et al., 2001; McDonagh et al., 2005).

Another approach used Grx for identification of *in vivo S*-glutathionylated proteins (Lind et al., 2002; Hamnell-Pamment et al., 2005). Here, accessible protein thiols were blocked *in vivo* with NEM and glutathione mixed disulphides were specifically reduced by Grx system after protein extraction. The newly liberated thiol groups were labelled with biotin-maleimide, and the biotionylated proteins were isolated by avidin affinity chromatography and separated by 2-DE. In a gel-free approach, proteins treated likewise with NEM, Grx system and biotin-maleimide were digested with trypsin and the biotionylated peptides were isolated by avidin affinity chromatography for analysis by LC-MS/MS and identification of the *S*-glutathionylated cysteine residues (Hamnell-Pamment et al., 2005).

A cell permeable ethyl ester derivative of GSH conjugated to biotin via a primary amine (Sullivan et al., 2000) has been used to identify proteins that are *S*-glutathionylated *in vivo* in *Arabidopsis thaliana* cell cultures (Ito et al., 2003). Briefly, the extracted proteins were fractionated by gel filtration, ion exchange and hydrophobic interaction chromatography and the biotinylated proteins were detected by using streptavidin-conjugated horseradish peroxidase. A cytosolic triose phosphate isomerase and a putative plastidic aldolase involved in the pathways of glycolysis and gluconeogenesis, respectively, were identified as *S*-glutathionylated proteins. *Arabidopsis* triose phosphate isomerase was produced in recombinant form and shown to be inhibited by *S*-glutathionylation. Inhibition of sugar metabolizing enzymes is suggested to occur under conditions of increased cellular ROS concentrations and negatively regulate the corresponding metabolic pathways to prevent further production of ROS in mitochondria and chloroplasts.

In a similar approach reported recently, *Arabidopsis* cell culture was treated with GSSH conjugated to biotin via a primary amine (GSSG-Biotin). *In vivo S*-glutathionylated proteins were affinity isolated on avidin columns and separated by 2-DE (Dixon et al., 2005b). A total of 79 proteins comprising *S*-glutathionylated proteins and proteins in complex with *S*-glutathionylated proteins were identified by MS (Dixon et al., 2005b).

4.3.4 *Cysteine SOH, SO_2H and SO_3H*

SOH represents a reversible modification of cysteine residues that is mainly formed after exposure to diverse oxidative conditions. In specific cases, SOH is also part of the catalytic cycle of enzymes, for example peroxiredoxins involved in ROS

removal (Claiborne et al., 2001). A proteomic method for identification of proteins susceptible to oxidation to SOH was described by Saurin et al. (2004). This procedure was based on selective reduction of SOH in protein extracts by arsenite and subsequent labelling of the reduced thiols by biotin-maleimide. By completely alkylating protein thiols prior to treatment with arsenite, proteins containing SOH were selectively biotinylated, detected by western blotting with streptavidin-conjugated horseradish peroxidase and isolated by avidin affinity chromatography. The method was applied to protein extracts from rat cardiac tissue.

SOH is a reactive species that can be reduced, form a disulphide, or be further oxidized to SO_2H and SO_3H. In contrast to SOH, SO_2H and SO_3H are more stable and are not reduced by common reductants such as DTT. Thus, oxidation to SO_2H and SO_3H can be observed as shifts in the migration of proteins in the first dimension of 2-DE due to the introduction of negative charges (Rabilloud et al., 2002; Wagner et al., 2002). These modifications can also be identified after enzymatic digestion using endoproteinase Asp-N that cleaves peptides on the N-terminal side of aspartic acid, SO_2H and SO_3H, but not cysteine (Drapeau, 1980). SO_2H and SO_3H modifications can thus be identified by peptide mass fingerprinting (Wagner et al., 2002). Furthermore, the mass increase of 32 Da (SO_2H) and 48 Da (SO_3H) relative to unmodified cysteine allows site-specific assignment of modified residues using MS/MS (Rabilloud et al., 2002).

4.3.5 *Trxs and disulphide reduction*

Trx was originally identified in *E. coli* as an electron donor for ribonucleotide reductase (Laurent et al., 1964). In addition to transferring reducing equivalents, Trxs specifically regulate the activity of various target proteins by disulphide bond reduction. Trx reduced and regulated the activity of the transcription factors NFκB and Ap-1 when transiently over-expressed in human cell cultures, suggesting regulatory roles of Trx in transcriptional processes (Schenk et al., 1994).

In plants, numerous Trx isoforms show diverse sub-cellular localizations (Section 4.2.1). Chloroplastic Trxs were originally identified as factors essential for photoactivation of the Calvin cycle enzyme fructose-1,6-bisphosphatase by reduction of its regulatory disulphide bond (Buchanan et al., 1971; Wolosiuk and Buchanan, 1977). In this light-dependent regulatory pathway, reducing equivalents are transferred from photosystem I to ferredoxin, an iron–sulphur protein and subsequently to Trxs via ferredoxin-dependent Trx reductase (Schürmann and Jacquot, 2000). The mainly cytosolic Trx h is abundant in seeds of different plants and is thought to be involved in the germination process (Yano et al., 2001; Marx et al., 2003). Although the functions of Trx h in seeds are poorly understood, germinating transgenic barley seeds over-expressing wheat Trx h show higher limit dextrinase activity and earlier increase in α-amylase activity compared to the non-transgenic seeds (Cho et al., 1999; Wong et al., 2002). Storage proteins in cereals are released from a disulphide-bound and poorly soluble form during germination, and Trx h has been shown to enhance this process *in vitro* (Kobrehel et al., 1992).

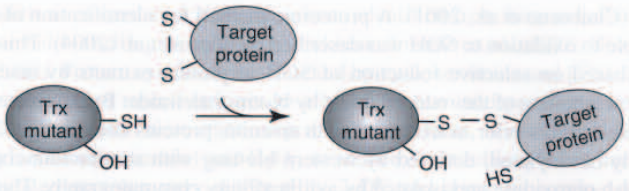

Figure 4.3 Formation of disulphide-bound complexes between thioredoxin Cys–Ser mutants and target proteins. The SH group of the most N-terminal cysteine (Cys_1) in the Trx active site carries out the initial nucleophilic attack on the target disulphide to form a intermolecular disulphide bond, whereas Cys_2 carries out the subsequent release of the reduced target protein. Thus, Trx where Cys_2 is mutated to serine forms disulphide-bound complexes with target proteins.

Recently, proteomics techniques have been applied in several studies for identification of Trx target proteins in plants. The approaches used can be categorized into three groups based on the techniques used to detect the target proteins: (1) isolation of target proteins by utilizing the formation of stable intermolecular disulphide bonds with Cys_2–Trx mutants (Verdoucq et al., 1999); (2) *in vitro* target reduction with Trxs followed by labelling of accessible thiol groups and detection of labelled proteins after 2-DE (Yano et al., 2001); (3) affinity isolation of protein–protein interaction partners of Trxs (Kumar et al., 2004).

The first strategy is based on knowledge of the reaction mechanism for the Trx catalysed reduction of disulphides in target proteins (Section 4.2.2). Thus, covalent intermediate Trx complexes with target proteins have been obtained with Trx having Cys_2 mutated to serine or alanine (Figure 4.3). By introducing polyhistidine extensions on such mutants, complexes formed between target proteins and Trx mutants can be isolated by nickel chromatography. This approach was used in yeast transformed with a mutant of *Arabidopsis* Trx h resulting in identification of a novel type of peroxiredoxin as an *in vivo* target (Verdoucq et al., 1999). Similarly, by using an immobilized Trx h mutant, a peroxiredoxin from *Chlamydomonas reinhardtii* was identified and shown to use Trx h as a hydrogen donor (Goyer et al., 2002). Immobilized Trx mutants have also been used in various other *in vitro* isolations of plant target proteins. Potential target proteins of Trx h have been identified from *Chlamydomonas reinhardtii* (Lemaire et al., 2004), from developing wheat seeds (Wong et al., 2004) and from *Arabidopsis* leaves (Yamazaki et al., 2004). Potential target proteins of f- and m-type chloroplastic Trx have also been identified from a stroma lysate of spinach chloroplasts (Motohashi et al., 2001; Balmer et al., 2003).

Fluorescence labelling of thiol groups has been applied in a survey of Trx targets in peanut seed (Yano et al., 2001). In this study, protein extracts were incubated in the presence of the Trx system (NADPH, Trx reductase and *E. coli* Trx) and subsequently labelled with the thiol-specific fluorescent reagent monobromobimane (mBBr). Control extracts were incubated in the absence of the Trx system. After separation by 2-DE, the labelled proteins were detected under ultraviolet light. By comparing

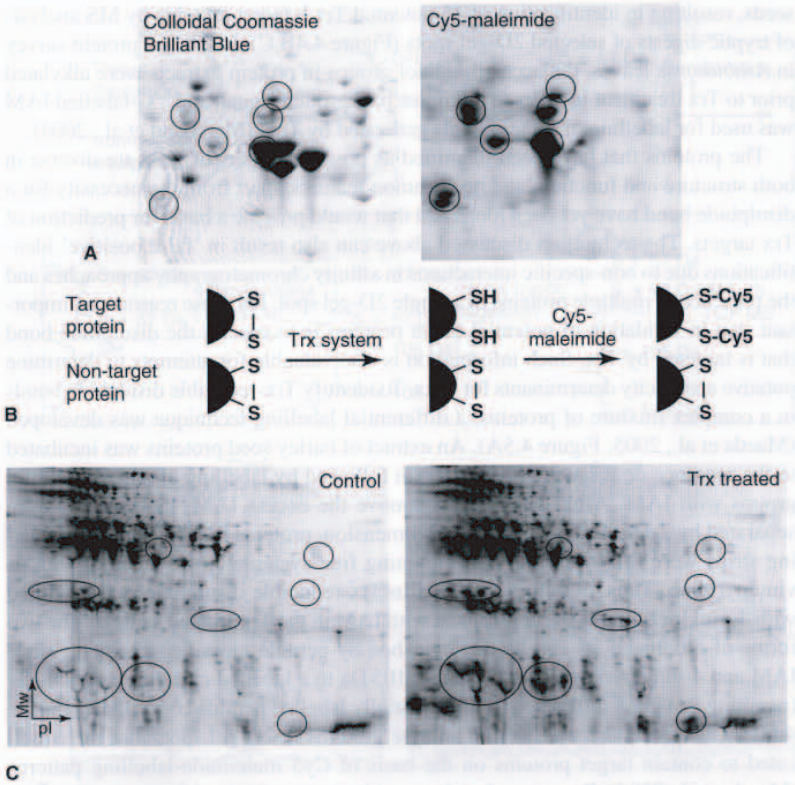

Figure 4.4 A strategy for detection of proteins targeted by Trx based on Cy5 maleimide-labelling of accessible thiol groups and 2-DE. A: Close-up view of a region in a 2D-gel of mature barley seed proteins treated with Cy5 maleimide (without reduction by Trx). Colloidal Coomassie Brilliant Blue-stained proteins (left) and Cy5 maleimide-labelled proteins (right). Proteins labelled with Cy5 maleimide are indicated with circles. **B:** The procedure for target protein identification of Trx based on Cy5 maleimide labelling (see Section 4.3.5). **C:** Cy5 maleimide-labelled proteins in barley seed extracts treated with (right) and without Trx system (left). Additional Cy5 labelled spots in the Trx-treated sample are indicated with circles. Modified from Maeda et al. (2004), with permission.

the resulting fluorescence spot patterns for the control and the Trx-treated sample, a number of proteins reduced *in vitro* by Trx were in-gel digested and identified by MS. A similar approach was used for identification of Trx-target proteins in embryos of germinated barley seeds (Marx et al., 2003). One disadvantage with mBBr is the relatively low sensitivity, thus only abundant proteins can be detected. This motivated the development of a procedure for highly sensitive and specific detection of proteins with accessible thiol groups, using the fluorescent reagent Cy5 maleimide (Maeda et al., 2004; Figure 4.4A). This method was applied on mature and germinated barley

seeds, resulting in identification of 16 potential Trx h target proteins by MS analysis of tryptic digests of selected 2D-gel spots (Figure 4.4B,C). In a target protein survey in *Arabidopsis* leaves, the accessible thiol groups in protein extracts were alkylated prior to Trx treatment in order to minimize background signal, and ^{14}C-labelled IAM was used for labelling of protein thiols generated by Trxs (Marchand et al., 2004).

The proteins that have been identified as possible targets of Trxs are diverse in both structure and function, and no common features apart from the necessity for a disulphide bond have yet been identified that would provide a basis for prediction of Trx targets. The techniques discussed above can also result in 'false positive' identifications due to non-specific interactions in affinity chromatography approaches and the presence of multiple proteins in a single 2D-gel spot. For these reasons, an important step in validation of potential target proteins is to specify the disulphide bond that is targeted by Trx. Such information is also valuable for attempts to determine putative specificity determinants for Trxs. To identify Trx-reducible disulphide bonds in a complex mixture of proteins, a differential labelling technique was developed (Maeda et al., 2005; Figure 4.5A). An extract of barley seed proteins was incubated in the presence or absence of barley Trx h followed by labelling of accessible thiol groups with IAM. After desalting to remove the excess IAM, the samples were separated by 2-DE. Prior to the second dimension, proteins in the isoelectric focusing strips were fully reduced and remaining free cysteines were labelled with 4-vinylpyridine. Thus, cysteines involved in Trx-reducible disulphides are modified with 4-vinylpyridine in the control and with IAM in the Trx-treated sample. The two forms of modifications can be distinguished by peptide mass fingerprinting since IAM and 4-vinylpyridine add 57 Da and 105 Da to a labelled cysteine, respectively (resulting in a mass difference for differentially labelled peptides of Δ 48 Da; Figure 4.5B). This procedure was used to analyse proteins in 2D-gel spots that were indicated to contain target proteins on the basis of Cy5 maleimide-labelling patterns (Maeda et al., 2004). By comparing the peptide masses obtained from samples incubated in the presence or absence of Trx, 9 disulphides in 8 proteins were identified as reducible by Trx h. This study provided an indication that some disulphides are more susceptible to Trx h reduction than others. Preferential reduction of one of the two surface-accessible disulphide bonds was observed in the barley α-amylase/subtilisin inhibitor (BASI) (Maeda et al., 2005).

Most of the approaches described so far for identification of Trx target proteins have been applied *in vitro* and therefore only indicate the susceptibility of proteins to undergo reduction. The identifications made using these methods include proteins involved in photosynthesis and carbon metabolism, defence against pathogens, oxidative stress responses and protein folding. Validation of these putative target proteins by other approaches will be required to confirm that they are targeted by Trx.

Finally, proteomics has been used to identify proteins involved in electrostatic protein–protein interactions with Trxs. Although these proteins are not necessarily reduced by Trxs, the interactions may influence the physiological roles of Trxs in redox-regulation mechanisms. In *E. coli*, 80 proteins associated *in vivo* with Trx were identified using a so-called tandem affinity purification tag containing a protein A

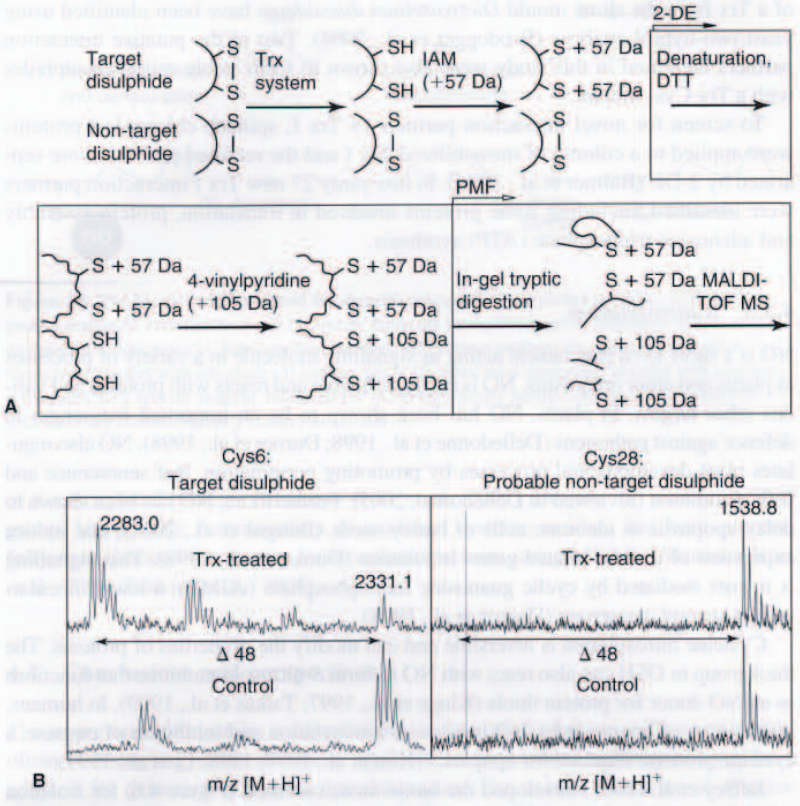

Figure 4.5 Identification of Trx reducible disulphide bonds in barley seed proteins based on differential labelling, 2-DE and MALDI-TOF MS. A: Overview of the differential labelling procedure for identification of Trx h reducible protein disulphides (see Section 4.3.5). **B:** Sections of MALDI-TOF MS spectra for the tryptic peptides of α-amylase inhibitor BMAI-1, showing differential labelling of Cys6 and Cys28, expected to be involved in different disulphide bonds (Maeda et al., 2005). In control (lower spectra), two peaks corresponding to residue 1-19 ($[M + H]^+$ 2331.1 (left)) and residue 26-39 ($[M + H]^+$ 1538.8. (right)) covering Cys6 and Cys28, respectively, in the pyridylethylated form were observed. When treated with Trx h (upper spectra), an additional peak of residue 1-19 at $[M + H]^+$ 2283.0 covering carbamidomethylated Cys6 appeared, showing that Cys6 in BMAI-1 is involved in a Trx h reducible disulphide. A peptide containing the carbamidomethylated form of Cys28 was not observed, indicating that the disulphide bond involving Cys28 is not Trx h reducible. Modified from Maeda et al. (2005), with permission.

moiety and a calmodulin-binding peptide (Kumar et al., 2004). A construct encoding Trx with the tag appended to the C-terminus was expressed in *E. coli*. Complexes associated with the tagged Trx were purified by applying *E. coli* culture extracts sequentially onto immobilized immunoglobulin G and calmodulin. Interaction partners

of a Trx from the slime mould *Dictyostelium discoideum* have been identified using yeast two-hybrid analysis (Brodegger et al., 2004). Two of the putative interaction partners identified in this study were also shown to form stable mixed disulphides with a Trx Cys_2 mutant.

To screen for novel interaction partners of Trx f, spinach chloroplast proteins were applied to a column of immobilized Trx f and the retained proteins were separated by 2-DE (Balmer et al., 2004). In this study 27 new Trx f interaction partners were identified, including some proteins involved in translation, protein assembly and adenosine triphosphate (ATP) synthesis.

4.3.6 S-*nitrosylation*

NO is a short-lived free radical acting as signalling molecule in a variety of processes in plants and other organisms. NO is easily diffusible and reacts with proteins and various other targets. In plants, NO has been shown to be an important messenger in defence against pathogens (Delledonne et al., 1998; Durner et al., 1998). NO also regulates plant developmental processes by promoting germination, leaf senescence and fruit maturation (reviewed in Delledonne, 2005). Furthermore, NO has been shown to delay apoptosis in aleurone cells of barley seeds (Beligni et al., 2002), and induce expression of disease-related genes in tobacco (Durner et al., 1998). This signalling is in part mediated by cyclic guanosine monophosphate (cGMP), a low-molecular-weight second messenger (Durner et al., 1998).

Cysteine nitrosylation is reversible and can modify the properties of proteins. The thiol group in GSH can also react with NO to form *S*-nitrosoglutathione that functions as an NO donor for protein thiols (Kluge et al., 1997; Tsikas et al., 1999). In humans, suppression of apoptosis by NO involves *S*-nitrosylation and inhibition of caspase, a cysteine protease required for apoptosis (Kim et al., 1997, 1998; Li et al., 1999).

Jaffrey et al. (2001) developed the biotin switch method (Figure 4.6) for isolation and identification of *in vitro* and *in vivo* *S*-nitrosylated proteins (Kuncewicz et al., 2003, Martinez-Ruiz et al., 2005). Briefly, free thiol forms of cysteine residues are blocked with the thiol-reactive reagent, methyl methanethiosulphonate. Subsequently, SNO groups are specifically reduced with ascorbate and the resulting free thiol groups are labelled with the thiol-specific biotin reagent, *N*-[6-(biotinamido) hexyl]-3′-(2′-pyridyldithio)propionamide (Biotin-HPDP).

Using the biotin switch method in combination with nano-LC-MS/MS, 63 *in vitro* *S*-nitrosylated proteins were identified in *Arabidopsis* cell cultures (Lindermayr et al., 2005). These included stress-related proteins, signalling and regulating proteins, redox-related proteins, cytoskeleton proteins, metabolic proteins and others. Moreover, 52 proteins from *Arabidopsis* leaves were identified to be *in vivo* *S*-nitrosylated, including several photosynthetic enzymes. These results suggest that *S*-nitrosylation, in addition to Trx-mediated regulation, is involved in the control of photosynthesis mediated through cysteine modifications (Lindermayr et al., 2005).

S-nitrosylation can also be detected using anti-SNO antibodies. These have been used to detect *S*-nitrosylation *in vivo* (Gow et al., 2002) and for immunoprecipitation

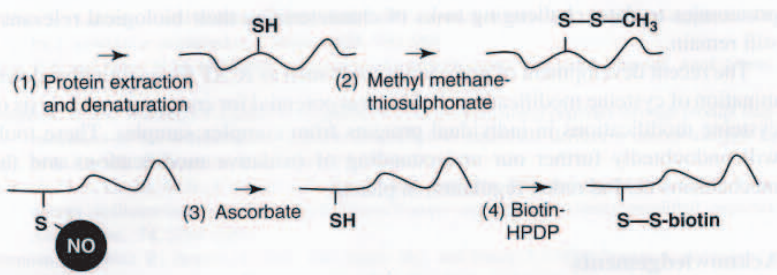

Figure 4.6 The biotin switch method for identification of *S*-nitrosylated proteins. Following protein extraction and denaturation (1), protein thiols are methylthiolated by treatment with methyl methanethiosulphonate (2). Subsequently, nitrosylated cysteine residues are reduced to the thiol forms by treatment with ascorbate (3) and the newly liberated thiol groups are labelled with a biotin-conjugated thiol-specific reagent, biotin-HPDP (4) to specifically purify *S*-nitrosylated proteins by avidin affinity chromatography (Jaffrey et al., 2001).

of *S*-nitrosylated proteins (Martinez-Ruiz et al., 2005). Despite the lability of SNO group, site-specific determination of modified cysteine residues has been successfully demonstrated for *in vitro* *S*-nitrosylated proteins using MS/MS (Martinez-Ruiz et al., 2005; Taldone et al., 2005).

4.4 Conclusions and perspectives

The importance of cysteine oxidoreduction in control of plant signalling and metabolism is becoming more and more apparent as proteomics techniques have been adapted for detection of cysteine modifications. The unique reactivity of cysteine thiol groups means that they are susceptible to modification by many molecules present in plant cells under different conditions, and it is likely that even more modification mechanisms remain to be identified. For each modification identified there may also be an associated regulatory protein to catalyse its removal, as in the case of the recently identified sulphiredoxin (Biteau et al., 2003).

Proteomics studies have led to the identification of many proteins that undergo cysteine oxidoreduction under various experimental conditions *in vitro* and *in vivo*. However, proteomics approaches require improvements if the whole picture of cysteine oxidoreduction in proteins is to be resolved. Proteome analysis of cysteine oxidoreduction has mostly been focused on abundant water-soluble proteins. Moreover, the identified candidate proteins for redox regulation must be validated by other means before the biological significance of the regulatory mechanism can be evaluated. In order to be biologically relevant, an experimentally observed cysteine oxidoreduction should occur under physiological conditions in response to a signal. The modification must also affect the function of the protein. Thus, although large numbers of proteins susceptible to cysteine modification have been identified by

proteomics to date, challenging tasks of characterizing their biological relevance still remain.

The recent development of proteomics tools such as ICAT for quantitative determination of cysteine modifications holds great potential for comparative analysis of cysteine modifications in individual proteins from complex samples. These tools will undoubtedly further our understanding of oxidative modifications and the mechanisms behind redox regulation in plants.

Acknowledgements

The authors acknowledge the Danish Technical Research Council (STVF) for financial support. C.F. is supported by a grant from the Danish Agricultural and Veterinary Research Council (SJVF). K.M. is supported by a Ph.D. scholarship from the Technical University of Denmark.

References

Åslund, F., Berndt, K.D. and Holmgren, A. (1997) Redox potentials of glutaredoxins and other thiol-disulfide oxidoreductases of the thioredoxin superfamily determined by direct protein-protein redox equilibria. *J. Biol. Chem.*, **272**, 30780–30786.

Bae, Y.S., Kang, S.W., Seo, M.S., Baines, I.C., Tekle, E., Chock, P.B. and Rhee, S.G. (1997) Epidermal growth factor (EGF)-induced generation of hydrogen peroxide. Role in EGF receptor-mediated tyrosine phosphorylation. *J. Biol. Chem.*, **272**, 217–221.

Bailey, J.L. (1967) *Techniques in Protein Chemistry*, Elsevier publishing company, Amsterdam.

Bailly, C. (2004) Active oxygen species and antioxidants in seed biology. *Seed Sci. Res.*, **14**, 93–107.

Balmer, Y., Koller, A., del Val, G., Manieri, W., Schurmann, P. and Buchanan, B.B. (2003) Proteomics gives insight into the regulatory function of chloroplast thioredoxins. *Proc. Natl Acad. Sci. USA*, **100**, 370–375.

Balmer, Y., Koller, A., del Val, G., Schürmann, P. and Buchanan, B.B. (2004) Proteomics uncovers proteins interacting electrostatically with thioredoxin in chloroplasts. *Photosynth. Res.*, **79**, 275–280.

Bandyopadhyay, S., Starke, D.W., Mieyal, J.J. and Gronostajski, R.M. (1998) Thioltransferase (glutaredoxin) reactivates the DNA-binding activity of oxidation-inactivated nuclear factor I. *J. Biol. Chem.*, **273**, 392–397.

Barrett, W.C., DeGnore, J.P., Keng, Y.F., Zhang, Z.Y., Yim, M.B. and Chock, P.B. (1999a) Roles of superoxide radical anion in signal transduction mediated by reversible regulation of protein-tyrosine phosphatase 1B. *J. Biol. Chem.*, **274**, 34543–34546.

Barrett, W.C., DeGnore, J.P., Konig, S., Fales, H.M., Keng, Y.F., Zhang, Z.Y., Yim, M.B. and Chock, P.B. (1999b) Regulation of PTP1B via glutathionylation of the active site cysteine 215. *Biochemistry*, **38**, 6699–6705.

Baty, J.W., Hampton, M.B. and Winterbourn, C.C. (2002) Detection of oxidant sensitive thiol proteins by fluorescence labeling and two-dimensional electrophoresis. *Proteomics*, **2**, 1261–1266.

Beer, S.M., Taylor, E.R., Brown, S.E., Dahm, C.C., Costa, N.J., Runswick, M.J. and Murphy, M.P. (2004) Glutaredoxin 2 catalyzes the reversible oxidation and glutathionylation of mitochondrial membrane thiol proteins: implications for mitochondrial redox regulation and antioxidant defense. *J. Biol. Chem.*, **279**, 47939–47951.

Beligni, M.V., Fath, A., Bethke, P.C., Lamattina, L. and Jones, R.L. (2002) Nitric oxide acts as an antioxidant and delays programmed cell death in barley aleurone layers. *Plant Physiol.*, **129**, 1642–1650.

Biteau, B., Labarre, J. and Toledano, M.B. (2003) ATP-dependent reduction of cysteine-sulphinic acid by *S. cerevisiae* sulphiredoxin. *Nature*, **425**, 980–984.

Boja, E.S. and Fales, H.M. (2001) Overalkylation of a protein digest with iodoacetamide. *Anal. Chem.*, **73**, 3576–3582.

Borges, C.R. and Watson, J.T. (2003) Recognition of cysteine-containing peptides through prompt fragmentation of the 4-dimethylaminophenylazophenyl-4′-maleimide derivative during analysis by MALDI-MS. *Protein Sci.*, **12**, 1567–1572.

Borisov, O.V., Goshe, M.B., Conrads, T.P., Rakov, V.S., Veenstra, T.D. and Smith, R.D. (2002) Low-energy collision-induced dissociation fragmentation analysis of cysteinyl-modified peptides. *Anal. Chem.*, **74**, 2284–2292.

Brennan, J.P., Wait, R., Begum, S., Bell, J.R., Dunn, M.J. and Eaton, P. (2004) Detection and mapping of widespread intermolecular protein disulfide formation during cardiac oxidative stress using proteomics with diagonal electrophoresis. *J. Biol. Chem.*, **279**, 41352–41360.

Brodegger, T., Stockmann, A., Oberstrass, J., Nellen, W. and Follmann, H. (2004) Novel thioredoxin targets in *Dictyostelium discoideum* identified by two-hybrid analysis: interactions of thioredoxin with elongation factor 1alpha and yeast alcohol dehydrogenase. *Biol. Chem.*, **385**, 1185–1192.

Brune, D.C. (1992) Alkylation of cysteine with acrylamide for protein sequence analysis. *Anal. Biochem.*, **207**, 285–290.

Buchanan, B.B. and Balmer, Y. (2005) Redox regulation: a broadening horizon. *Annu. Rev. Plant Biol.*, **56**, 187–220.

Buchanan, B.B., Schurmann, P. and Kalberer, P.P. (1971) Ferredoxin-activated fructose diphosphatase of spinach chloroplasts. Resolution of the system, properties of the alkaline fructose diphosphatase component, and physiological significance of the ferredoxin-linked activation. *J. Biol. Chem.*, **246**, 5952–5959.

Chan, H.L., Gharbi, S., Gaffney, P.R., Cramer, R., Waterfield, M.D. and Timms, J.F. (2005) Proteomic analysis of redox- and ErbB2-dependent changes in mammary luminal epithelial cells using cysteine- and lysine-labelling two-dimensional difference gel electrophoresis. *Proteomics*, **5**, 2908–2926.

Cho, M.J., Wong, J.H., Marx, C., Jiang, W., Lemaux, P.G. and Buchanan, B.B. (1999) Overexpression of thioredoxin h leads to enhanced activity of starch debranching enzyme (pullulanase) in barley grain. *Proc. Natl Acad. Sci. USA*, **96**, 14641–14646.

Chrestensen, C.A., Starke, D.W. and Mieyal, J.J. (2000) Acute cadmium exposure inactivates thioltransferase (Glutaredoxin), inhibits intracellular reduction of protein-glutathionyl-mixed disulfides, and initiates apoptosis. *J. Biol. Chem.*, **275**, 26556–26565.

Claiborne, A., Mallett, T.C., Yeh, J.I., Luba, J. and Parsonage, D. (2001) Structural, redox, and mechanistic parameters for cysteine-sulfenic acid function in catalysis and regulation. *Adv. Protein Chem.*, **58**, 215–276.

Clements, A., Johnston, M.V., Larsen, B.S. and McEwen, C.N. (2005) Fluorescence-based peptide labeling and fractionation strategies for analysis of cysteine-containing peptides. *Anal. Chem.*, **77**, 4495–4502.

Conrads, T.P., Alving, K., Veenstra, T.D., Belov, M.E., Anderson, G.A., Anderson, D.J., Lipton, M.S., Pasa-Tolic, L., Udseth, H.R., Chrisler, W.B., Thrall, B.D. and Smith, R.D. (2001) Quantitative analysis of bacterial and mammalian proteomes using a combination of cysteine affinity tags and 15N-metabolic labelling. *Anal. Chem.*, **73**, 2132–2139.

Cunsolo, V., Foti, S. and Saletti, R. (2004) Mass spectrometry in the characterization of cereal seed proteins. *Eur. J. Mass Spectrom.*, **10**, 359–370.

Deitz, K.J. (2003) Plant peroxiredoxins. *Annu. Rev. Plant Biol.*, **54**, 93–107.

Delledonne, M. (2005) NO news is good news for plants. *Curr. Opin. Plant Biol.*, **8**, 390–396.

Delledonne, M., Xia, Y., Dixon, R.A. and Lamb, C. (1998) Nitric oxide functions as a signal in plant disease resistance. *Nature*, **394**, 585–588.

Denu, J.M. and Tanner, K.G. (1998) Specific and reversible inactivation of protein tyrosine phosphatases by hydrogen peroxide: evidence for a sulfenic acid intermediate and implications for redox regulation. *Biochemistry*, **37**, 5633–5642.

Dixon, D.P., Fordham-Skelton, A.P. and Edwards, R. (2005a) Redox regulation of a soybean tyrosine-specific protein phosphatase. *Biochemistry*, **44**, 7696–7703.

Dixon, D.P., Skipsey, M., Grundy, N.M. and Edwards, R. (2005b) Stress-induced protein S-glutathionylation in *Arabidopsis*. *Plant Physiol.*, **138**, 2233–2244.

Drapeau, G.R. (1980) Substrate specificity of a proteolytic enzyme isolated from a mutant of *Pseudomonas fragi*. *J. Biol. Chem.*, **255**, 839–840.

Durner, J., Wendehenne, D. and Klessig, D.F. (1998) Defense gene induction in tobacco by nitric oxide, cyclic GMP, and cyclic ADP-ribose. *Proc. Natl Acad. Sci. USA*, **95**, 10328–10333.

Eaton, P. and Shattock, M.J. (2002) Purification of proteins susceptible to oxidation at cysteine residues: identification of malate dehydrogenase as a target for S-glutathiolation. *Ann. NY Acad. Sci.*, **973**, 529–532.

Fischer, W.H., Rivier, J.E. and Craig, A.G. (1993) *In situ* reduction suitable for matrix-assisted laser desorption/ionization and liquid secondary ionization using tris(2-carboxyethyl)phosphine. *Rapid Commun. Mass Spectrom.*, **7**, 225–228.

Friedman, M., Krull, L.H. and Cavins, J.F. (1970) The chromatographic determination of cystine and cysteine residues in proteins as s-beta-(4-pyridylethyl)cysteine. *J. Biol. Chem.*, **245**, 3868–3871.

Foyer, C.H. and Noctor, G. (2005) Oxidant and antioxidant signalling in plants: a re-evaluation of the concept of oxidative stress in a physiological context. *Plant Cell Environ.*, **28**, 1056–1071.

Fratelli, M., Demol, H., Puype, M., Casagrande, S., Eberini, I., Salmona, M., Bonetto, V., Mengozzi, M., Duffieux, F., Miclet, E., Bachi, A., Vandekerckhove, J., Gianazza, E. and Ghezzi, P. (2002) Identification by redox proteomics of glutathionylated proteins in oxidatively stressed human T lymphocytes. *Proc. Natl Acad. Sci. USA*, **99**, 3505–3510.

Galvani, M., Rovatti, L., Hamdan, M., Herbert, B. and Righetti, P.G. (2001) Protein alkylation in the presence/absence of thiourea in proteome analysis: a matrix assisted laser desorption/ionization-time of flight-mass spectrometry investigation. *Electrophoresis*, **22**, 2066–2074.

Gan, Z.R., Sardana, M.K., Jacobs, J.W. and Polokoff, M.A. (1990) Yeast thioltransferase – the active site cysteines display differential reactivity. *Arch. Biochem. Biophys.*, **282**, 110–115.

Gevaert, K., Ghesquiere, B., Staes, A., Martens, L., Van Damme, J., Thomas, G.R. and Vandekerckhove, J. (2004) Reversible labeling of cysteine-containing peptides allows their specific chromatographic isolation for non-gel proteome studies. *Proteomics*, **4**, 897–908.

Ghezzi, P. and Bonetto, V. (2003) Redox proteomics: identification of oxidatively modified proteins. *Proteomics*, **3**, 1145–1153.

Gorman, J.J., Wallis, T.P. and Pitt, J.J. (2002) Protein disulfide bond determination by mass spectrometry. *Mass Spectrom. Rev.*, **21**, 183–216.

Gow, A.J., Chen, Q.P., Hess, D.T., Day, B.J., Ischiropoulos, H. and Stamler, J.S. (2002) Basal and stimulated protein S-nitrosylation in multiple cell types and tissues. *J. Biol. Chem.*, **277**, 9637–9640.

Goyer, A., Haslekas, C., Miginiac-Maslow, M., Klein, U., Le Marechal, P., Jacquot, J.P. and Decottignies, P. (2002) Isolation and characterization of a thioredoxin-dependent peroxidase from *Chlamydomonas reinhardtii*. *Eur. J. Biochem.*, **269**, 272–282.

Gravina, S.A. and Mieyal, J.J. (1993) Thioltransferase is a specific glutathionyl mixed disulfide oxidoreductase. *Biochemistry*, **32**, 3368–3376.

Gupta, R. and Luan, S. (2003) Redox control of protein tyrosine phosphatases and mitogen-activated protein kinases in plants. *Plant Physiol.*, **132**, 1149–1152.

Gupta, R., Ting, J.T., Sokolov, L.N., Johnson, S.A. and Luan, S. (2002) A tumor suppressor homolog, AtPTEN1, is essential for pollen development in *Arabidopsis*. *Plant Cell*, **14**, 2495–2507.

Gygi, S.P., Rist, B., Gerber, S.A., Turecek, F., Gelb, M.H. and Aebersold, R. (1999) Quantitative analysis of complex protein mixtures using isotope-coded affinity tags. *Nat. Biotechnol.*, **17**, 994–999.

Hamnell-Pamment, Y., Lind, C., Palmberg, C., Bergman, T. and Cotgreave, I.A. (2005) Determination of site-specificity of *S*-glutathionylated cellular proteins. *Biochem. Biophys. Res. Commun.*, **332**, 362–369.

Holmgren, A. (1979) Glutathione-dependent synthesis of deoxyribonucleotides. Characterization of the enzymatic mechanism of *Escherichia coli* glutaredoxin. *J. Biol. Chem.*, **254**, 3672–3678.

Holmgren, A. (1985) Thioredoxin. *Annu. Rev. Biochem.*, **54**, 237–271.

Hwang, C., Sinskey, A.J. and Lodish, H.F. (1992) Oxidized redox state of glutathione in the endoplasmic reticulum. *Science*, **25**, 1496–1502.

Ito, H., Iwabuchi, M. and Ogawa, K. (2003) The sugar-metabolic enzymes aldolase and triose-phosphate isomerase are targets of glutathionylation in *Arabidopsis thaliana*: detection using biotinylated glutathione. *Plant Cell Physiol.*, **44**, 655–660.

Jaffrey, S.R., Erdjument-Bromage, H., Ferris, C.D., Tempst, P. and Snyder, S.H. (2001) Protein S-nitrosylation: a physiological signal for neuronal nitric oxide. *Nat. Cell. Biol.*, **3**, 193–197.

Jones, M.D., Patterson, S.D. and Lu, H.S. (1998) Determination of disulfide bonds in highly bridged disulfide-linked peptides by matrix-assisted laser desorption/ionization mass spectrometry with postsource decay. *Anal. Chem.*, **70**, 136–143.

Kallis, G.B. and Holmgren, A. (1980) Differential reactivity of the functional sulfhydryl groups of cysteine-32 and cysteine-35 present in the reduced form of thioredoxin from *Escherichia coli*. *J. Biol. Chem.*, **255**, 10261–10265.

Kim, Y.M., Talanian, R.V. and Billiar, T.R. (1997) Nitric oxide inhibits apoptosis by preventing increases in caspase-3-like activity via two distinct mechanisms. *J. Biol. Chem.*, **272**, 31138–31148.

Kim, Y.M., Talanian, R.V., Li, J. and Billiar, T.R. (1998) Nitric oxide prevents IL-1β and IFN-γ-inducing factor (IL-18) release from macrophages by inhibiting caspase-1 (IL-1β-converting enzyme). *J. Immunol.*, **161**, 4122–4128.

Kim, J.R., Yoon, H.W., Kwon, K.S., Lee, S.R. and Rhee, S.G. (2000) Identification of proteins containing cysteine residues that are sensitive to oxidation by hydrogen peroxide at neutral pH. *Anal. Biochem.*, **283**, 214–221.

Klatt, P., Pineda Molina, E., Perez-Sala, D. and Lamas, S. (2000) Novel application of S-nitrosoglutathione-Sepharose to identify proteins that are potential targets for S-nitrosoglutathione-induced mixed-disulphide formation. *Biochem. J.*, **349**, 567–578.

Kluge, I., Gutteck-Amsler, U., Zollinger, M. and Do, K.Q. (1997) *S*-nitrosoglutathione in rat cerebellum: identification and quantification by liquid chromatography-mass spectrometry. *J. Neurochem.*, **69**, 2599–2607.

Kobayashi, T., Kishigami, S., Sone, M., Inokuchi, H., Mogi, T. and Ito, K. (1997) Respiratory chain is required to maintain oxidized states of the DsbA-DsbB disulfide bond formation system in aerobically growing *Escherichia coli* cells. *Proc. Natl Acad. Sci. USA*, **94**, 11857–11862.

Kobrehel, K., Wong, J.H., Balogh, A., Kiss, F., Yee, B.C. and Buchanan, B.B. (1992) Specific reduction of wheat storage proteins by thioredoxin h. *Plant Physiol.*, **99**, 919–924.

Kumar, J.K., Tabor, S. and Richardson, C.C. (2004) Proteomic analysis of thioredoxin-targeted proteins in *Escherichia coli*. *Proc. Natl Acad. Sci. USA*, **101**, 3759–3764.

Kuncewicz, T., Sheta, E.A., Goldknopf, I.L. and Kone, B.C. (2003) Proteomic analysis of S-nitrosylated proteins in mesangial cells. *Mol. Cell. Proteomics*, **2**, 156–163.

Lapko, V.N., Smith, D.L. and Smith, J.B. (2000) Identification of an artifact in the mass spectrometry of proteins derivatized with iodoacetamide. *J. Mass Spectrom.*, **35**, 572–575.

Laragione, T., Bonetto, V., Casoni, F., Massignan, T., Bianchi, G., Gianazza, E. and Ghezzi, P. (2003) Redox regulation of surface protein thiols: identification of integrin α-4 as a molecular target by using redox proteomics *Proc. Natl Acad. Sci. USA*, **100**, 14737–14741.

Laurent, T.C., Moore, E.C. and Reichard, P. (1964) Enzymatic synthesis of deoxyribonucleotides. IV. Isolation and characterization of thioredoxin, the hydrogen donor from *Escherichia coli* B. *J. Biol. Chem.*, **239**, 3436–3444.

Lee, S.R., Kwon, K.S., Kim, S.R. and Rhee, S.G. (1998) Reversible inactivation of protein-tyrosine phosphatase 1B in A431 cells stimulated with epidermal growth factor. *J. Biol. Chem.*, **273**, 15366–15372.

Lee, K., Lee, J., Kim, Y., Bae, D., Kang, K.Y., Yoon, S.C. and Lim, D. (2004) Defining the plant disulfide proteome. *Electrophoresis*, **25**, 532–541.

Lemaire, S.D., Guillon, B., Le Marechal, P., Keryer, E., Miginiac-Maslow, M. and Decottignies, P. (2004) New thioredoxin targets in the unicellular photosynthetic eukaryote *Chlamydomonas reinhardtii*. *Proc. Natl Acad. Sci. USA*, **101**, 7475–7480.

Li, J., Bombeck, C.A., Yang, S., Kim, Y.M. and Billiar, T.R. (1999) Nitric oxide suppresses apoptosis via interrupting caspase activation and mitochondrial dysfunction in cultured hepatocytes. *J. Biol. Chem.*, **274**, 17325–17333.

Lin, T.K., Hughes, G., Muratovska, A., Blaikie, F.H., Brookes, P.S., Darley-Usmar, V., Smith, R.A. and Murphy, M.P. (2002) Specific modification of mitochondrial protein thiols in response to oxidative stress: a proteomics approach. *J. Biol. Chem.*, **277**, 17048–17056.

Lind, C., Gerdes, R., Hamnell, Y., Schuppe-Koistinen, I., von Lowenhielm, H.B., Holmgren, A. and Cotgreave, I.A. (2002) Identification of S-glutathionylated cellular proteins during oxidative stress and constitutive metabolism by affinity purification and proteomic analysis. *Arch. Biochem. Biophys.*, **406**, 229–240.

Lindermayr, C., Saalbach, G. and Durner, J. (2005) Proteomic identification of S-nitrosylated proteins in *Arabidopsis*. *Plant Physiol.*, **137**, 921–930.

Lindorff-Larsen, K. and Winther, J.R. (2000) Thiol alkylation below neutral pH. *Anal. Biochem.*, **286**, 308–310.

Luche, S., Diemer, H., Tastet, C., Chevallet, M., Van Dorsselaer, A., Leize-Wagner, E. and Rabilloud, T. (2004) About thiol derivatization and resolution of basic proteins in two-dimensional electrophoresis. *Proteomics*, **4**, 551–561.

MacRobbie, E.A. (2002) Evidence for a role for protein tyrosine phosphatase in the control of ion release from the guard cell vacuole in stomatal closure. *Proc. Natl Acad. Sci. USA*, **99**, 11963–11968.

Maeda, K., Finnie, C. and Svensson, B. (2004) Cy5 maleimide labelling for sensitive detection of free thiols in native protein extracts: identification of seed proteins targeted by barley thioredoxin h isoforms. *Biochem. J.*, **378**, 497–507.

Maeda, K., Finnie, C. and Svensson, B. (2005) Identification of thioredoxin h-reducible disulphides in proteomes by differential labelling of cysteines: insight into recognition and regulation of proteins in barley seeds by thioredoxin h. *Proteomics*, **5**, 1634–1644.

Marchand, C., Le Marechal, P., Meyer, Y., Miginiac-Maslow, M., Issakidis-Bourguet, E. and Decottignies, P. (2004) New targets of *Arabidopsis* thioredoxins revealed by proteomic analysis. *Proteomics*, **4**, 2696–2706.

Marley, K., Mooney, D.T., Clark-Scannell, G., Tong, T.T., Watson, J., Hagen, T.M., Stevens, J.F. and Maier, C.S. (2005) Mass tagging approach for mitochondrial thiol proteins. *J. Proteome Res.*, **4**, 1403–1412.

Martin, J.L. (1995) Thioredoxin – a fold for all reasons. *Structure*, **3**, 245–250.

Martinez-Ruiz, A., Villanueva, L., Gonzalez de Orduna, C., Lopez-Ferrer, D., Higueras, M.A., Tarin, C., Rodriguez-Crespo, I., Vazquez, J. and Lamas, S. (2005) S-nitrosylation of Hsp90 promotes the inhibition of its ATPase and endothelial nitric oxide synthase regulatory activities. *Proc. Natl Acad. Sci. USA*, **102**, 8525–8530.

Marx, C., Wong, J.H. and Buchanan, B.B. (2003) Thioredoxin and germinating barley: targets and protein redox changes. *Planta*, **216**, 454–460.

McDonagh, B., Tyther, R. and Sheehan, D. (2005) Carbonylation and glutathionylation of proteins in the blue mussel *Mytilus edulis* detected by proteomic analysis and Western blotting: Actin as a target for oxidative stress. *Aquat. Toxicol.*, **73**, 315–326.

Meier, B., Radeke, H.H., Selle, S., Younes, M., Sies, H., Resch, K. and Habermehl, G.G. (1989) Human fibroblasts release reactive oxygen species in response to interleukin-1 or tumour necrosis factor-α. *Biochem. J.*, **263**, 539–545.

Meinhard, M. and Grill, E. (2001) Hydrogen peroxide is a regulator of ABI1, a protein phosphatase 2C from *Arabidopsis*. *FEBS Lett.*, **508**, 443–446.

Meyer, Y., Vignols, F. and Reichheld, J.P. (2002) Classification of plant thioredoxins by sequence similarity and intron position; *Method Enzymol.*, **347**, 394–402.

Motohashi, K., Kondoh, A., Stumpp, M.T. and Hisabori, T. (2001) Comprehensive survey of proteins targeted by chloroplast thioredoxin. *Proc. Natl Acad. Sci. USA*, **98**, 11224–11229.

Mouaheb, N., Thomas, D., Verdoucq, L., Monfort, P. and Meyer, Y. (1998) *In vivo* functional discrimination between plant thioredoxins by heterologous expression in the yeast *Saccharomyces cerevisiae*. *Proc. Natl Acad. Sci. USA*, **95**, 3312–3317.

Ogawa, K., Tasaka, Y., Mino, M., Tanaka, Y. and Iwabuchi, M. (2001) Association of glutathione with flowering in *Arabidopsis thaliana*. *Plant Cell Physiol.*, **42**, 524–530.

Patterson, S.D. and Katta, V. (1994) Prompt fragmentation of disulfide-linked peptides during matrix-assisted laser desorption ionization mass spectrometry. *Anal. Chem.*, **66**, 3727–3732.

Plapp, B.V., Raftery, M.A. and Cole, R.D. (1967) The tryptic digestion of S-aminoethylated ribonuclease. *J. Biol. Chem.*, **242**, 265–270.

Potters, G., de Gara, L., Asard, H. and Horemans, N. (2002) Ascorbate and Gutathione: guardians of the cell cycle, partners in crime? *Plant Physiol. Biochem.*, **40**, 537–548.

Qin, J. and Chait, B.T. (1997) Identification and characterization of posttranslational modifications of proteins by MALDI ion trap mass spectrometry. *Anal. Chem.*, **69**, 4002–4009.

Rabilloud, T., Heller, M., Gasnier, F., Luche, S., Rey, C., Aebersold, R., Benahmed, M., Louisot, P. and Lunardi, J. (2002) Proteomics analysis of cellular response to oxidative stress. Evidence for *in vivo* overoxidation of peroxiredoxins at their active site. *J. Biol. Chem.*, **277**, 19396–19401.

Ren, D., Julka, S., Inerowicz, H.D. and Regnier, F.E. (2004) Enrichment of cysteine-containing peptides from tryptic digests using a quaternary amine tag. *Anal. Chem.*, **76**, 4522–4530.

Riener, C.K., Kada, G., and Gruber, H.J. (2002) Quick measurement of protein sulfhydryls with Ellman's reagent and with 4,4′-dithiodipyridine. *Anal. Bioanal. Chem.*, **373**, 266–276.

Rouhier, N., Gelhaye, E. and Jacquot, J.P. (2002a) Exploring the active site of plant glutaredoxin by site-directed mutagenesis. *FEBS Lett.*, **511**, 145–149.

Rouhier, N., Gelhaye, E. and Jacquot, J.P. (2002b) Glutaredoxin-dependent peroxiredoxin from poplar: protein-protein interaction and catalytic mechanism. *J. Biol. Chem.*, **277**, 13609–13614.

Rouhier, N., Gelhaye, E. and Jacquot, J.P. (2004) Plant glutaredoxins: still mysterious reducing systems. *Cell Mol. Life Sci.*, **61**, 1266–1277.

Sarkar, N., Lemaire, S., Wu-Scharf, D., Issakidis-Bourguet, E. and Cerutti, H. (2005) Functional specialization of *Chlamydomonas reinhardtii* cytosolic thioredoxin h1 in the response to alkylation-induced DNA damage. *Eukaryot. Cell.*, **4**, 262–273.

Saurin, A.T., Neubert, H., Brennan, J.P. and Eaton, P. (2004) Widespread sulfenic acid formation in tissues in response to hydrogen peroxide. *Proc. Natl Acad. Sci. USA*, **101**, 17982–17987.

Schenk, H., Klein, M., Erdbrugger, W., Droge, W. and Schulze-Osthoff, K. (1994) Distinct effects of thioredoxin and antioxidants on the activation of transcription factors NF-κB and AP-1. *Proc. Natl Acad. Sci. USA*, **91**, 1672–1676.

Schürmann, P. and Jacquot, J.P. (2000) Plant thioredoxin systems revisited. *Annu. Rev. Plant Physiol. Plant Mol. Biol.*, **51**, 371–400.

Sebastiano, R., Citterio, A., Lapadula, M. and Righetti, P.G. (2003) A new deuterated alkylating agent for quantitative proteomics. *Rapid Commun. Mass Spectrom.*, **17**, 2380–2386.

Sechi, S. and Chait, B.T. (1998) Modification of cysteine residues by alkylation. A tool in peptide mapping and protein identification. *Anal. Chem.*, **70**, 5150–5158.

Sethuraman, M., McComb, M.E., Huang, H., Huang, S., Heibeck, T., Costello, C.E. and Cohen, R.A. (2004) Isotope-coded affinity tag (ICAT) approach to redox proteomics: identification and quantitation of oxidant-sensitive cysteine thiols in complex protein mixtures. *J. Proteome Res.*, **3**, 1228–1233.

Shevchenko, A., Wilm, M., Vorm, O. and Mann, M. (1996) Mass spectrometric sequencing of proteins silver-stained polyacrylamide gels. *Anal. Chem.*, **68**, 850–858.

Shaw, J., Rowlinson, R., Nickson, J., Stone, T., Sweet, A., Williams, K. and Tonge, R. (2003) Evaluation of saturation labelling two-dimensional difference gel electrophoresis fluorescent dyes. *Proteomics*, **3**, 1181–1195.

Sommer, A. and Traut, R.R. (1974) Diagonal polyacrylamide-dodecyl sulfate gel electrophoresis for the identification of ribosomal proteins crosslinked with methyl-4-mercaptobutyrimidate. *Proc. Natl Acad. Sci. USA*, **71**, 3946–3950.

Taldone, F. S., Tummala, M., Goldstein, E. J., Ryzhov, V., Ravi, K., Black, S. M. (2005) Studying the S-nitrosylation of model peptides and eNOS protein by mass spectrometry. *Nitric Oxide*, **13**, 176–187.

Thevis, M., Ogorzalek Loo, R.R. and Loo, J.A. (2003) In-gel derivatization of proteins for cysteine-specific cleavages and their analysis by mass spectrometry. *J. Proteome Res.*, **2**, 163–172.

Tie, J.K., Jin, D.Y., Loiselle, D.R., Pope, R.M., Straight, D.L. and Stafford, D.W. (2004) Chemical modification of cysteine residues is a misleading indicator of their status as active site residues in the vitamin K-dependent gamma-glutamyl carboxylation reaction. *J. Biol. Chem.*, **279**, 54079–54087.

Tiessen, A., Hendriks, J.H., Stitt, M., Branscheid, A., Gibon, Y., Farre, E.M. and Geigenberger, P. (2002) Starch synthesis in potato tubers is regulated by post-translational redox modification of ADP-glucose pyrophosphorylase: a novel regulatory mechanism linking starch synthesis to the sucrose supply. *Plant Cell*, **14**, 2191–2213.

Toriumi, C. and Imai, K. (2003) An identification method for altered proteins in tissues utilizing fluorescence derivatization, liquid chromatography, tandem mass spectrometry, and a database-searching algorithm. *Anal. Chem.*, **75**, 3725–3730.

Trebitsh, T., Meiri, E., Ostersetzer, O., Adam, Z. and Danon, A. (2001) The protein disulfide isomerase-like RB60 is partitioned between stroma and thylakoids in *Chlamydomonas reinhardtii* chloroplasts. *J. Biol. Chem.*, **276**, 4564–4569.

Tsikas, D., Sandmann, J., Rossa, S., Gutzki, F.M. and Frolich, J.C. (1999) Investigations of S-transnitrosylation reactions between low- and high-molecular-weight S-nitroso compounds and their thiols by high-performance liquid chromatography and gas chromatography-mass spectrometry. *Anal. Biochem.*, **270**, 231–241.

Verdoucq, L., Vignols, F., Jacquot, J.P., Chartier, Y. and Meyer, Y. (1999) *In vivo* characterization of a thioredoxin h target protein defines a new peroxiredoxin family. *J. Biol. Chem.*, **274**, 19714–19722.

Vestweber, D. and Schatz, G. (1988) Mitochondria can import artificial precursor proteins containing a branched polypeptide chain or a carboxy-terminal stilbene disulfonate. *J. Cell Biol.*, **107**, 2045–2049.

Wagner, E., Luche, S., Penna, L., Chevallet, M., Van Dorsselaer, A., Leize-Wagner, E. and Rabilloud, T. (2002) A method for detection of overoxidation of cysteines: peroxiredoxins are oxidized *in vivo* at the active-site cysteine during oxidative stress. *Biochem. J.*, **366**, 777–785.

Wallis, T.P., Pitt, J.J. and Gorman, J.J. (2001) Identification of disulfide-linked peptides by isotope profiles produced by peptic digestion of proteins in 50% ^{18}O water. *Protein Sci.*, **10**, 2251–2271.

Wang, J., Boja, E.S., Tan, W., Tekle, E., Fales, H.M., English, S., Mieyal, J.J. and Chock, P.B. (2001) Reversible glutathionylation regulates actin polymerization in A431 cells. *J. Biol. Chem.*, **276**, 47763–47766.

Wilkinson, B. and Gilbert, H.F. (2004) Protein disulfide isomerase. *Biochim. Biophys. Acta.*, **1699**, 35–44.

Wolosiuk, R.A. and Buchanan, B.B. (1977) Thioredoxin and glutathione regulate photosynthesis in chloroplasts. *Nature*, **266**, 565–567.

Wolosiuk, R.A., Crawford, N.A., Yee, B.C. and Buchanan, B.B. (1979) Isolation of three thioredoxins from spinach leaves. *J. Biol. Chem.*, **254**, 1627–1632.

Wong, J.H., Kim, Y.B., Ren, P.H., Cai, N., Cho, M.J., Hedden, P., Lemaux, P.G. and Buchanan, B.B. (2002) Transgenic barley grain overexpressing thioredoxin shows evidence that the starchy endosperm communicates with the embryo and the aleurone. *Proc. Natl Acad. Sci. USA*, **99**, 16325–16330.

Wong, J.H., Cai, N., Balmer, Y., Tanaka, C.K., Vensel, W.H., Hurkman, W.J. and Buchanan, B.B. (2004) Thioredoxin targets of developing wheat seeds identified by complementary proteomic approaches. *Phytochemistry*, **65**, 1629–1640.

Wu, J. and Watson, J.T. (1997) A novel methodology for assignment of disulfide bond pairings in proteins. *Protein Sci.*, **6**, 391–398.

Wu, Y, Kwon, K.S. and Rhee, S.G. (1998) Probing cellular protein targets of H_2O_2 with fluorescein-conjugated iodoacetamide and antibodies to fluorescein. *FEBS Lett.*, **440**, 111–115.

Xiao, R., Wilkinson, B., Solovyov, A., Winther, J.R., Holmgren, A., Lundstrom-Ljung, J. and Gilbert, H.F. (2004) The contributions of protein disulfide isomerase and its homologues to oxidative protein folding in the yeast endoplasmic reticulum. *J. Biol. Chem.*, **279**, 49780–49786.

Yamazaki, D., Motohashi, K., Kasama, T., Hara, Y. and Hisabori, T. (2004) Target proteins of the cytosolic thioredoxins in *Arabidopsis thaliana*. *Plant Cell Physiol.*, **45**, 18–27.

Yanagida, M., Mino, M., Iwabuchi, M. and Ogawa, K. (2004) Reduced glutathione is a novel regulator of vernalization-induced bolting in the rosette plant *Eustoma grandiflorum*. *Plant Cell Physiol.*, **45**, 129–137.

Yang, Y., Jao, S., Nanduri, S., Starke, D.W., Mieyal, J.J. and Qin, J. (1998) Reactivity of the human thioltransferase (glutaredoxin) C7S, C25S, C78S, C82S mutant and NMR solution structure of its glutathionyl mixed disulfide intermediate reflect catalytic specificity. *Biochemistry*, **37**, 17145–17156.

Yano, H., Wong, J.H., Lee, Y.M., Cho, M.J. and Buchanan, B.B. (2001) A strategy for the identification of proteins targeted by thioredoxin. *Proc. Natl Acad. Sci. USA*, **98**, 4794–4799.

Yen, T.Y., Joshi, R.K., Yan, H., Seto, N.O., Palcic, M.M. and Macher, B.A. (2000) Characterization of cysteine residues and disulfide bonds in proteins by liquid chromatography/electrospray ionization tandem mass spectrometry. *J. Mass Spectrom.*, **35**, 990–1002.

Yen, T.Y., Yan, H. and Macher, B.A. (2002) Characterizing closely spaced, complex disulfide bond patterns in peptides and proteins by liquid chromatography/electrospray ionization tandem mass spectrometry. *J. Mass Spectrom.*, **37**, 15–30.

Zubarev, R.A., Kruger, N.A., Fridriksson, E.K., Lewis, M.A., Horn, D.M., Carpenter, B.K. and McLafferty, F.W. (1999) Electron capture dissociation of gaseous multiply-charged proteins is favored at disulfide bonds and other sites of high hydrogen atom affinity. *J. Am. Chem. Soc.*, **121**, 2857–2862.

Appendix II

Structure *14*, 1701–1710, November 2006 DOI 10.1016/j.str.2006.09.012

Structural Basis for Target Protein Recognition by the Protein Disulfide Reductase Thioredoxin

Kenji Maeda,[1,5] Per Hägglund,[1,5] Christine Finnie,[1] Birte Svensson,[1,3,*] and Anette Henriksen[2,4,*]
[1] Enzyme and Protein Chemistry
BioCentrum-DTU
Søltofts Plads
Building 224
Technical University of Denmark
DK-2800 Kgs. Lyngby
Denmark
[2] Biostructure Group
Carlsberg Laboratory
Gamle Carlsberg Vej 10
DK-2500 Valby
Denmark

Summary

Thioredoxin is ubiquitous and regulates various target proteins through disulfide bond reduction. We report the structure of thioredoxin (HvTrxh2 from barley) in a reaction intermediate complex with a protein substrate, barley α-amylase/subtilisin inhibitor (BASI). The crystal structure of this mixed disulfide shows a conserved hydrophobic motif in thioredoxin interacting with a sequence of residues from BASI through van der Waals contacts and backbone-backbone hydrogen bonds. The observed structural complementarity suggests that the recognition of features around protein disulfides plays a major role in the specificity and protein disulfide reductase activity of thioredoxin. This novel insight into the function of thioredoxin constitutes a basis for comprehensive understanding of its biological role. Moreover, comparison with structurally related proteins shows that thioredoxin shares a mechanism with glutaredoxin and glutathione transferase for correctly positioning substrate cysteine residues at the catalytic groups but possesses a unique structural element that allows recognition of protein disulfides.

Introduction

Thioredoxins (Trxs) are ubiquitous small proteins (~12–14 kDa) with protein disulfide reductase activity that play central roles in cellular metabolic activities by donating electrons to enzymes such as ribonucleotide reductase, methionine sulfoxide reductases, and peroxiredoxins (Arnér and Holmgren, 2000). In addition, an array of target proteins ranging from mammalian transcription factors to plant enzymes involved in photosynthesis are regulated by Trx-catalyzed disulfide bond reduction (Schenk et al., 1994; Buchanan and Balmer, 2005). Despite the importance of Trx in a wide variety of biological processes, it is not known to what extent the disulfide reductase activity of Trx depends on recognition of a structural motif in the protein substrates. This lack of insight into the substrate interaction features has to date been a hindrance for a complete mapping of redox signaling pathways involving Trx.

The structure of Trx is highly conserved among species, with a central five-stranded β sheet surrounded by four α helices in a βαβαβαββα topology that includes the so-called Trx fold (βαβαββα) (Holmgren et al., 1975; Katti et al., 1990; Weichsel et al., 1996; Menchise et al., 2001). In spite of considerable variation in overall structures, sequences, and functions, the Trx fold is also present in glutaredoxin (Grx), which catalyzes protein deglutathionylation, glutathione transferase (GST), protein disulfide isomerase (PDI), glutathione peroxidase, and the disulfide-forming protein DsbA (reviewed in Martin, 1995). The redox activity of Trx involves two cysteines in the conserved active site motif $WC_NG(P)PC_C$. The cysteines form an intramolecular disulfide in the oxidized state and universally receive reducing equivalents from either NADPH via Trx reductase (Arnér and Holmgren, 2000) or in plant chloroplasts via ferredoxin and ferredoxin-Trx reductase (Buchanan and Balmer, 2005). In the reduced dithiol state, the surface-exposed cysteine at the N-terminal side of the motif (C_N) attacks disulfide bonds in protein substrates with formation of an intermolecular disulfide intermediate (Kallis and Holmgren, 1980) (Figure 1A). This mixed disulfide is subsequently attacked by the buried C-terminal cysteine (C_C), resulting in release of the reduced target protein and the oxidized Trx.

Even though Trx is proposed to act as a general protein disulfide reductase, examinations of individual disulfide proteins and proteomics-based surveys for target proteins have shown substrate selectivity of Trx for certain protein disulfides (Østergaard et al., 2001; Yano et al., 2001; Maeda et al., 2004, 2005). Moreover, although Trx shares the Trx fold and catalytic sequence motif CXXC with Grx (typically CPYC in Grx), Trx reduces glutathione mixed disulfides much less efficiently and thus differs in specificity from Grx (reviewed in Fernandes and Holmgren, 2004). Mutational analysis of the specific redox regulation of fructose-1,6-bisphosphatase by chloroplastic Trx has suggested charge complementarity to influence the specificity of Trx (de Lamotte-Guery et al., 1991; Geck et al., 1996; Mora-García et al., 1997). However, the only structural studies to date of the interaction between Trx and target proteins are NMR structure determinations of two disulfide-bonded complexes between a mutant of human Trx and short synthetic peptide fragments derived from transcription factors NF-κB and Ref-1 (Qin et al., 1995, 1996). Protein disulfides can be structurally diverse in various aspects, such as their surface exposure and their locations in secondary structure elements, the dihedral angles around the disulfide bond, and the identity of the amino acids present at spatially and sequentially close locations (Bhattacharyya et al., 2004). Thus, determination of the structure of a Trx-target protein-protein

*Correspondence: bis@biocentrum.dtu.dk (B.S.), anette@crc.dk (A.H.)
[3] Lab address: http://www.epc.biocentrum.dtu.dk
[4] Lab address: http://www.crc.dk
[5] These authors contributed equally to this work.

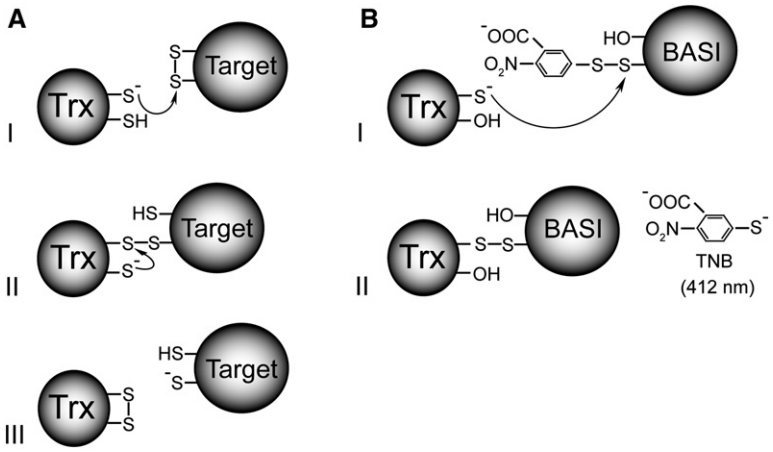

Figure 1. Mechanisms of Trx Disulfide Reductase Activity and the Strategy Used Here to Form a Kinetically Stable Mixed Disulfide

(A) The N-terminal, exposed cysteine (C_N) in the Trx active site sequence motif $WC_NG(P)PC_C$ makes a nucleophilic attack on the target disulfide bond (I) to form an intermolecular mixed-disulfide intermediate (II), which is subjected to intramolecular attack from the C-terminal, buried cysteine (C_C) to release the reduced target protein and oxidized Trx (III).

(B) Activated disulfides formed by conjugation of TNB to single cysteines $C148_{BASI}$ and $C144_{BASI}$ in the BASI-target disulfide mutants C144S and C148S are attacked by C_N (C46) in an HvTrxh2 mutant that lacks C_C (C49S) (I), to form stable mixed disulfides between BASI and HvTrxh2 (II). The reaction is monitored spectrophotometrically by following the release of TNB at 412 nm.

complex is essential to fully reveal the structural features involved in recognition of protein disulfides by Trx.

Plants contain multiple Trxs that show diverse subcellular locations and have been classified into groups (e.g., h, f, and m types) based on sequence similarity (Gelhaye et al., 2005). The h-type thioredoxins are found in cytosol, nucleus, mitochondria, and phloem sieve tubes. Our previous screenings for target proteins in barley seed extracts have shown that disulfide C144-C148 in α-amylase/subtilisin inhibitor (BASI) is reduced with high efficiency by h-type Trx, and that this disulfide is preferentially reduced compared to the other disulfide C43-C90 in BASI (Maeda et al., 2003, 2004, 2005). Here, the barley Trx h isoform 2 (HvTrxh2)-catalyzed disulfide reduction of BASI is used as a model system to investigate structural requirements for recognition of a target protein disulfide bond by Trx. The crystal structure is solved for HvTrxh2-S-S-BASI, a trapped mixed disulfide that mimics the reaction intermediate of the reductase in complex with its target protein.

Results

Production of the HvTrxh2-S-S-BASI Mixed Disulfide

To form a kinetically stable complex mimicking the intermolecular mixed-disulfide intermediate in the disulfide reductase reaction pathway of Trx (Figure 1A), an HvTrxh2 mutant of C_C (C49S) in the active site motif WC_NGPC_C and BASI mutants C144S and C148S from the target disulfide C144-C148 were used (Figure 1B). Briefly, the single cysteines $C148_{BASI}$ and $C144_{BASI}$ in C144S and C148S, respectively, were conjugated to 2-nitro-5-thiobenzoate (TNB) and subsequently incubated with HvTrxh2 C49S to substitute TNB with $C46_{HvTrxh2}$ (Figure 1B). To determine whether $C144_{BASI}$ or $C148_{BASI}$ are accessible to nucleophilic attack from $C46_{HvTrxh2}$, the rate of the reaction was monitored spectrophotometrically by following the release of TNB (Figure 1B). The reaction progressed rapidly with C144S, whereas almost no substitution was observed for C148S (Figure 2A). The results suggest that essentially only $C148_{BASI}$ is accessible to $C46_{HvTrxh2}$. This is in agreement with the Sγ atom of $C148_{BASI}$ being surface exposed and covering the Sγ atom of $C144_{BASI}$ in the crystal structure of BASI in complex with barley α-amylase 2 (AMY2/BASI) (Protein Data Bank [PDB] ID code 1AVA; Vallée et al., 1998) (Figure 2B). According to the mechanism of bimolecular nucleophilic substitution, the thiolate anion of $C46_{HvTrxh2}$ must perform the nucleophilic attack on an Sγ atom of a disulfide from a direction 180° away from the other Sγ atom that acts as a leaving group. Thus, the relative accessibilities of the two Sγ atoms permit $C46_{HvTrxh2}$ to only attack on C148 of disulfide C144-C148 of BASI. $C148_{BASI}$ was therefore concluded to form an intermolecular disulfide bond in the Trx reaction intermediate, and the $C46_{HvTrxh2}$-$C148_{BASI}$ mixed disulfide (HvTrxh2-S-S-BASI) was prepared in large scale for crystallization.

Architecture of HvTrxh2-S-S-BASI

The final electron density map of HvTrxh2-S-S-BASI at 2.3 Å resolution (PDB ID code 2IWT) unambiguously displays the covalent and noncovalent contacts between Trx and BASI in the single mixed-disulfide complex present in the asymmetric unit (Figure 3A). The structural model comprises residues 13–120 of HvTrxh2 (122 amino acids), while the 12 residue N-terminal segment is not visible in the final 1σ $2F_o - F_c$ electron density map, presumably due to high flexibility. Residues 59–64, 94–101, and 112–120 of HvTrxh2, located distantly from the BASI interface, exhibit relatively high B factors, presumably due to the small number of contacts with symmetry-related molecules (in total 214 for HvTrxh2 versus 818 for BASI). HvTrxh2 has the typical fold of Trx with a five-stranded β sheet surrounded by four α helices in a βαβαβαββα topology. The overall structure of HvTrxh2 is representative for Trxs, as the Cα atoms can be superimposed on the crystal structures of oxidized Trxs from *Escherichia coli* (PDB ID code 2TRX, molecule A; Katti et al., 1990), *Homo sapiens* (PDB ID code 1ERU; Weichsel et al., 1996), and the green alga *Chlamydomonas reinhardtii* (h type) (PDB ID code 1EP7, molecule A; Menchise et al., 2001) with root-mean-square difference (rmsd) values of 0.9, 1.1, and 0.8 Å, respectively (70, 86, and 102 Cα atoms are used, respectively). Major deviations are observed for residues at the most N- and C-terminal ends and around α1, which in HvTrxh2 (residues 20–32) is particularly extended in comparison to Trxs from *E. coli* (residues

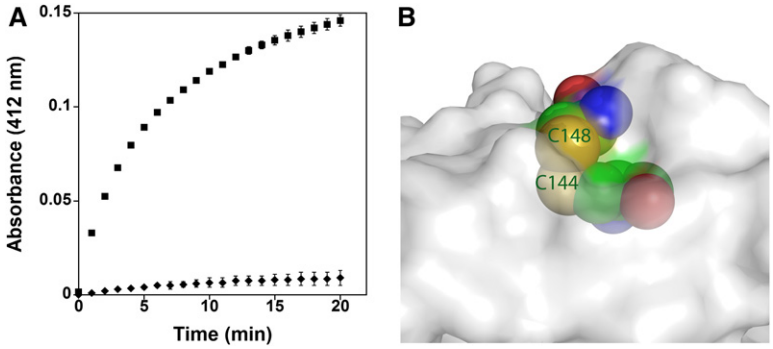

Figure 2. Accessibility of the Cysteines in the BASI C144-C148 Disulfide Bond

(A) The time course of the reaction between C49S HvTrxh2 (16.4 μM) and TNB-conjugated C144S (■) (11.9 μM) and C148S BASI (◆) (11.9 μM) is monitored by the liberation of TNB at 412 nm. Error bars indicate the maxima and minima from duplicate measurements.

(B) Close-up view of the disulfide C144-C148 in the crystal structure of BASI in complex with barley α-amylase 2 (PDB ID code 1AVA, molecule D; Vallée et al., 1998) showing that C148 Sγ is exposed and shields C144 Sγ. The exposed surface is shown in white except for C144 and C148. For C144 and C148, carbon, oxygen, nitrogen, and sulfur atoms are shown as van der Waals spheres and colored green, red, blue, and yellow, respectively.

12–15, molecule A) or *H. sapiens* (residues 8–17). The β-trefoil topology of BASI could be traced in the structure except for an alanine residue at the C terminus. The global structure of the BASI mutant in HvTrxh2-S-S-BASI is superimposable on the wild-type in AMY2/BASI (molecule D) with rmsd of 0.5 Å using 161 Cα atoms (PDB ID code 1AVA; Vallée et al., 1998). The intermolecular disulfide bond is as expected formed between $C46_{HvTrxh2}$ and $C148_{BASI}$. Neither of the bonded cysteines is in a strained conformation as the χ1 angle of $C46_{HvTrxh2}$ is 175°, close to the values reported in reduced Trxs from other species such as human Trx (χ1 = 192°, C32) (PDB ID code 1ERT; Weichsel et al., 1996), while the χ1 angle of $C148_{BASI}$ is −60° and comparable to that of C148 from the intact disulfide in wild-type BASI (PDB ID code 1AVA; Vallée et al., 1998) (χ1 = −71° in molecule C and χ1 = −64° in molecule D). The intermolecular disulfide bond displays an architecture common to right-handed disulfide bonds (Petersen et al., 1999), with dihedral angles defined by $C\alpha_i$-$C\beta_i$-$S\gamma_i$-$S\gamma_j$, $C\alpha_j$-$C\beta_j$-$S\gamma_j$-$S\gamma_i$, and $C\beta_i$-$S\gamma_i$-$S\gamma_j$-$C\beta_j$ (i = $C46_{HvTrxh2}$ and j = $C148_{BASI}$) of 71°, 112°, and 95°, respectively.

The Protein-Protein Interface of HvTrxh2-S-S-BASI

In total, 762 $Å^2$ of accessible surface area is buried in the protein interface of HvTrxh2-S-S-BASI. This value is smaller than the reported average interface area of

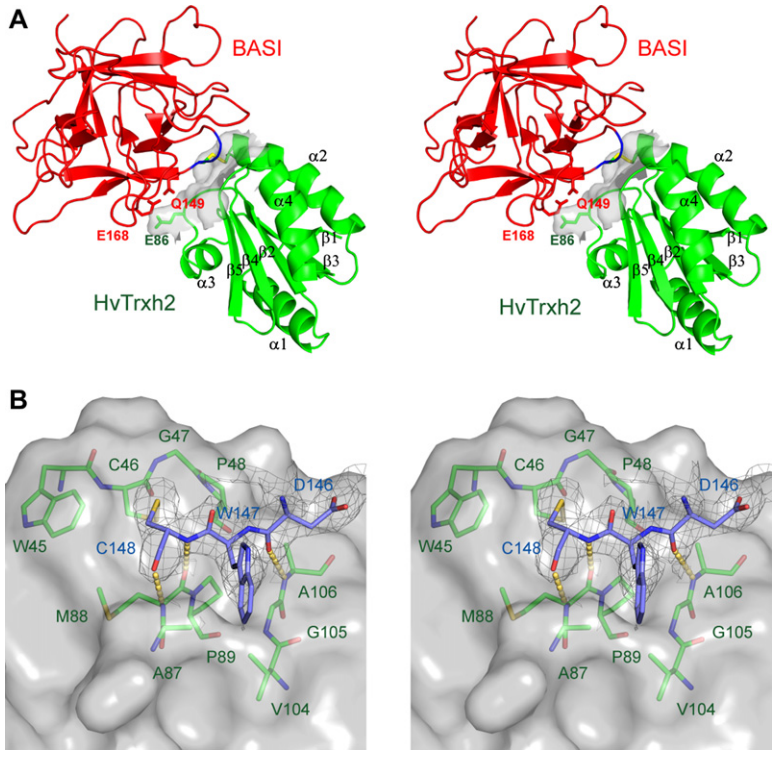

Figure 3. The Crystal Structure of HvTrxh2-S-S-BASI

(A) Stereo view of the overall structure of HvTrxh2-S-S-BASI in cartoon display. HvTrxh2 and BASI are colored green and red, respectively. Secondary structure elements in HvTrxh2 are labeled. The segment $_{146}DWC_{148}$ in BASI is blue. The side chains of the disulfide-bound $C46_{HvTrxh2}$ and $C148_{BASI}$, and the residues $Q149_{BASI}$, $E168_{BASI}$, and $E86_{HvTrxh2}$, are shown in stick representation. $Q149_{BASI}$ and $E168_{BASI}$ are colored and labeled in red and $E86_{HvTrxh2}$ in green. In $C46_{HvTrxh2}$ and $C148_{BASI}$, the carbon and sulfur atoms are colored green and yellow, respectively. The solvent-accessible surface is shown in transparent gray for the residues of HvTrxh2 that are in contact with BASI.

(B) Close-up stereo view of the interaction between HvTrxh2 and BASI. The solvent-accessible surface of HvTrxh2 is colored gray and shown transparent. Segment $_{146}DWC_{148}$ of BASI and the substrate recognition loop motif composed of $_{45}WCGP_{48}$, $_{87}AMP_{89}$, and $_{104}VGA_{106}$ of HvTrxh2 are shown in stick representation. Oxygen, nitrogen, and sulfur atoms are in red, blue, and yellow, respectively. Carbon atoms are in green and blue for HvTrxh2 and BASI, respectively. Intermolecular hydrogen bonds are shown as dashed yellow lines. The $2F_o - F_c$ electron density map is presented as a dark gray isosurface mesh at the 1.0σ level to a distance of 1.0 Å from $_{146}DWC_{148}$ of BASI. Labels on residues from BASI and HvTrxh2 are in blue and green, respectively.

1906 Å^2 in 70 assemblies of proteins or the interface area of 1140 Å^2 in a well-characterized example of an electron-transfer complex between cytochrome *c* peroxidase and cytochrome *c* (Pelletier and Kraut, 1992; Chakrabarti and Janin, 2002). The structure of HvTrxh2-S-S-BASI shows that BASI is recognized by HvTrxh2 primarily through $C148_{BASI}$ and two immediately preceding residues. This $_{146}DWC_{148}$ segment is stabilized by a spatially defined motif on the HvTrxh2 surface composed of $_{45}WCGP_{48}$, $_{87}AMP_{89}$, and $_{104}VGA_{106}$ (referred to in the following as the substrate recognition loop motif) from three neighboring loops between β2-α2, α3-β4, and β5-α4 and the adjacent α2 and β5, all belonging to the core of the Trx fold (Figures 3A and 3B). The substrate recognition loop motif constitutes a hydrophobic groove along which the backbone atoms of $_{146}DWC_{148}$ from BASI are positioned and form van der Waals interactions and backbone-backbone hydrogen bonds (Figure 3B). Although the conserved *cis* proline, $P89_{HvTrxh2}$, is buried and has no direct contact with BASI, it plays an essential structural role in this protein-protein interaction. The conformation of the *cis* peptide bond determines the direction of the main chain at the N terminus of β4. Thereby the backbone amino and carbonyl groups of the adjacent $M88_{HvTrxh2}$ are exposed on the surface, where they make two intermolecular backbone-backbone hydrogen bonds in an antiparallel fashion to $C148_{BASI}$ (Figure 3B). In an adjacent loop between β5 and α4, the backbone amino group of $A106_{HvTrxh2}$ stabilizes the backbone carbonyl group of $D146_{BASI}$ through a hydrogen bond. The side chain of $P48_{HvTrxh2}$ in the conserved active site sequence motif WCGPC further stabilizes the main chain of BASI by van der Waals contacts to five backbone atoms of $D146_{BASI}$ and $W147_{BASI}$. The indole ring of $W147_{BASI}$ is accommodated between the two segments $_{87}AMP_{89}$ and $_{104}VGA_{106}$ of HvTrxh2 and makes hydrophobic interactions with the side chains of $A87_{HvTrxh2}$ and $V104_{HvTrxh2}$ (Figure 3B). Finally, the side chain of $C148_{BASI}$ fits into a shallow groove between the hydrophobic side chains of $W45_{HvTrxh2}$ and $P48_{HvTrxh2}$. In addition to the segment $_{146}DWC_{148}$, $E168_{BASI}$ and $Q149_{BASI}$ make van der Waals interactions with $E86_{HvTrxh2}$ (Figure 3A).

Conservation of the Substrate Recognition Loop Motif among Trx-Fold Proteins

The coordinates of the main-chain atoms of $_{45}WCGP_{48}$, $_{87}AMP_{89}$, and $_{104}VGA_{106}$ from HvTrxh2 that constitute the substrate recognition loop motif, interacting with $_{146}DWC_{148}$ of BASI, were used to search for similar motifs in the existing PDB entries using the SPASM server (http://portray.bmc.uu.se/cgi-bin/spasm/scripts/spasm.pl; Kleywegt, 1999). The result shows that the main-chain structure and a major part of the sequence in this motif is conserved among Trxs from diverse species (Table 1; maximum rmsd set to 1.0 Å for the initial search). For example, the corresponding motifs in Trxs from *H. sapiens* (PDB ID code 1ERT, reduced form) and *E. coli* (PDB ID code 2TRX, oxidized form) are superimposed on that of HvTrxh2 with rmsd values of 0.39 Å and 0.48 Å, respectively. Motifs with highly similar main-chain structures are also identified in PDIs from *E. coli* (DsbC, PDB ID code 1EEJ; DsbG, PDB ID code 1V58) that catalyze formation and isomerization of disulfides in proteins, and in GSTs of classes delta (PDB ID codes 1V2A and 1R5A), kappa (PDB ID codes 1R4W and 1YZX), and tau (PDB ID code 1GWC) that catalyze transfer of the cysteine thiol group in glutathione (Table 1). The other matched proteins have various functions, overall structures, and sequences—nevertheless they all contain the Trx fold (Table 1). The conservation of the substrate recognition loop motif in these proteins might therefore only reflect the conserved domain structure. To test this, the conservation of the overall Trx fold in the identified proteins was examined by searching in the SPASM server using spatially defined fingerprint motifs from secondary structure elements in the Trx fold of HvTrxh2. The fingerprint motifs β2α2α3, β2α3α4, and β2α2α4 were formed by combining the main-chain atoms of segments 38–41 (β2), 53–55 (α2), 78–80 (α3), and 112–114 (α4). A majority of the Trxs that matched the substrate recognition loop motif also superimposed well with the fingerprint motifs from HvTrxh2, whereas most other Trx-fold proteins were either not identified or superimposed poorly with the fingerprint motifs (Table 1). Thus, the spatially defined substrate recognition loop motif of HvTrxh2 is more conserved than the overall Trx fold, supporting its functional significance proposed here.

Comparison with the Glutathione Recognition Mechanisms of GST and Grx

The motif comprised of residues $_{15}LSPY_{18}$, $_{182}GLP_{184}$, and $_{198}FGS_{200}$ in rat mitochondrial class kappa GST (PDB ID code 1R4W; Ladner et al., 2004) can be superimposed with the substrate recognition loop motif of HvTrxh2 (Table 1). This motif plays a central part in the interaction with the substrate glutathione (Ladner et al., 2004). Visual inspection of the aligned structural motifs reveals remarkable similarities as well as differences in the interactions that stabilize their respective substrate complexes (Figure 4A; aligned using Cα atoms only). Segment $_{182}GLP_{184}$ in rat class kappa GST has a function analogous to the structural counterpart $_{87}AMP_{89}$ of HvTrxh2. It binds the cysteine residue of glutathione through backbone-backbone hydrogen bonds from the residue preceding a *cis* proline in an antiparallel fashion. The cysteine thiol group of glutathione is thereby situated at the catalytic hydroxyl group of S16 in GST (Ladner et al., 2004), superimposed on C46 in HvTrxh2 in the alignment. Segment $_{198}FGS_{200}$ in rat class kappa GST involved in the specific recognition of glutathione corresponds to $_{104}VGA_{106}$ of HvTrxh2. The side chain and the backbone amino group of the conserved serine (S200, superimposed on $A106_{HvTrxh2}$) in this segment form hydrogen bonds to the γ-glutamate residue of glutathione (Figure 4A).

The search in the SPASM server using the substrate recognition loop motif of HvTrxh2 only identified a single Grx, Grx-2 from *E. coli*, with an unusual C-terminal helical domain and overall structural similarity to mammalian GST (Xia et al., 2001) (Table 1). The absence of typical Grxs with a βαβαββα topology among the matched structures reveals that the region corresponding to the substrate recognition loop motif of HvTrxh2 differs in typical Grxs in spite of the high functional and structural similarity to Trx (Eklund et al., 1984). The substrate recognition loop motif of HvTrxh2 is aligned with the motif comprised

Table 1. Proteins with Motifs Superimposable to the Substrate Recognition Loop Motif in HvTrxh2 Identified Using the SPASM Server

PDB ID Code	Protein	Sequence	Rmsd[b] (Å)			
		WCGP-AMP-VGA[a]	Loop Motif[c]	β2α2α3[d]	β2α3α4[d]	β2α2α4[d]
Trxs						
1ERT	*H. sapiens*	WCGP-CMP-SGA	0.39	0.64	0.56	0.81
1XWA	*Drosophila melanogaster*	WCGP-SMP-AGA	0.40	0.56	0.57	0.62
2CVK	*Thermus thermophilus*	WCAP-SIP-VGA	0.45	0.41	0.78	—
1SYR	*Plasmodium falciparum*	WCGP-SMP-LGA	0.46	0.59	0.55	0.67
1EP7	*C. reinhardtii*	WCGP-AMP-VGA	0.47	0.63	0.60	0.60
1R26	*Trypanosoma brucei brucei*	WCGP-QLP-IGA	0.47	—	0.60	—
1T00	*Streptomyces coelicolor*	WCGP-SIP-VGA	0.47	0.52	0.85	0.91
2TRX	*E. coli*	WCGP-GIP-VGA	0.48	0.52	0.93	—
1V98	*T. thermophilus*	WCGP-SVP-VGA	0.55	0.55	0.92	0.98
1FB6	*Spinacia oleracea*	WCGP-SIP-IGA	0.59	0.42	0.88	—
2F51	*Trichomonas vaginalis*	WCGP-SIP-VGA	0.60	1.22	1.04	—
1THX	*Anabaena sp.*	WCGP-GVP-EGV	0.67	0.48	0.92	—
1W4V	*H. sapiens*	WCGP-AVP-VGI	0.69	—	—	—
1DBY	*C. reinhardtii*	WCGP-SIP-IGA	0.78	0.62	—	0.95
GSTs						
1R4W	Class kappa, *Rattus norvegicus*	LSPY-GLP-FGS	0.40	—	—	—
1YZX	Class kappa, *H. sapiens*	LSPY-GLP-FGS	0.45	—	—	—
1V2A	Class delta, *Anopheles dirus*	ISPP-TIP-WES	0.78	—	—	—
1GWC	Class tau, *Aegilops tauschii*	PSPF-KIP-CES	0.82	—	—	—
1R5A	Class delta, *A. dirus*	ASPP-CIP-WES	0.87	—	—	—
PDIs						
1EEJ	DsbC, *E. coli*	TCGY-GTP-PGY	0.65	—	1.27	—
1V58	DsbG, *E. coli*	FCPY-VTP-VGL	0.76	—	—	—
Other Proteins						
1ST9	Cytochrome *c* biosynthesis protein	WCEP-PLP-TGT	0.43	0.85	—	—
1J08	Glutaredoxin-like protein	TCPY-AVP-EGA	0.46	—	0.97	—
1GH2	Thioredoxin-like protein	GCGP-ATP-QGA	0.50	0.50	0.51	0.63
1VRS	Electron-transfer protein DsbD	WCVA-GLP-TGF	0.52	—	—	—
1HYU	Alkyl hydroperoxide reductase	SCHN-GVP-QGR	0.66	—	—	—
1JFU	Thioredoxin-like protein	WCVP-GMP-AGP	0.67	0.84	—	—
1A8L	Protein disulfide oxidoreductase	TCPY-AVP-EGA	0.78	—	1.00	—
1Z3E	Transcriptional regulator	SCTS-RRP-VGY	0.80	—	—	—
1G7O	Glutaredoxin-2	HCPY-QVP-PES	0.84	—	—	—
1RW1	Hypothetical protein	ACDT-KRP-VGF	0.91	—	—	—
1Z6N	Hypothetical protein	WCPD-AIP-VER	1.11	—	—	—

[a] Sequence of the three segments constituting the substrate recognition loop motif of HvTrxh2.
[b] Rmsd values for the superimposition of 40 matched main-chain atoms.
[c] Main-chain atoms for the substrate recognition loop motif of HvTrxh2 constituted of residues 45–48, 87–89, and 104–106 used as a search model.
[d] Coordinates for the main-chain atoms of residues in secondary structure elements β2 (residues 38–41), α2 (residues 53–55), α3 (residues 78–80), and α4 (residues 112–114) constituted fingerprint motifs β2α2α3, β2α3α4, and β2α2α4, used as search models to track fold conservation. Proteins not identified using the fingerprint motifs are marked —.

of residues $_{36}$SCSY$_{39}$, $_{80}$TVP$_{82}$, and $_{92}$GGA$_{94}$ from the crystal structure of human Grx in complex with glutathione (Figure 4B; PDB ID code 2FLS). The main-chain Cα atoms of segments $_{36}$SCSY$_{39}$ and $_{80}$TVP$_{82}$ of human Grx superimpose well on the corresponding segments $_{45}$WCGP$_{48}$ and $_{87}$AMP$_{89}$ from HvTrxh2 and stabilize the substrate cysteine residue in the same manner as observed in rat mitochondrial class kappa GST and in HvTrxh2-S-S-BASI (Figures 4A and 4B). In contrast, the position and orientation of the main-chain Cα atoms of segment $_{92}$GGA$_{94}$ in human Grx and the corresponding segment $_{104}$VGA$_{106}$ in HvTrxh2 clearly diverge. Whereas segment $_{104}$VGA$_{106}$ constitutes a section of the elongated substrate binding groove in HvTrxh2 (Figure 3B), segment $_{92}$GGA$_{94}$ and the side chain of the succeeding residue T95 block the corresponding groove section in human Grx and form hydrogen bonds with the γ-glutamate residue of glutathione (Figure 4B). Moreover, whereas A106$_{HvTrxh2}$ and D146$_{BASI}$ are in an antiparallel-like orientation appropriate for backbone-backbone hydrogen bond formation (Figure 3B), the main chain of A94 in human Grx is oriented almost perpendicularly to the substrate binding surface (Figure 4B).

Discussion

The involvement of protein-protein interactions in the disulfide reductase activity of Trx toward a broad range of protein substrates has been the subject of extensive discussions (Holmgren, 1984; Meyer et al., 2002; Buchanan and Balmer, 2005). In the present study, van der Waals contacts and three intermolecular backbone-backbone hydrogen bonds involving a structural motif created by the $_{45}$WCGP$_{48}$, $_{87}$AMP$_{89}$, and $_{104}$VGA$_{106}$ loops

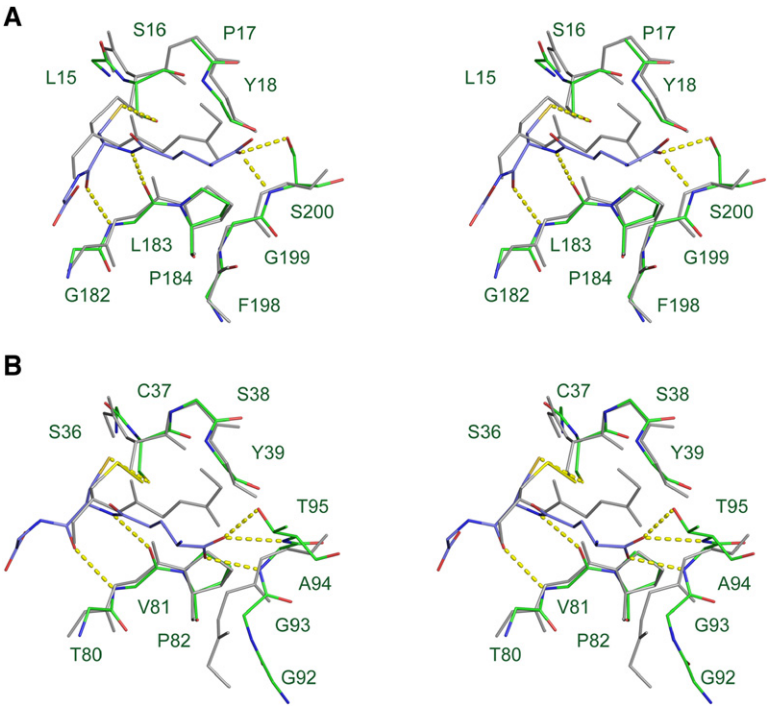

Figure 4. Comparison with the Glutathione Recognition Mechanisms of GST and Grx

Stereo views showing the alignment of Cα atoms in the substrate recognition loop motif of HvTrxh2 composed of $_{45}$WCGP$_{48}$, $_{87}$AMP$_{89}$, and $_{104}$VGA$_{106}$ with Cα atoms in (A) residues $_{15}$LSPY$_{18}$, $_{182}$GLP$_{184}$, and $_{198}$FGS$_{200}$ of rat mitochondrial GST (PDB ID code 1R4W; Ladner et al., 2004) and (B) residues $_{36}$SCSY$_{39}$, $_{80}$TVP$_{82}$, and $_{92}$GGA$_{94}$ of human Grx (PDB ID code 2FLS; C. Johansson, C. Smee, K. Kavanagh, J. Debreczeni, U. Oppermann, and M. Sundström, personal communication) in complex with glutathione. HvTrxh2 and $_{146}$DWC$_{148}$ of BASI are in gray except for the cysteine Sγ atoms in yellow. For GST and Grx, carbon, oxygen, nitrogen, and sulfur atoms are colored green, red, blue, and yellow, respectively. Side chains are not shown except for glutathione, the *cis* proline, and the catalytic cysteine and serine residues. For rat GST (A), the side chain of S200 is also shown. For human Grx (B), the main chain and the side chain of T95 are also shown. Intermolecular hydrogen bonds are shown as dashed yellow lines.

of HvTrxh2 are shown to stabilize the HvTrxh2-S-S-BASI reaction intermediate. HvTrxh2-S-S-BASI has a small interface area and differs largely in the overall interaction features from the two NMR structures of Trx-peptide mixed disulfides, in which at least 9 residues of the 13 residue long synthetic peptides interact with extended surface areas of human Trx (Qin et al., 1995, 1996). The larger number of residues involved in these Trx-peptide interactions most likely reflects the higher conformational freedom of a short peptide compared to a folded protein. Nevertheless, the intermolecular hydrogen bonding pattern observed in the present study is in accordance with the NMR structure of human Trx in complex with a peptide from Ref-1 (Qin et al., 1996). Moreover, a pattern of intermolecular backbone-backbone hydrogen bonds, essentially identical to that in HvTrxh2-S-S-BASI, is also observed in the crystal structure of a mixed-disulfide protein-protein complex between the N- and C-terminal domains of the electron-transfer protein DsbD (DsbD$_N$ and DsbD$_C$) from *E. coli* (PDB ID code 1VRS; Rozhkova et al., 2004; included in Table 1). DsbD$_C$, which transfers electrons to DsbD$_N$, displays disulfide reductase activity and is structurally similar to Trx with a βαβααβαβαβα topology and an active site sequence motif WCVAC. The crystal structure of a protein-protein mixed-disulfide complex, which displays the interactions occurring during the transfer of electrons from DsbD$_N$ to the Trx folded domain of DsbC (PDB ID code 1JZB; Haebel et al., 2002), also includes the pattern of intermolecular hydrogen bonds observed in HvTrxh2-S-S-BASI. We postulate that the mode of interaction observed in HvTrxh2-S-S-BASI is a general feature of Trx-target protein complexes, as the essential parts of the identified substrate recognition loop motif are conserved among Trxs from different species. In the NMR structure of human Trx in complex with a peptide from NF-κB, the parts of Trx forming intermolecular backbone-backbone hydrogen bonds agree with the present study, but the direction of the bound peptide is reversed (Qin et al., 1995), suggesting that multiple patterns of Trx-target interactions may exist.

The conserved *cis* proline is present in various Trx-fold proteins (Martin, 1995), and structural studies have suggested its importance for peptide binding in Trx (Qin et al., 1995, 1996) and glutathione binding in Grx (Nordstrand et al., 1999) and in GST (Reinemer et al., 1991). In addition, the functional importance of the *cis* proline for Grx, GST, and DsbA activity has been demonstrated by site-directed mutagenesis (Nikkola et al., 1991; Charbonnier et al., 1999; Nathaniel et al., 2003; Kadokura et al., 2004). The residue preceding the *cis* proline P89 in HvTrxh2 is shown here to stabilize the target cysteine residue of an intact target protein, supporting that this *cis* peptide bond is also important in Trx for correct positioning of the disulfide from the substrate at the catalytic site. On the other hand, the $_{104}$VGA$_{106}$ segment of the substrate recognition loop motif from HvTrxh2 is shown here to contribute to the unique specificity of Trx. Accordingly, conserved polar and charged residues at the corresponding segments in structures of the diverse classes of GSTs are found to be crucial for the interactions with glutathione (reviewed in Oakley, 2005). The absence of polar or charged residues in Trxs at positions corresponding to $_{104}$VGA$_{106}$ in HvTrxh2 most likely impairs glutathione recognition. An NMR study of an *E. coli* Grx-glutathione mixed disulfide has suggested that Trx with its hydrophobic active site surface is deficient in groups that complement the charged and polar groups of glutathione (Nordstrand et al., 1999). The present study, however, emphasizes the genuine structure-based specificity of Trx that cannot solely be explained by this inability to match with glutathione. The structurally conserved segment $_{104}$VGA$_{106}$ of HvTrxh2 creates a hydrophobic and elongated groove that specifically

interacts with a continuous peptide chain from a protein substrate. In contrast, this part of the Grx structure has an alternative main-chain conformation and seems to be inappropriate for the recognition of protein substrates.

Trx also shares the redox active sequence motif CXXC and the *cis* proline with prokaryotic Trx-fold proteins DsbA, DsbC, and DsbG, responsible for the formation of correct disulfide bonds in periplasmic proteins (reviewed in Kadokura et al., 2003). However, in the structures of DsbC and DsbG from *E. coli* (both included in Table 1; McCarthy et al., 2000; Heras et al., 2004), tyrosine and leucine residues, respectively, substitute A106 of HvTrxh2. In *E. coli* DsbA, conserved uncharged and hydrophobic residues present around the loop corresponding to β5-α4 (residues 105–107) of HvTrxh2 are proposed to participate in interactions with unfolded and misfolded protein substrates (Guddat et al., 1997).

The small interface area that HvTrxh2 forms with a target protein in HvTrxh2-S-S-BASI could account for the broad specificity of Trx toward protein disulfides. The interactions observed in HvTrxh2-S-S-BASI also provide, however, a structural basis to explain protein substrate discrimination by Trx. One of the cysteines in a target protein disulfide should ideally fulfill three structural criteria for optimal interaction with Trx: (1) The backbone amino and carbonyl groups of the cysteine residue, and the carbonyl group of the residue positioned two residues toward the N terminus, should be solvent exposed and free of intramolecular contacts (such as backbone-backbone hydrogen bond arrangements in secondary structure elements) to allow the formation of backbone-backbone hydrogen bonds with Trx. (2) The peptide chain between the cysteine and the other residue forming intermolecular hydrogen bonds to Trx should have an extended main-chain conformation without a turn or a bend to allow the best fit into the substrate binding groove in Trx. (3) The Sγ atom of the cysteine residue must be solvent exposed in order to receive the nucleophilic attack from C_N in Trx. There are only a few well-established Trx-target proteins for which 3D structures have been solved and the redox active disulfide bond has been identified. Nevertheless, visual inspection of the structures shows that the proposed three criteria are fulfilled for the redox active intramolecular disulfide of oxidized *E. coli* 2-Cys peroxiredoxin (PDB ID code 1QXH; Choi et al., 2003), the redox active intermolecular disulfide formed between subunits of rat 2-Cys peroxiredoxin in a homodimer (PDB ID code 1QQ2; Hirotsu et al., 1999), and for the C-terminal regulatory disulfide in the oxidized sorghum malate dehydrogenase (PDB ID code 7MDH; Johansson et al., 1999). Insulin is widely used as a substrate to assay Trx activity (Holmgren, 1979). C7 in chain B of insulin (involved in one of the two interchain disulfides) fulfills all the proposed criteria except that the backbone amino group of H10 in the subsequent α-helical region donates a hydrogen bond to the solvent-exposed carbonyl group of C7 (PDB ID code 1APH; Gursky et al., 1992). The redox active disulfide in $DsbD_N$ that receives electrons from the Trx folded $DsbD_C$ and donates them to periplasmic Trx-fold proteins such as DsbC also fulfills the proposed criteria (PDB ID code 1JZB; Haebel et al., 2002). Also in support of these propositions, a disulfide bond in a mutant of green fluorescent protein that connects two β strands in the β-barrel structure is susceptible to reduction by reduced glutathione but not by Trx (Østergaard et al., 2001), presumably because the backbone atoms are unavailable for hydrogen bonding to Trx and thus criterion (1) is not fulfilled. In addition to the proposed criteria, the van der Waals interactions with $W147_{BASI}$ observed in HvTrxh2-S-S-BASI indicate that a hydrophobic side chain at this position interacting with A87 and V104 may promote the recognition. This is in agreement with our previous observation that hydrophobic residues are overrepresented in the sequences adjacent to the disulfides in barley-seed proteins efficiently reduced by barley Trx h (Maeda et al., 2005). A87 and V104 of HvTrxh2, however, are not conserved among Trxs; these positions are occupied respectively by cysteine and serine in human Trx (PDB ID code 1ERT) and by glycine and valine in *E. coli* Trx (PDB ID code 2TRX). Thus, amino acid residues at these positions may contribute to the variation in target specificity among Trxs.

The surface charge distribution patterns also differ greatly among the Trx structures reported so far. Even though no charge-charge interactions are observed in HvTrxh2-S-S-BASI, the Trx-target interaction suggests that charge distribution could affect the specificity of Trxs by favoring or disfavoring Trx-target complex formation. In HvTrxh2-S-S-BASI, $E86_{HvTrxh2}$ is within van der Waals distance from $E168_{BASI}$ (Figure 3A), and one may speculate that substitution by a basic amino acid would favor complex formation. In the crystal structures of the oxidized form of pea chloroplastic fructose-1,6-bisphosphatase (PDB ID codes 1DCU and 1D9Q; Chiadmi et al., 1999), C173 in the regulatory disulfide C153-C173 has a solvent-exposed Sγ atom with exposed backbone amino and carbonyl groups, but is situated in an α helix and thus does not fulfill criteria (1) and (2) for target disulfide bonds of Trx proposed here. Indeed, most Trxs poorly reduce plant fructose-1,6-bisphosphatase (Meyer et al., 2002). On the other hand, chloroplastic f-type Trx, which uniquely possesses several surface-exposed basic residues at positions surrounding the substrate recognition loop motif defined in the present work, interacts with a cluster of acidic residues in fructose-1,6-bisphosphatase and efficiently reduces this disulfide bond (de Lamotte-Guery et al., 1991; Geck et al., 1996; Mora-García et al., 1997).

In conclusion, the present study reveals that structural features around disulfides in proteins are recognized by Trx. This insight is of great importance for understanding the target specificity of Trx. An array of proteomics techniques developed in recent years has been applied for identification of Trx-target proteins (Verdoucq et al., 1999; Yano et al., 2001; Maeda et al., 2004) and Trx-target disulfide bonds (Maeda et al., 2005). The structural information provided here can be applied for validation of identified target disulfides and prediction of novel redox regulatory pathways. Finally, the detailed knowledge about the structure-function relationship of Trx obtained here opens possibilities for manipulation of protein-protein interactions involving Trx and contributes to the characterization of the numerous other Trx-fold proteins with unresolved functions and specificities.

Experimental Procedures

Construction of Mutants

Mutagenesis was performed using the QuikChange Site-Directed Mutagenesis Kit (Stratagene). The genes encoding HvTrxh2 inserted into plasmid pET15b (contains a plasmid-encoded thrombin-cleavable N-terminal His tag) and His-tagged BASI (Bønsager et al., 2003) inserted into plasmid pET11a were used as templates. The following primers were used for mutagenesis; HvTrxh2 mutant C49S: 5′-TGCATCATGGTGCGGACCATCGAGAATCATGGCTCCAG TTTTCG-3′ and 5′-CGAAAACTGGAGCCATGATTCTCGATGGTCCG CACCATGATGCA-3′; BASI mutant C144S: 5′-GTACAAGCTGATGTC CTCAGGGGACTGGTGCCAGG-3′ and 5′-CCTGGCACCAGTCCCCT GAGGACATCAGCTTGTAC-3′; and BASI mutant C148S: 5′-GCGGG GACTGGTCTCAGGACCTCGGCG-3′ and 5′-CGCCGAGGTCCTGA G-ACCAGTCCCCGC-3′. The polymerase chain reaction (PCR) products were treated with DpnI (Invitrogen) to hydrolyze the template plasmid, and transformed into *E. coli* DH5α. All mutations were confirmed by DNA sequencing at MWG Biotech (Ebersberg, Germany).

Protein Expression and Purification

His-tagged C49S HvTrxh2 mutant was expressed in *E. coli* Rosetta cells at 37°C for 3 hr after induction with 100 μM isopropyl β-D-1-thiogalactopyranoside (IPTG). His-tagged BASI mutants C144S and C148S were expressed as described previously for wild-type BASI with minor modifications (Bønsager et al., 2003). Proteins were extracted with Bugbuster protein extraction reagent including benzonase nuclease (Novagen) and the supernatants were applied onto His-Trap HP columns (Amersham Biosciences) preequilibrated with loading buffer (10 mM imidazole, 500 mM NaCl, 30 mM Tris-HCl [pH 8.0]) and eluted in a gradient of 10–200 mM imidazole. Fractions containing C49S HvTrxh2 were dialyzed against 30 mM Tris [pH 8.0]. For thiol conjugation to TNB, the fractions containing BASI mutants C144S and C148S were incubated with an excess of 5,5′-dithiobis(2-nitrobenzoic acid) (DTNB) for 1 hr at room temperature. TNB-conjugated BASI mutants were purified using HiLoad 16/60 Superdex 75 preparative-grade gel-filtration columns (Amersham Biosciences) equilibrated with 30 mM Tris (pH 8.0). TNB conjugation of the BASI mutants C144S and C148S was confirmed by adding dithiothreitol (DTT) (10 mM) and quantifying the released TNB spectrophotometrically at 412 nm. Protein concentrations were deduced by aid of amino-acid analysis.

Trx-Complex Formation

Analytical scale formation of mixed disulfides between TNB-conjugated C144S or C148S BASI mutants (11.9 μM) and C49S HvTrxh2 (16.4 μM) in a reaction volume of 126 μl was monitored spectrophotometrically at 412 nm by the release of TNB. For production in preparative scale of HvTrxh2-S-S-BASI, C49S HvTrxh2 (44.7 μM) was incubated with TNB-conjugated C144S BASI (32.5 μM) in a reaction volume of 15 ml for 1 hr at room temperature and purified using a HiLoad 26/60 Superdex 75 preparative-grade gel-filtration column (Amersham Biosciences) equilibrated with 50 mM ammonium acetate (pH 6.0), 200 mM NaCl. Fractions containing HvTrxh2-S-S-BASI were treated with immobilized thrombin (Calbiochem) in a 1:100 enzyme:substrate molar ratio for approximately 40 hr to remove the N-terminal His tag from C49S HvTrxh2. Subsequently, HvTrxh2-S-S-BASI was purified on a His-Trap HP column as described above.

Crystallization and X-Ray Crystallography

HvTrxh2-S-S-BASI was dialyzed against 10 mM ammonium acetate (pH 6.0) and concentrated to 8 mg/ml using Centricon 10 (Millipore) filter units. Crystals of HvTrxh2-S-S-BASI were obtained using the hanging-drop vapor-diffusion method at room temperature with 2 μl each of protein solution and a reservoir solution containing 0.1 M citric acid (pH 5.0), 12% (w/v) polyethylene glycol (PEG) 6000. All attempts to cryoprotect the crystals by soaking in cryoprotectants resulted in loss of resolution, and the crystals suffered from radiation damage when data were collected at room temperature. The best data (present study) was obtained by flash freezing the crystals directly from the crystallization drop (the cover slide was removed from the crystallization plate a few minutes before freezing the crystals to evaporate water from the crystallization drop and increase the PEG 6000 concentration to some extent). Diffraction data were collected on a Rigaku RU-H3RHB rotating Cu anode X-ray generator equipped with an R-AXIS IV++ imaging plate detector, a 700 series cryostream cooler from Oxford Cryosystems operated at −160°C, and Molecular Structure Corporation (MSC)/confocal Max-Flux mirrors. Reflections were indexed, integrated, and scaled with MOSFLM (Leslie, 1994) and SCALA (Kabsch, 1988). A high Wilson B factor (48.3) is presumably due to the relatively high crystal mosaicity (estimated to 0.6°–0.8° in MOSFLM) and incomplete cryoprotection of the crystal. A minor ice ring at ~3.7 Å is observed in collected diffraction data. The crystal structures of AMY2/BASI (Vallée et al., 1998) and the oxidized HvTrxh2 (K.M., P.H., C.F., J. Winther, B.S., and A.H., unpublished data) were used as search models for molecular replacement of HvTrxh2-S-S-BASI in MOLREP (Vagin and Teplyakov, 1997). The refinement was carried out with the program CNS (Brünger et al., 1998). Using the simulated annealing protocol against the MLF target function, individual, but restrained, B factors were refined after building the protein model. The X-ray/geometry weight was optimized by the automated CNS procedure. A nonuniform electron-density quality with quite poor electron-density contrast in some parts of the HvTrxh2 molecule probably made the assignment of one overall X-ray/geometry weight insufficient. Bearing the intermediate resolution of the data (2.3 Å) in mind, it was judged inappropriate to solve this problem by using a less restricted B factor refinement. Water molecules and ions were added in the graphic program Coot (Emsley and Cowtan, 2004), also used for manual model rebuilding. The geometries of the refined structure were checked with PROCHECK (Laskowski et al., 1993). The resultant Ramachandran plot has a relatively low (compared to better than 2 Å resolution structures with R factors < 20%) proportion of residues in the most favored areas of the plot, but 99.6% of residues are within the allowed regions and none are in the disallowed

Table 2. Crystallographic Data and Refinement Statistics

	HvTrxh2-S-S-BASI
Data Collection	
Space group	$P\,4_12_12$
Cell dimensions	
a, *b*, *c* (Å)	76.1, 76.1, 129.4
Resolution (Å)	65.7–2.3
R_{sym}	0.079 (0.429)[a]
$I/\sigma I$	6.6 (1.7)[a]
Completeness (%)	99.3 (99.7)[a]
Redundancy	4.4 (4.6)[a]
Wilson B factor	48.3
Refinement	
Resolution (Å)	24.9–2.3
Number of reflections	17,377
R_{work}/R_{free}	22.4 (32.5)[b]/26.4 (38.0)[b]
Number of atoms	
HvTrxh2	841
BASI	1404
Ligand/ion	26
Water	125
B factors	
HvTrxh2	59.7
BASI	43.0
Ligand/ion	57.5
Water	45.4
Rmsd	
Bond lengths (Å)	0.009
Bond angles (°)	1.4
Ramachandran Plot Regions (%)	
Most favored	86.5
Additional allowed	13.1
Generously allowed	0.4
Disallowed	0.0

[a] Highest resolution data shell 2.4–2.3.
[b] Highest resolution data shell 2.4–2.3.

regions. The coordinates and structure factors of HvTrxh2-S-S-BASI have been deposited in the Protein Data Bank under ID code 2IWT. The protein-protein interface in HvTrxh2-S-S-BASI was analyzed using AREAIMOL (Lee and Richards, 1971) and NCONT (CCP4, 1994). The numbers of contacts HvTrxh2 and BASI make with symmetry-related atoms were determined by CONTACT (CCP4, 1994) with a cutoff distance of 5.0 Å. Figures of protein structures were made in PyMOL (http://pymol.sourceforge.net/; DeLano, 2002). The statistics are listed in Table 2.

Search for Structural Motifs in PDB Entries

The searches were performed in the SPASM server (http://portray.bmc.uu.se/cgi-bin/spasm/scripts/spasm.pl; Kleywegt, 1999) with standard settings except that Cα atoms and main-chain atoms only were used for the first and finer screenings, respectively. The minimum number of matched atoms was set to 40 and maximum superimposing rmsd was set to 1 Å (when the substrate recognition loop motif was used as a template) and 1.3 Å (when the fingerprint motifs were used as templates). Matched PDB ID codes of mutant proteins were excluded from Table 1 except for PDB ID code 1VRS. The substrate recognition loop motif was constituted of residues 45–48, 87–89, and 104–106 of HvTrxh2. Residues 38–41, 53–55, 78–80, and 112–114 situated in the central parts of β2, α2, α3, and α4, respectively, were combined to constitute fingerprint motifs β2α2α3, β2α3α4, and β2α2α4.

Acknowledgments

Mette Therese Christensen and Karina Rasmussen are acknowledged for technical assistance. Anne Blicher is thanked for performing amino acid analysis. Jakob R. Winther (Copenhagen University) is gratefully thanked for helpful discussions. The Danish Technical Research Council (STVF, grant 26-03-0194) and the Carlsberg Foundation are acknowledged for financial support to B.S. C.F. receives a grant as a young research leader (grant 23-03-0073) from the Danish Agricultural and Veterinary Research Council (SJVF). K.M. holds a Ph.D. scholarship from the Technical University of Denmark.

Received: August 1, 2006
Revised: September 21, 2006
Accepted: September 24, 2006
Published: November 14, 2006

References

Arnér, E.S.J., and Holmgren, A. (2000). Physiological functions of thioredoxin and thioredoxin reductase. Eur. J. Biochem. *267*, 6102–6109.

Bhattacharyya, R., Pal, D., and Chakrabarti, P. (2004). Disulfide bonds, their stereospecific environment and conservation in protein structures. Protein Eng. Des. Sel. *17*, 795–808.

Bønsager, B.C., Praetorius-Ibba, M., Nielsen, P.K., and Svensson, B. (2003). Purification and characterization of the β-trefoil fold protein barley α-amylase/subtilisin inhibitor overexpressed in *Escherichia coli*. Protein Expr. Purif. *30*, 185–193.

Brünger, A.T., Adams, P.D., Clore, G.M., DeLano, W.L., Gros, P., Grosse-Kunstleve, R.W., Jiang, J.S., Kuszewski, J., Nilges, M., Pannu, N.S., et al. (1998). Crystallography and NMR system: a new software suite for macromolecular structure determination. Acta Crystallogr. D Biol. Crystallogr. *54*, 905–921.

Buchanan, B.B., and Balmer, Y. (2005). Redox regulation: a broadening horizon. Annu. Rev. Plant Biol. *56*, 187–220.

CCP4 (Collaborative Computational Project, Number 4) (1994). The CCP4 suite: programs for protein crystallography. Acta Crystallogr. D Biol. Crystallogr. *50*, 760–763.

Chakrabarti, P., and Janin, J. (2002). Dissecting protein-protein recognition sites. Proteins *47*, 334–343.

Charbonnier, J.B., Belin, P., Moutiez, M., Stura, E.A., and Quéméneur, E. (1999). On the role of the *cis*-proline residue in the active site of DsbA. Protein Sci. *8*, 96–105.

Chiadmi, M., Navaza, A., Miginiac-Maslow, M., Jacquot, J.P., and Cherfils, J. (1999). Redox signalling in the chloroplast: structure of oxidized pea fructose-1,6-bisphosphate phosphatase. EMBO J. *18*, 6809–6815.

Choi, J., Choi, S., Choi, J., Cha, M.K., Kim, I.H., and Shin, W. (2003). Crystal structure of *Escherichia coli* thiol peroxidase in the oxidized state: insights into intramolecular disulfide formation and substrate binding in atypical 2-Cys peroxiredoxins. J. Biol. Chem. *278*, 49478–49486.

de Lamotte-Guery, F., Miginiac-Maslow, M., Decottignies, P., Stein, M., Minard, P., and Jacquot, J.P. (1991). Mutation of a negatively charged amino acid in thioredoxin modifies its reactivity with chloroplastic enzymes. Eur. J. Biochem. *196*, 287–294.

DeLano, W.L. (2002). The PyMOL Molecular Graphics System (San Carlos, CA: DeLano Scientific).

Eklund, H., Cambillau, C., Sjöberg, B.M., Holmgren, A., Jörnvall, H., Höög, J.O., and Brändén, C.I. (1984). Conformational and functional similarities between glutaredoxin and thioredoxins. EMBO J. *3*, 1443–1449.

Emsley, P., and Cowtan, K. (2004). Coot: model-building tools for molecular graphics. Acta Crystallogr. D Biol. Crystallogr. *60*, 2126–2132.

Fernandes, A.P., and Holmgren, A. (2004). Glutaredoxins: glutathione-dependent redox enzymes with functions far beyond a simple thioredoxin backup system. Antioxid. Redox Signal. *6*, 63–74.

Geck, M.K., Larimer, F.K., and Hartman, F.C. (1996). Identification of residues of spinach thioredoxin f that influence interactions with target enzymes. J. Biol. Chem. *271*, 24736–24740.

Gelhaye, E., Rouhier, N., Navrot, N., and Jacquot, J.P. (2005). The plant thioredoxin system. Cell. Mol. Life Sci. *62*, 24–35.

Guddat, L.W., Bardwell, J.C., Zander, T., and Martin, J.L. (1997). The uncharged surface features surrounding the active site of *Escherichia coli* DsbA are conserved and are implicated in peptide binding. Protein Sci. *6*, 1148–1156.

Gursky, O., Badger, J., Li, Y., and Caspar, D.L. (1992). Conformational changes in cubic insulin crystals in the pH range 7–11. Biophys. J. *63*, 1210–1220.

Haebel, P.W., Goldstone, D., Katzen, F., Beckwith, J., and Metcalf, P. (2002). The disulfide bond isomerase DsbC is activated by an immunoglobulin-fold thiol oxidoreductase: crystal structure of the DsbC-DsbDα complex. EMBO J. *21*, 4774–4784.

Heras, B., Edeling, M.A., Schirra, H.J., Raina, S., and Martin, J.L. (2004). Crystal structures of the DsbG disulfide isomerase reveal an unstable disulfide. Proc. Natl. Acad. Sci. USA *101*, 8876–8881.

Hirotsu, S., Abe, Y., Okada, K., Nagahara, N., Hori, H., Nishino, T., and Hakoshima, T. (1999). Crystal structure of a multifunctional 2-Cys peroxiredoxin heme-binding protein 23 kDa/proliferation-associated gene product. Proc. Natl. Acad. Sci. USA *96*, 12333–12338.

Holmgren, A. (1979). Thioredoxin catalyzes the reduction of insulin disulfides by dithiothreitol and dihydrolipoamide. J. Biol. Chem. *254*, 9627–9632.

Holmgren, A. (1984). Enzymatic reduction-oxidation of protein disulfides by thioredoxin. Methods Enzymol. *107*, 295–300.

Holmgren, A., Söderberg, B.O., Eklund, H., and Bränden, C.I. (1975). Three-dimensional structure of *Escherichia coli* thioredoxin-S_2 to 2.8 Å resolution. Proc. Natl. Acad. Sci. USA *72*, 2305–2309.

Johansson, K., Ramaswamy, S., Saarinen, M., Lemaire-Chamley, M., Issakidis-Bourguet, E., Miginiac-Maslow, M., and Eklund, H. (1999). Structural basis for light activation of a chloroplast enzyme: the structure of sorghum NADP-malate dehydrogenase in its oxidized form. Biochemistry *38*, 4319–4326.

Kabsch, W. (1988). Evaluation of single-crystal X-ray-diffraction data from a position-sensitive detector. J. Appl. Crystallogr. *21*, 916–924.

Kadokura, H., Katzen, F., and Beckwith, J. (2003). Protein disulfide bond formation in prokaryotes. Annu. Rev. Biochem. *72*, 111–135.

Kadokura, H., Tian, H., Zander, T., Bardwell, J.C., and Beckwith, J. (2004). Snapshots of DsbA in action: detection of proteins in the process of oxidative folding. Science *303*, 534–537.

Kallis, G.B., and Holmgren, A. (1980). Differential reactivity of the functional sulfhydryl groups of cysteine-32 and cysteine-35 present

in the reduced form of thioredoxin from *Escherichia coli*. J. Biol. Chem. *255*, 10261–10265.

Katti, S.K., LeMaster, D.M., and Eklund, H. (1990). Crystal structure of thioredoxin from *Escherichia coli* at 1.68 Å resolution. J. Mol. Biol. *212*, 167–184.

Kleywegt, G.J. (1999). Recognition of spatial motifs in protein structures. J. Mol. Biol. *285*, 1887–1897.

Ladner, J.E., Parsons, J.F., Rife, C.L., Gilliland, G.L., and Armstrong, R.N. (2004). Parallel evolutionary pathways for glutathione transferases: structure and mechanism of the mitochondrial class kappa enzyme rGSTK1-1. Biochemistry *43*, 352–361.

Laskowski, R.A., McArthur, M.W., Moss, D.S., and Thornton, J.M. (1993). PROCHECK: a program to check the stereochemical quality of protein structures. J. Appl. Crystallogr. *26*, 283–291.

Lee, B., and Richards, F.M. (1971). The interpretation of protein structures: estimation of static accessibility. J. Mol. Biol. *55*, 379–400.

Leslie, A.G.W. (1994). Mosflm User Guide, Mosflm Version 5.30 (Cambridge, UK: MRC Laboratory of Molecular Biology).

Maeda, K., Finnie, C., Østergaard, O., and Svensson, B. (2003). Identification, cloning and characterization of two thioredoxin h isoforms, HvTrxh1 and HvTrxh2, from the barley seed proteome. Eur. J. Biochem. *270*, 2633–2643.

Maeda, K., Finnie, C., and Svensson, B. (2004). Cy5 maleimide labelling for sensitive detection of free thiols in native protein extracts: identification of seed proteins targeted by barley thioredoxin h isoforms. Biochem. J. *378*, 497–507.

Maeda, K., Finnie, C., and Svensson, B. (2005). Identification of thioredoxin h-reducible disulphides in proteomes by differential labelling of cysteines: insight into recognition and regulation of proteins in barley seeds by thioredoxin h. Proteomics *5*, 1634–1644.

Martin, J.L. (1995). Thioredoxin—a fold for all reasons. Structure *3*, 245–250.

McCarthy, A.A., Haebel, P.W., Torronen, A., Rybin, V., Baker, E.N., and Metcalf, P. (2000). Crystal structure of the protein disulfide bond isomerase, DsbC, from *Escherichia coli*. Nat. Struct. Biol. *7*, 196–199.

Menchise, V., Corbier, C., Didierjean, C., Saviano, M., Benedetti, E., Jacquot, J.P., and Aubry, A. (2001). Crystal structure of the wild-type and D30A mutant thioredoxin h of *Chlamydomonas reinhardtii* and implications for the catalytic mechanism. Biochem. J. *359*, 65–75.

Meyer, Y., Miginiac-Maslow, M., Schürmann, P., and Jacquot, J.P. (2002). Protein-protein interactions in plant thioredoxin dependent systems. In Protein-Protein Interactions in Plant Biology, The Annual Plant Reviews, Volume 7, M.T. McManus, W. Laing, and A. Allan, eds. (Sheffield, UK: Sheffield Academic Press), pp. 1–29.

Mora-García, S., Rodríguez-Suárez, R., and Wolosiuk, R.A. (1997). Role of electrostatic interactions on the affinity of thioredoxin for target proteins. Recognition of chloroplast fructose-1,6-bisphosphatase by mutant *Escherichia coli* thioredoxins. J. Biol. Chem. *273*, 16273–16280.

Nathaniel, C., Wallace, L.A., Burke, J., and Dirr, H.W. (2003). The role of an evolutionarily conserved *cis*-proline in the thioredoxin-like domain of human class α glutathione transferase A1-1. Biochem. J. *372*, 241–246.

Nikkola, M., Gleason, F.K., Saarinen, M., Joelson, T., Björnberg, O., and Eklund, H. (1991). A putative glutathione-binding site in T4 glutaredoxin investigated by site-directed mutagenesis. J. Biol. Chem. *266*, 16105–16112.

Nordstrand, K., Åslund, F., Holmgren, A., Otting, G., and Berndt, K.D. (1999). NMR structure of *Escherichia coli* glutaredoxin 3-glutathione mixed disulfide complex: implications for the enzymatic mechanism. J. Mol. Biol. *286*, 541–552.

Oakley, A.J. (2005). Glutathione transferases: new functions. Curr. Opin. Struct. Biol. *15*, 716–723.

Østergaard, H., Henriksen, A., Hansen, F.G., and Winther, J.R. (2001). Shedding light on disulfide bond formation: engineering a redox switch in green fluorescent protein. EMBO J. *20*, 5853–5862.

Pelletier, H., and Kraut, J. (1992). Crystal structure of a complex between electron transfer partners, cytochrome *c* peroxidase and cytochrome *c*. Science *258*, 1748–1755.

Petersen, M.T.N., Jonson, P.H., and Petersen, S.B. (1999). Amino acid neighbours and detailed conformational analysis of cysteines in proteins. Protein Eng. *12*, 535–548.

Qin, J., Clore, G.M., Kennedy, W.M., Huth, J.R., and Gronenborn, A.M. (1995). Solution structure of human thioredoxin in a mixed disulfide intermediate complex with its target peptide from the transcription factor NFκB. Structure *3*, 289–297.

Qin, J., Clore, G.M., Kennedy, W.P., Kuszewski, J., and Gronenborn, A.M. (1996). The solution structure of human thioredoxin complexed with its target from Ref-1 reveals peptide chain reversal. Structure *4*, 613–620.

Reinemer, P., Dirr, H.W., Ladenstein, R., Schäffer, J., Gallay, O., and Huber, R. (1991). The three-dimensional structure of class π glutathione S-transferase in complex with glutathione sulfonate at 2.3 Å resolution. EMBO J. *10*, 1997–2005.

Rozhkova, A., Stirnimann, C.U., Frei, P., Grauschopf, U., Brunisholz, R., Grütter, M.G., Capitani, G., and Glockshuber, R. (2004). Structural basis and kinetics of inter- and intramolecular disulfide exchange in the redox catalyst DsbD. EMBO J. *23*, 1709–1719.

Schenk, H., Klein, M., Erdbrügger, W., Dröge, W., and Schulze-Osthoff, K. (1994). Distinct effects of thioredoxin and antioxidants on the activation of transcription factors NF-κB and AP-1. Proc. Natl. Acad. Sci. USA *91*, 1672–1676.

Vagin, A., and Teplyakov, A. (1997). MOLREP: an automated program for molecular replacement. J. Appl. Crystallogr. *30*, 1022–1025.

Vallée, F., Kadziola, A., Bourne, Y., Juy, M., Rodenburg, K.W., Svensson, B., and Haser, R. (1998). Barley α-amylase bound to its endogenous protein inhibitor BASI: crystal structure of the complex at 1.9 Å resolution. Structure *6*, 649–659.

Verdoucq, L., Vignols, F., Jacquot, J.P., Chartier, Y., and Meyer, Y. (1999). In vivo characterization of a thioredoxin h target protein defines a new peroxiredoxin family. J. Biol. Chem. *274*, 19714–19722.

Weichsel, A., Gasdaska, J.R., Powis, G., and Montfort, W.R. (1996). Crystal structures of reduced, oxidized, and mutated human thioredoxins: evidence for a regulatory homodimer. Structure *4*, 735–751.

Xia, B., Vlamis-Gardikas, A., Holmgren, A., Wright, P.E., and Dyson, H.J. (2001). Solution structure of *Escherichia coli* glutaredoxin-2 shows similarity to mammalian glutathione-S-transferases. J. Mol. Biol. *310*, 907–918.

Yano, H., Wong, J.H., Lee, Y.M., Cho, M.J., and Buchanan, B.B. (2001). A strategy for the identification of proteins targeted by thioredoxin. Proc. Natl. Acad. Sci. USA *98*, 4794–4799.

Accession Numbers

The coordinates and structure factors of HvTrxh2-S-S-BASI have been deposited in the Protein Data Bank under ID code 2IWT.